國 立 交 通 大 學

電子工程學系 電子研究所碩士班

碩 士 論 文

多輸入多輸出正交分頻多工通信之通道估測技術研究

On Channel Estimations for MIMO OFDM Systems

研 究 生：詹偉廷

指導教授：陳紹基 博士

中 華 民 國 九 十 四 年 八 月

多輸入多輸出正交分頻多工通信之通道估測技術研究

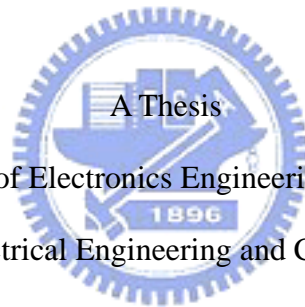# On Channel Estimations for MIMO OFDM Systems

研 究 生：詹偉廷　　　　　　　Student：Wei-Ting Chan

指導教授：陳紹基 博士　　　　　Advisor：Sau-Gee Chen

國 立 交 通 大 學

電子工程學系　電子研究所所碩士班

碩 士 論 文

A Thesis

Submitted to Department of Electronics Engineering & Institute of Electronics

College of Electrical Engineering and Computer Science

National Chiao Tung University

in Partial Fulfillment of the Requirements

for the Degree of

Master

in

Electronics Engineering

August 2005

Hsinchu, Taiwan, Republic of China

中華民國九十四年八月

多輸入多輸出正交分頻多工通信之通道估測技術研究

學生: 詹偉廷　　　　　　　　　　　指導老師: 陳紹基博士

國立交通大學

電子工程學系　電子研究所碩士班

摘　　要

在本篇論文中探討了數種多輸入多輸出正交多工分頻系統中的通道估測技術。我們所主要討論的系統平台包含採用梳狀式(comb-type)傳輸的 802.16a 時空碼模式以及採用區塊式(block-type)傳輸的 802.11n-like 系統，並且配合不同引導訊號的使用。以採分散式(scattered)導引訊號的 802.11n-like 系統來說，我們主要討論內插技巧對這個系統的影響。為了克服非整數取樣空間通道的問題，我們嘗試了離散式餘弦轉換式內插法。模擬結果證實在此系統中較採用傳統離散式傳立葉轉換有所改善。而在含有時空碼先導訊號的 802.11n-like 系統中，我們利用通道追蹤(tracking)的技巧來改善在時變通道下的效能。在討論使用全引導訊號式(all-pilot preamble)的 MIMO 系統時，我們也討論基於最小平方差的估測技巧，並為現有的簡化作法提出一個簡單的通道長度估測法。我們利用 WWiSE 提案的系統進行全引導訊號式系統的模擬，證實了此一方法適合在WWiSE 的標準下中使用。至於對具有時空碼結構的梳狀式傳輸系統，我們則以含有時空碼的 802.16a 系統作為模擬平台，評估各種內插方式的效能。
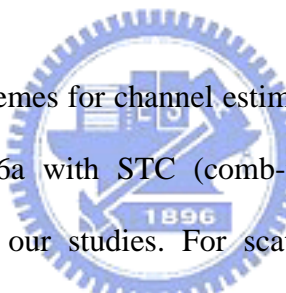
On Channel Estimations for MIMO OFDM Systems

Student: Chan Wei-Ting   Advisor: Dr. Chen Sau-Gee

Department of Electronics Engineering &

Institute of Electronics

National Chiao Tung University

ABSTRACT

In this thesis, several schemes for channel estimation for MIMO OFDM systems are investigated. Both 802.16a with STC (comb-type) and 802.11n-like systems (block-type) are explored in our studies. For scattered preamble in 802.11n-like systems, different interpolation skills are evaluated. To overcome the effect of non-sample spaced channel, DCT-based interpolation is tried. The simulation results show that it is better than DFT-based estimator in this MIMO system. For STBC preamble in 802.11n-like systems, a channel tracking skill is used to improve its performance under time-varying channel. For all-pilot preamble in 802.11n-like systems, a LS-based estimation method is studied. A simple method to detect the length of channel is proposed for this method. With WWiSE standard, this estimation method is evaluated and shown to be suitable for this standard. Also, estimation schemes for comb-type MIMO OFDM systems are also explored in thesis. We evaluate the performances of interpolation techniques applied to 802.16a system with STC.

致謝

　　完成這份碩士學位論文後，不可免俗的要向諸位對我助益良多的師長朋友表達感謝之意。首先最重要的，我必須感謝我的指導教授陳紹基老師。在兩年內，老師在研究方法，專業探討，以及處事態度上給我許多建言，在此深深向老師致謝。作論文的這段時間內，實驗室同學承穎，世民給了我許多有形無形的幫助；佳旻，元志和觀易在口試前的這段時間給了我很多建議以及協助，並且在論文的用詞遣字字上提供建言；另外感謝特別曲建全學長兩年來的照顧，教導我許多研究以外的事情。雅娣在這段時間中除了在寫作上給予很多專業建議外，在我陷入低潮的時候也花許多時間為我分擔煩惱，是這段忙碌時期的一盞引路燈。我也要感謝我的家人，除了讓我在物質生活上不需煩憂，能夠專心求學外，也時常給我很多必要的建言。更重要的是感謝父母給予我生命以及心靈，使我有機會體驗這個世界的驚喜。

　　我算不上是一個創造論者，但倘若這充滿難解矛盾以及神秘美感的世界真是由造物主所創生的，在此對其致上謝意。

Content

List of Tables

List of Figures

Chapter 1
Introduction

MIMO transmission techniques have attracted much attention, since a few years ago. For recent communication system, the desire for high efficiency wireless communication is exploding due to the high demand and high bit-rate telecommunication. To serve these new applications of wireless communication, video on demand (VoD), and etc, IEEE starts to establish new standards that adopt MIMO techniques. One of the most significant standards is WMAN 802.16a with space-time coding, and another is WLAN 802.11n, which is a performance-enhanced version of 802.11a. Both two standards adopt MIMO techniques to achieve higher bandwidth efficiency.

Combined with MIMO technique, space-time coding is a typical method for enhancing transmitter diversity. It is a special arrangement of data in both spatial and time domains. There are two typical kinds of space-time coding in recent research [1,2]. There are space-time block coding (STBC) and space-time trellis coding (STTC). STBC is popular in present MIMO systems due to simple involved encoding and decoding processes. For this reason, only STBC is considered in this thesis. STBC can be only used in flat fading systems. However, this problem is much reduced in STBC-OFDM systems.

While STBC-OFDM system is used, channel estimation techniques are very important. To solve space-time coded data, accurate channel state information is required. Compared to conventional SISO OFDM systems, the estimations in MIMO systems are more difficulty due to transmitter diversity. Several types of pilot

arrangements are discussed in Chapter 4 to facilitate channel estimations. The pilot arrangement strategies and corresponding estimation methods are investigated in this thesis.

For the nature of wireless channels, there is non-sample spaced channel path delay and distorted aliasing effect in channel estimations. DCT-based channel estimators are applied to those conditions and reduce aliasing problem. Results show better performance than DFT-based channel estimators. The results of improvement in MIMO OFDM systems are also revealed in Chapter 5.

The thesis is organized as follows. In Chapter 2, the OFDM concepts are reviewed first. After that, a multipath fading channel simulator with spatial correlation is explored. Simulation data are shown to indicate that this simulator can generate channels with desired correlations. In Chapter 3, two standards 802.16a with STC and WWiSE proposal are introduced briefly. The baseband concepts and frame formats are the major focus in this chapter. Pilot arrangement strategies and estimation methods are introduced in Chapter 4. In this chapter, a simple method to detect length of channel is proposed. This additional channel information can aid the LS estimator for all-pilot MIMO preamble. Besides, a decision-direct channel tracking skill is applied to the STBC preamble system to enhance its performance. After that, Matlab simulations are shown in Chapter 5 for the evaluation of the algorithms mentioned in Chapter 4. At last, briefly conclusion and future works are presented in Chapter 6.

Chapter 2
Fundamentals of MIMO OFDM
Systems

Orthogonal Frequency Division Multiplexing (OFDM) is an important communication technique adopted by many modern wireless and wired communication systems, such as IEEE 802.11 a/g, IEEE 802.16a, ADSL, and VDSL system (also known as Discrete Multi-Tone Modulation, DMT in wired system). In traditional communication systems, modulation skills applied to single carrier lead to limited performance. By utilizing multiple-carrier transmitting, data can be sent at the same time on different isolated bands. In 1966, a new idea was proposed by Chang [3] that uses Frequency Division Multiplexing (FDM) to transmit data on non-overlapping subchannels, which experiences less inter-channel interference (ICI) and inter-symbol interference (ISI) under band-limited channel condition. The idea of OFDM became practical in 1971. Weinstein proposed a DFT-based architecture to implement OFDM system [4]. The demand for multiple oscillators to generate multiple carrier frequencies was replaced by a baseband DFT processor, which can be implemented easily by FFT algorithms.

2.1 OFDM System Model

In this section, we will introduce an overview of mathematical expression of SISO OFDM before we start the studies on MIMO OFDM. Both continuous-time model and discrete-time model will be explored in this thesis. After this introduction,

we will further discuss some design issues and transmission environment of wireless radio channel.

2.1.1 Continuous and Discrete-Time Models of OFDM Systems

In this section, the system model of a typical OFDM system will be investigated. In OFDM transmitter, the raw data stream is spilt into N data sub-streams before IFFT. After IFFT, the parallel output data will be sent in serial via radio channel. In receiver, the data will be detected on each sub-channel after FFT operations, and then the parallel output data are converted into serial again. In this way, the original data can be reconstructed. In our discussion, only the baseband DSP skills are concerned. In Figure 2.1(a), the architecture of OFDM modulation is exhibited. The raw data are separated into N sub-streams, and then each sub-stream is loaded to corresponding subcarrier produced by N independent oscillators. In Figure 2.1(b), the OFDM receiver architecture is shown. In this architecture, N matched filters are used to detect all symbols on each subcarrier. Figure 2.2 shows the spectrum plot of OFDM system, and the property of high bandwidth efficiency in OFDM system is illustrated.

$$\Phi_k(t) = \begin{cases} e^{\frac{j2\pi(k-1)(t-T_g)}{T}} & 0 \le t \le T_s \\ 0 & otherwise \end{cases}$$
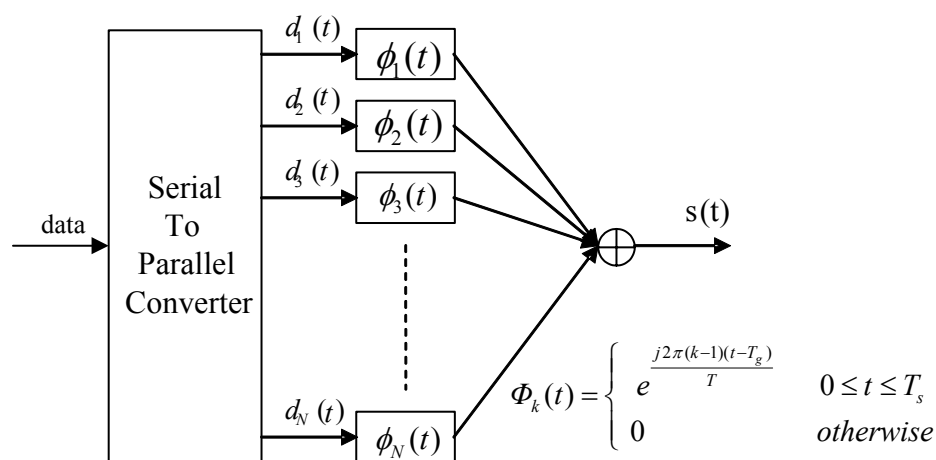
Figure 2.1(a) Continuous model of OFDM modulator

$$\Psi_k(t) = \begin{cases} \dfrac{1}{T} e^{\frac{j2\pi(k-1)t}{T}} = \dfrac{1}{T} \Phi_k^{\ *}(T_s - t) & 0 \le t \le T \\ 0 & otherwise \end{cases}$$
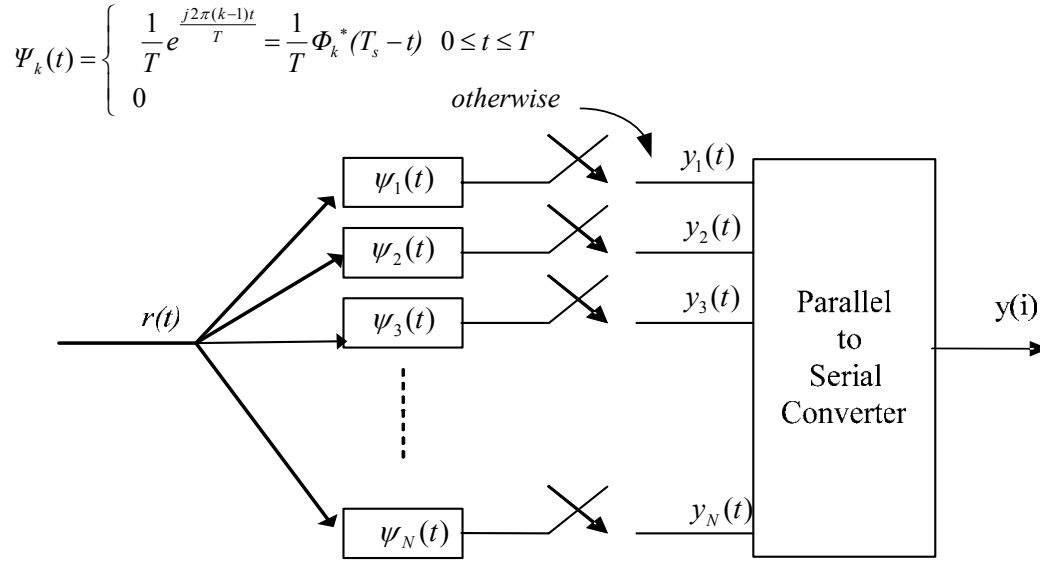
Figure 2.1(b) Continuous model of OFDM demodulator
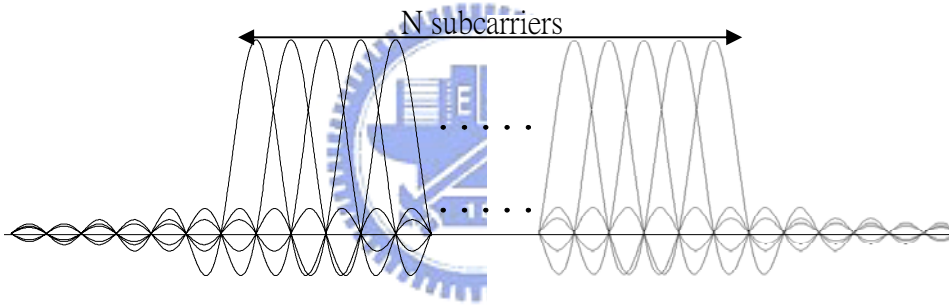
Figure 2.2 Spectrum of a single OFDM symbol

In [4], Weinstein suggested that OFDM modulation can be realized by IDFT / DFT in baseband processing. The concept can be expressed in the equations (2.1) and (2.2).

$$s(i) = \sum_{k=0}^{N-1} d(k) e^{j\frac{2\pi}{N}ki} \tag{2.1}$$

$$y(i) = \sum_{k=0}^{N-1} r(k) e^{-j\frac{2\pi}{N}ki} \tag{2.2}$$

The operations of OFDM modulation and demodulation are just identical to IDFT / DFT operations, and therefore FFT algorithm can be applied to simplify OFDM system.
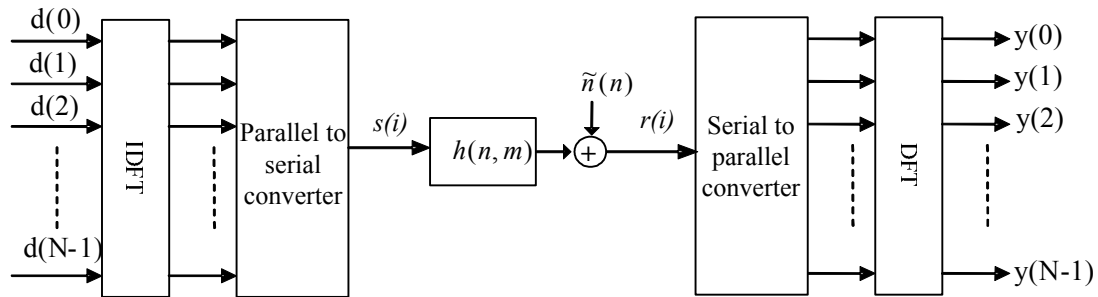
Figure 2.3 Discrete system model of OFDM system

2.1.2 The Concept of Guard Interval and Cyclic Prefix

In a high throughput OFDM wireless communication system, reduction efficiency of ISI and ICI is highly dependent on OFDM symbol formats. In ideal transmission environments, data symbols are delivered directly to the receiver via radio channel. However, the nature of the physical channel, such as reflection, diffraction, and interference will make the scenario much more complicated. In Figure 2.4, we can see how multi-path effect causes ISI in a communication system. An intuitive solution to reduce ISI is to add a null guard interval (GI) in front of each symbol. However, it would bring overhead in transmission. In OFDM system, the data streams are separated into N subchannels (where N is the FFT length). If the same transmission rate as that of single carrier system is assumed, the processed transmission rate on each subcarrier is 1/N that of the single carrier system and ISI effect can be reduced because the OFDM symbol length is N times that of the single carrier symbol.

ISI effect
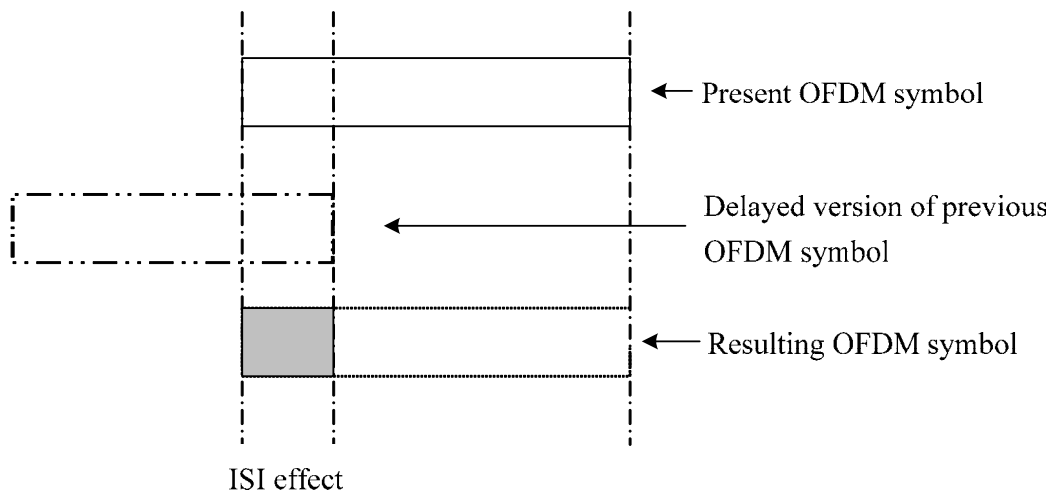
Figure 2.4 Inter-symbol-interference of wireless propagation

Although the OFDM system uses multiple orthogonal carriers to modulate all the data stream, null guard intervals will destroy the ideal orthogonal property within the symbol duration. In [5], Peled and Ruiz proposed a method of cyclic prefix (CP) to combat ICI in this case. Figure 2.5 illustrates concept of CP. It is a duplicated tail of the combined multicarrier symbol, and it is placed right in front of the OFDM symbol. This kind of guard band can avoid discontinuity in a single OFDM symbol, which will introduce severely ICI. If the length of CP is larger than the time dispersive channel, it can eliminate ISI effect as well as ICI.
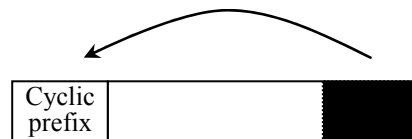
Figure 2.5 Cyclic prefix of an OFDM symbol

2.1.3 The Properties of Transmission Channels in Wireless Communication

Compared with relative static channels in wired transmission systems, channel characteristic of wireless transmissions are more complicated. In a wireless transmission environment, obstacles between the transmitter and receiver can result in reflections and diffractions, and these phenomenons bring multi-path effect, as discussed in section 2.1.2. When multi-path effect is observed from frequency domain, the delayed paths in time domain are transformed into different attenuation on each subcarrier. This is called frequency-selective channel for its varying gains on subcarriers. For a varying transmission medium, the characteristic of a radio channel is not always static. It changes across OFDM symbol sequences.

Two parameters are defined to measure variation [5] of the channel in both time and frequency domains.

Coherent bandwidth: This parameter is a criterion to tell if the channel is flat or frequency-selective in frequency domain. While the coherent bandwidth is larger than channel bandwidth, it means the flat region of radio channel is wide enough, and this channel is close to a flat one. Denser pilot subcarriers are usually required in preamble design if the channel is frequency selective. In [3], the coherent bandwidth is proportional to reciprocal of channel RMS delay spread, which can be found in typical industrial standards and technical reports.

Coherent time: The response of radio channel is time-variant if transmitter and receiver are not relatively stationary or properties of the medium changes. Hence coherent time is defined to be a criterion of static duration of a radio channel. The value of coherent time is inversely proportional to the Doppler frequency defined

as $f_d = f_c \cdot \dfrac{V}{C}$, where f_c is center frequency of the concerned system, V is the relative speed between transmitter and receiver, and C is speed of light. The ratio of coherent time and symbol duration in wireless system is usually estimated. If coherent time is relative short compared with symbol time, the channel is considered fast changing in time domain. Then it is a fast fading channel. The channel condition can be categorized into several types according to coherent bandwidth and coherent time.

2.2 Studies and Simulations of MIMO Channels

Recently, some MIMO channel models are proposed for MIMO-OFDM systems, and for example, the channel conditions related to 802.11n standard. Most of those channel models are based on a conventional fading channel simulator, which is well known as the Jakes' model. This conventional model utilizes a few oscillators to model fading effect with multiple sinusoidal waves. However, there have been studies revealing some non-ideal properties of this model and try to compensate those non-ideal properties, because Jakes' model was proposed long time ago in 1974. For example, Jakes' model can not produce multiple uncorrelated channels easily, for its deterministic parameter settings. When a MIMO system is simulated, such drawbacks may be confusing. In [6,7], the problem is analyzed and a solution using additive initial phase is proposed.

2.2.1 Wireless MIMO Channel Simulators

To simulate wireless MIMO channels, there are several important parameters to consider [8], namely:

Spatial correlation coefficients: factor that decides the correlation between different antennas

Steering matrix: matrices composed of transmission gains between different antenna pairs

Power delay profiles: delayed impulses that define the multipath power of wireless channels

Fading Characteristics: characteristics that describe the time-varying properties of channels

The channel simulator mentioned in [8] is illustrated in Figure 2.6, and these parameters can be set according to some measurements of the physical channels. With such channel model, multiple fading channels with specific spatial correlation matrix can be simulated. Like conventional SISO system, a certain power delay profile can be applied to simulate a typical wireless channel, given a Doppler frequency. In [9], correlated channels can be derived from uncorrelated channels with some matrix mapping. The procedure can be explained as follows.

$$H(\tau) = \sum_{l=1}^{L} A_l \delta(\tau - \tau_l) \qquad \text{where } H \text{ is the steering matrix,}$$
$$\text{and } \tau_l \text{ is the tap delay of the channel} \qquad (2.3)$$

$$A_l = \begin{bmatrix} a_{11}^{(l)} & a_{12}^{(l)} & \cdots & a_{1N}^{(l)} \\ a_{21}^{(l)} & a_{22}^{(l)} & \cdots & a_{2N}^{(l)} \\ \vdots & \vdots & \ddots & \vdots \\ a_{M1}^{(l)} & a_{M2}^{(l)} & \cdots & a_{MN}^{(l)} \end{bmatrix} \quad (2.4)$$

where $a_{mn}^{(l)}$ is the complex transmission coefficient from antenna m to n.

Hence the relationship between received signal $y(t)$ and transmitted signal $s(t)$ can be expressed as.

$$y(t) = \int H(\tau)s(t-\tau)d\tau \quad (2.5)$$

$$s(t) = \int H^T(\tau)y(t-\tau)d\tau \quad (2.6)$$

And the averaged power of the transmission coefficient can be defined as

$$P_l = E\left\{ \left| a_{mn}^{(l)} \right|^2 \right\} \quad (2.7)$$

The correlation between Tx antennas can be formulated in such form as

$$\rho_{m_1 m_2}^{BS} = \left\langle \left| a_{m_1 n}^{(l)} \right|^2, \left| a_{m_2 n}^{(l)} \right|^2 \right\rangle \quad (2.8)$$

where $\langle a, b \rangle$ is the inner product of a and b.

And the correlation between Rx antennas can also be formulated as

$$\rho_{n_1 n_2}^{MS} = \left\langle \left| a_{mn_1}^{(l)} \right|^2, \left| a_{mn_2}^{(l)} \right|^2 \right\rangle \quad (2.9)$$

From these two correlation coefficients, correlation matrixes R_{BS} and R_{MS} can be defined as,

$$R_{BS} = \begin{bmatrix} \rho_{11}^{BS} & \rho_{12}^{BS} & \cdots & \rho_{1M}^{BS} \\ \rho_{21}^{BS} & \rho_{22}^{BS} & \cdots & \rho_{2M}^{BS} \\ \vdots & \vdots & & \vdots \\ \rho_{M1}^{BS} & \rho_{M2}^{BS} & \cdots & \rho_{MM}^{BS} \end{bmatrix}_{M \times M} \quad (2.10)$$

$$R_{MS} = \begin{bmatrix} \rho_{11}^{MS} & \rho_{12}^{MS} & \cdots & \rho_{1N}^{MS} \\ \rho_{21}^{MS} & \rho_{22}^{MS} & \cdots & \rho_{2N}^{MS} \\ \vdots & \vdots & & \vdots \\ \rho_{N1}^{MS} & \rho_{N2}^{MS} & \cdots & \rho_{NN}^{MS} \end{bmatrix}_{N \times N} \qquad (2.11)$$

Finally, one can define

$$\rho_{n_2 m_2}^{n_1 m_1} = \left\langle \left| a_{m_2 n_1}^{(l)} \right|^2, \left| a_{m_2 n_2}^{(l)} \right|^2 \right\rangle \qquad (2.12)$$

$$\rho_{n_2 m_2}^{n_1 m_1} = \rho_{n_1 n_2}^{MS} \rho_{m_1 m_2}^{BS} \qquad (2.13)$$

To generate a set of correlated vectors, the method in [10] can be applied. Assume $x_1, x_2 \ldots x_N$ are independent vector elements, and a certain desired correlated vector Y composed of $y_1, y_2, \ldots, y_N$ can be generated in the following way:

$$y_1 = c_{11}x_1 + c_{12}x_2 + \ldots + c_{1N}x_N$$
$$y_2 = c_{21}x_1 + c_{22}x_2 + \ldots + c_{2N}x_N$$
$$\vdots \qquad\qquad\qquad\qquad (2.14)$$
$$y_N = c_{N1}x_1 + c_{N2}x_2 + \ldots + c_{NN}x_N$$

It can be expressed in the following matrix form

$$Y = CX, \qquad (2.15)$$

where C is the square root of the desired correlation matrix Γ and

$$\Gamma = CC^T \qquad (2.16)$$

And Γ is derived from the correlation matrices of R_{BS} and R_{MS}

$$\Gamma = R_{BS} \otimes R_{MS} \qquad (2.17)$$

where $\otimes$ is the Kronecker product of two matrices

To generate correlated fading channels, the mentioned skill can be applied to a set of uncorrelated fading channels, that is

$$\widetilde{A}_l = \sqrt{P_l} Ca_l \qquad (2.18)$$

$$\tilde{A}_l = \begin{bmatrix} \tilde{a}_{11}^{(l)} \\ \tilde{a}_{21}^{(l)} \\ \vdots \\ \tilde{a}_{M1}^{(l)} \\ \tilde{a}_{12}^{(l)} \\ \tilde{a}_{22}^{(l)} \\ \vdots \\ \tilde{a}_{M1}^{(l)} \\ \tilde{a}_{13}^{(l)} \\ \vdots \\ \tilde{a}_{MN}^{(l)} \end{bmatrix}_{MN \times 1} \qquad a_l = \begin{bmatrix} a_1^{(l)} \\ a_2^{(l)} \\ a_3^{(l)} \\ \vdots \\ a_{MN}^{(l)} \end{bmatrix}_{MN \times 1} \qquad (2.19)$$

where a_l is a vector with $M \times N$ uncorrelated fading elements. The simulator structure proposed in [9] is illustrated in Figure 2.6. First the target simulation environment is decided. Next, the simulation parameters are set according to the chosen environment. From the desired parameters, the spatial correlation matrix, the power delay profile and the Doppler shift can also be chosen properly. Note that in Figure 2.6(a), s(t) and y(t) are transmitting and received signals in MIMO systems.

(a)

(b)
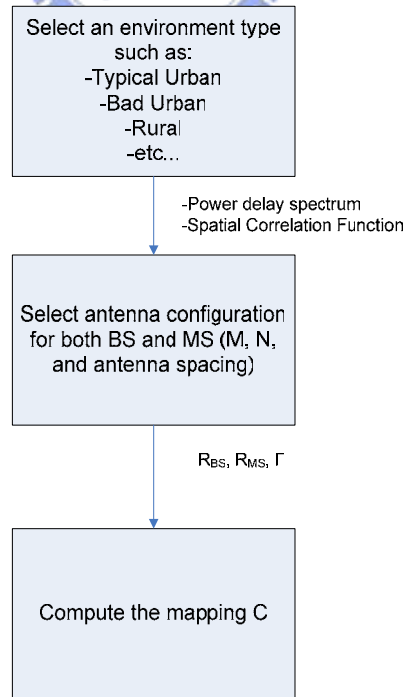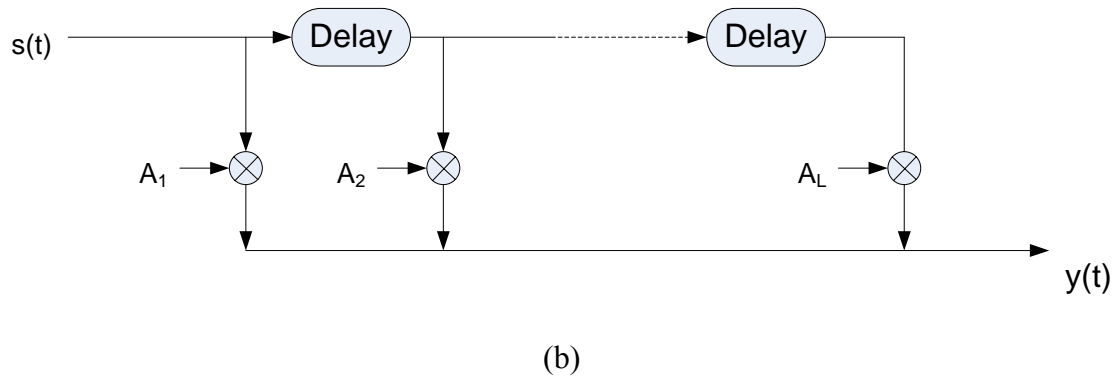
Figure 2.6 Simulator structure diagram for generating spatial correlated fading

model (a) simulator flow diagram (b) signal flow diagram

2.2.2 Studies and Simulation Results

Our Matlab simulation flow is shown in Figure 2.7. First of all, a single fading channel is constructed based on Jakes' model. After that, spatial correlation property is added to the channel simulator. At last, the channel response is produced by this MIMO channel simulator.
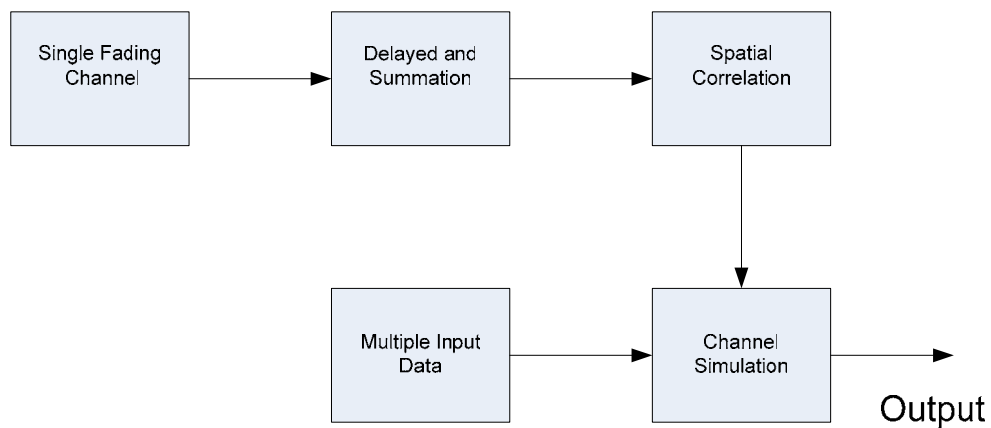
Figure 2.7 Simulation flow of the adopted MIMO channel simulator
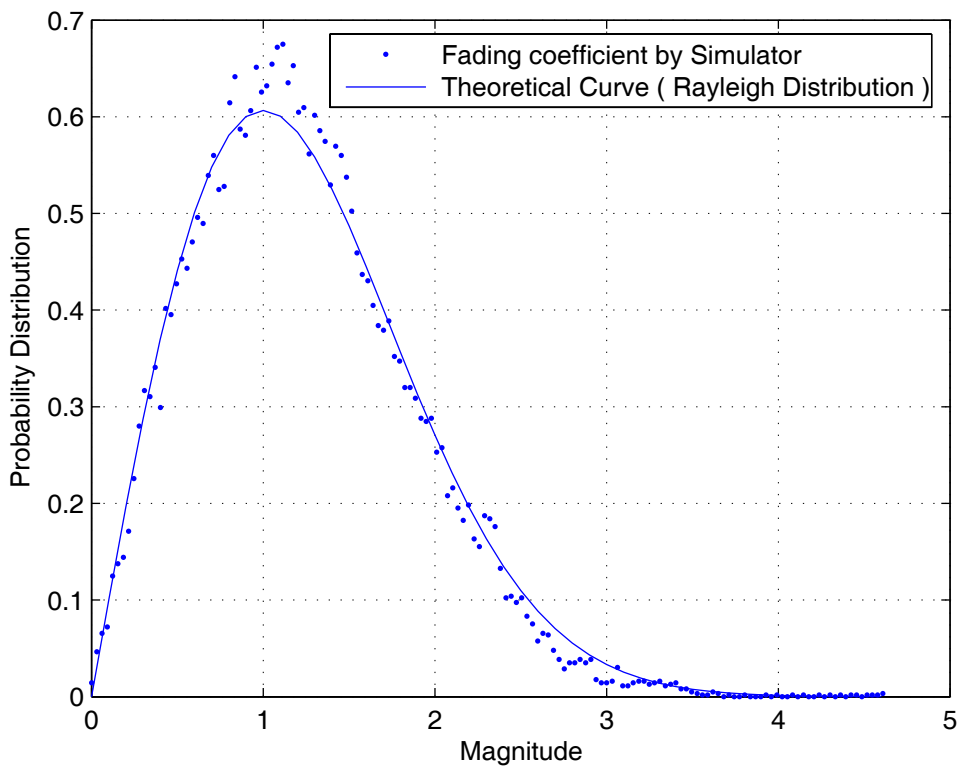
Figure 2.8 Magnitude distribution of four correlated fading channels

In the simulation, it shows that Jakes' model can model the Rayleigh fading channel precisely. The distribution of amplitude fits Rayleigh distribution and the phase variation is also uniformly distributed. In Figure 2.8 and 2.9, it can be observed that the distributions of magnitude and phase are close to the theoretical curve.
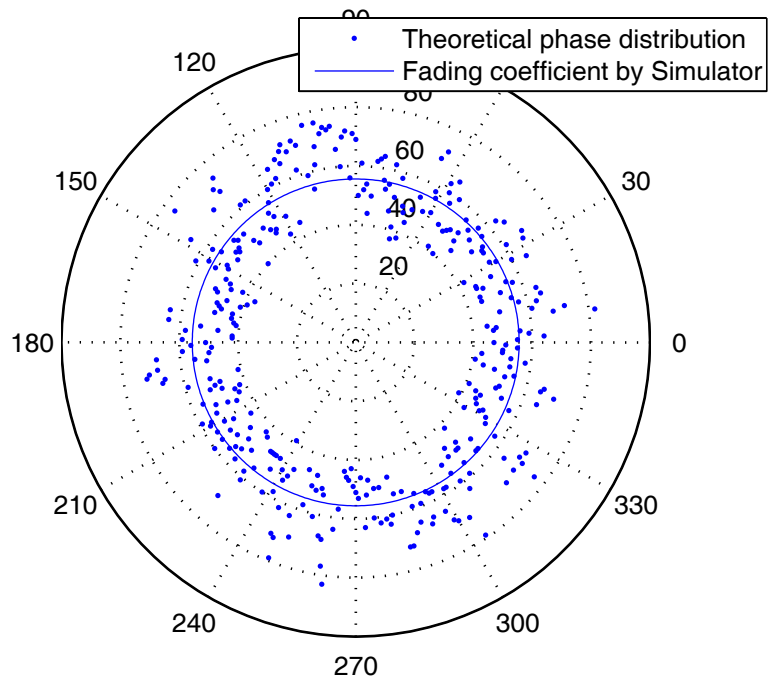
Figure 2.9 Phase distribution of four correlated fading channels (polar plot)

To verify the spatial correlation property, a 4 by 4 correlation matrix (as listed in Table 2.1) is selected to be target correlation matrix as an example.

Table 2.1 Desired spatial correlation matrix of the channel simulator

	Channel 1	Channel 2	Channel 3	Channel 4
Channel 1	1	0.3	0.3	0.3
Channel 2	0.3	1	0.3	0.3
Channel 3	0.3	0.3	1	0.3
Channel 4	0.3	0.3	0.3	1

Table 2.2 Resulting spatial correlation matrix of the channel simulator

	Channel 1	Channel 2	Channel 3	Channel 4
Channel 1	1	0.324	0.2655	0.2863
Channel 2	0.324	1	0.2898	0.2436
Channel 3	0.2655	0.2898	1	0.2831
Channel 4	0.2863	0.2436	0.2831	1

In the simulation, the resulting correlation matrix (as listed in Table 2.2) approximates to the desired matrix. This method can model the spatial correlation well. If we can adjust the number of oscillator in the Jakes' model, the matrix can be more precise, but it will take more computation time (i.e., take more iterations for simulation).

Chapter 3
Standards of IEEE 802.11n (WWiSE)
and IEEE 802.16a

For the rapid increase of broadband wireless communication, MIMO techniques are integrated into communication system to enhance system performance. However, the adoption of MIMO OFDM architectures may cause some difficulties in synchronization and channel equalization. For this reason, some efficient channel estimation schemes must be studied. Since a few years ago, some new communication standards have been discussed in the forums held by global engineering society, such as IEEE. One of them is MIMO 802.11n, which is a performance-enhanced version of 802.11-series standards. Another standard is 802.16a for wireless metropolitan area network (Wireless MAN). It also defines a specific optional mode with space-time block coding (STBC). In this chapter, we will make a simple introduction for both existing industrial standards with MIMO OFDM architectures.

3.1 IEEE 802.16a standard

The first version of P802.16a draft was issued on 30 November 2001. The last version of draft P802.16/D7 (draft version 7) was issued on 11 December 2002. The formal document of IEEE 802.16a (also known as WinMax) was approved as an IEEE standard on 29 January 2003 by IEEE Standard Association. The standard is developed by IEEE 802.16 Working Group and then the IEEE 802 Executive Committee. IEEE 802.16a focuses on the application of wireless metropolitan area,

network (Wireless MAN). This application may replace present 'last mile' technology between users' terminals and Internet service providers (ISP). Wireless MAN may be a threatening competitor against wired communication technologies, such as ADSL or VDSL. We will introduce main features of 802.16a in the following subsections.

802.16a defines three system modes: single carrier (SC), OFDM, and OFDMA. Each mode corresponds to different applications. OFDMA mode with space-time coding will be focused in this thesis. Table 3.1 shows the key baseband parameters of 802.16a-2003 standards. Some common abbreviations and expressions of 802.16a OFDMA PHY standard are listed below before introducing technical detail for conciseness.

(1) SS (subscriber station): usually known as user station or mobile stations.

(2) BS (base station): equipment sets providing connectivity, management, and control of subscriber stations.

(3) MAC (media access control): used to control system access and provides links of data from upper layer (data link layer) and lower layer (physical layer).

(4) PHY (physical layer): handles the data transmission and may include use of multiple transmission technologies, each appropriate to a certain frequency and application.

(7) TDD (time division duplexing): a single channel is used for both upstream and downstream transmission, but at different time.

(8) FDD (frequency division duplexing): requires two different channel pairs, one for upstream and another for downstream data transmission.

(9) STC (space-time coding): a coding skill applied on spatial and time domains

Table 3.1 Main baseband features of 802.16a-2003

Band Allocation	2-11Ghz
Throughput	1.0-75.0Mbps
Coverage range	Most 32km,(6-9km is a typical range)
Mobility	Fixed
Channel model	nLOS
Bandwidth	1.25-20Mhz
PHY	SCa, OFDM,OFDMA

3.1.1 802.16a OFDMA Frame and Symbol Structures

The adopted duplexing methods are either FDD or TDD. The frame structures are different in these two duplexing methods. In license-exempt bands, the duplexing method is defined as TDD, which will be described in the following part. A typical OFDMA TDD time frame is shown in Figure 3.1. We can see that the DL and UL bursts are inserted into different time slots on all the subchannels. Between DL and UL bursts, narrow time gaps are inserted to protect different bursts from inter-frame interference. The time gaps are named as Tx/Rx transition gap (TTG) and Rx/Tx transition gap (RTG). The receivers at BS and SS should detect the beginnings of their corresponding bursts, and then start other following detection steps.
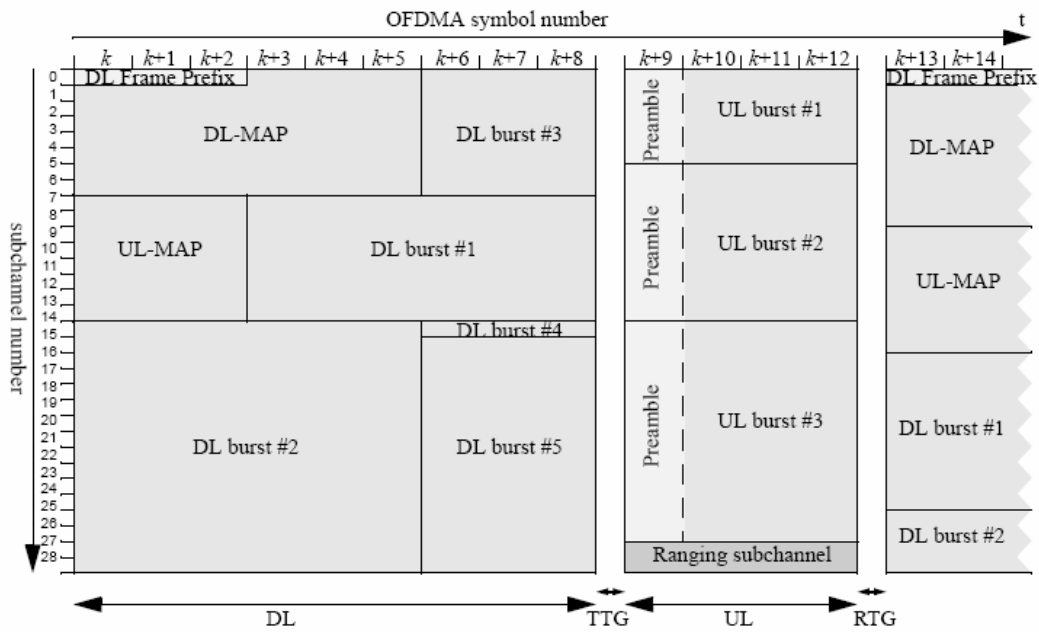
Figure 3.1 Frame structure of 802.16a OFDMA [11]

As described in Chapter 2 and Figure 3.2, a symbol (T_s) of 802.16a is composed of useful symbol (T_b) and guard interval (GI). The purpose of GI is to reserve orthogonality of each subcarrier, as we have described in Chapter 2.
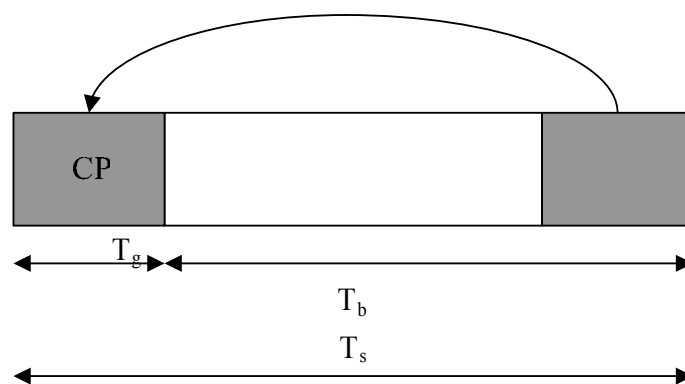
Figure 3.2 Time-domain structure of a 802.16a symbol

In frequency domain, all the subcarriers are either data carriers, pilot carriers, or guard band carriers. The purpose of guard band carriers are to avoid interference from other radiation sources or communication systems located at nearby bands, and the pilot carriers are for channel estimation or other tracking procedures. The data carriers are grouped into several subchannels, and data streams from different SS may transmit on different subchannels. The frequency domain description is shown in Figure 3.3.
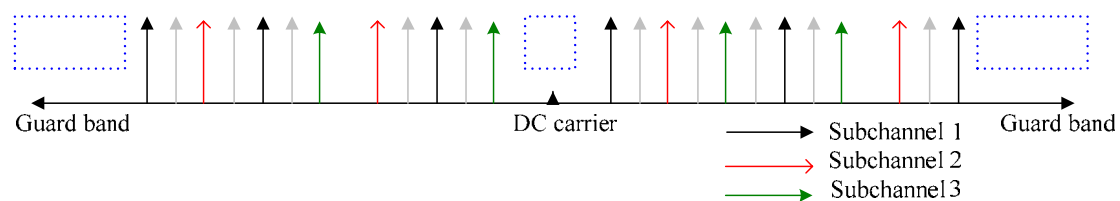
Figure 3.3 802.16a symbol frequency domain structure

3.1.2 802.16a OFDMA Carrier Allocation

In 802.16a OFDMA, the standard specifies the data tones and pilot tones in different ways for downlink and uplink. In general, an OFDMA symbol obtains a set of used subcarriers excluding DC subcarrier and guard band subcarriers. In both uplink and downlink, these used subcarriers are divided into data tones and pilot tones. However, the allocation of data and pilot tones is different in uplink and downlink. The main difference is that the pilot carriers are allocated first and then all the other data carriers are grouped into 32 subchannels in downlink, and the pilot carriers are allocated in each subchannel. But in uplink, each subchannel has its own set of pilot carriers. This allocation corresponds to the fact that BS broadcasts to all SS in the downlink transmission, and SS delivers data stream individually to BS in the uplink transmission. In this thesis, we will mainly discuss the design of channel estimation in DL.

In DL of 802.16a OFDMA, all of the subcarriers can be divided into pilot tones and data tones according to the different purpose in data transmission. The pilot tones can be categorized into fixed location pilots and variable location pilots. There are 32 fixed-location pilot in an OFDM symbol, and their exact positions are listed in the 14th row of Table 3.2. The allocations of DC subcarrier and guard band subcarriers are also listed in the first three rows of Table 3.2. These special tones are allocated at the same places in every OFDM symbol. However, there are many variable location pilots other than those fixed-location ones. These variable location pilots repeat with a period of four OFDM symbols. The placement of variable location pilots is decided by equation (3.1).

$$varLocPilot_k = 3L + 12P_k,$$
where
L is the offset that cycles through the values 0,1,2,3, periodically.
$$P_k \in \{0,1,2,\cdots141\}$$

(3.1)

The variable location pilots described in (3.1) are specially designed that the number of overall pilot tones are the same in every OFDM symbol even if there are variable location pilots coinciding with fixed location pilots. Additionally, there won't be all -pilot preamble in the DL OFDM symbols. Five 802.16a OFDMA DL symbols are illustrated in Figure 3.4 to show how these pilot tones are allocated, and the periodicity of variable pilots is also shown.
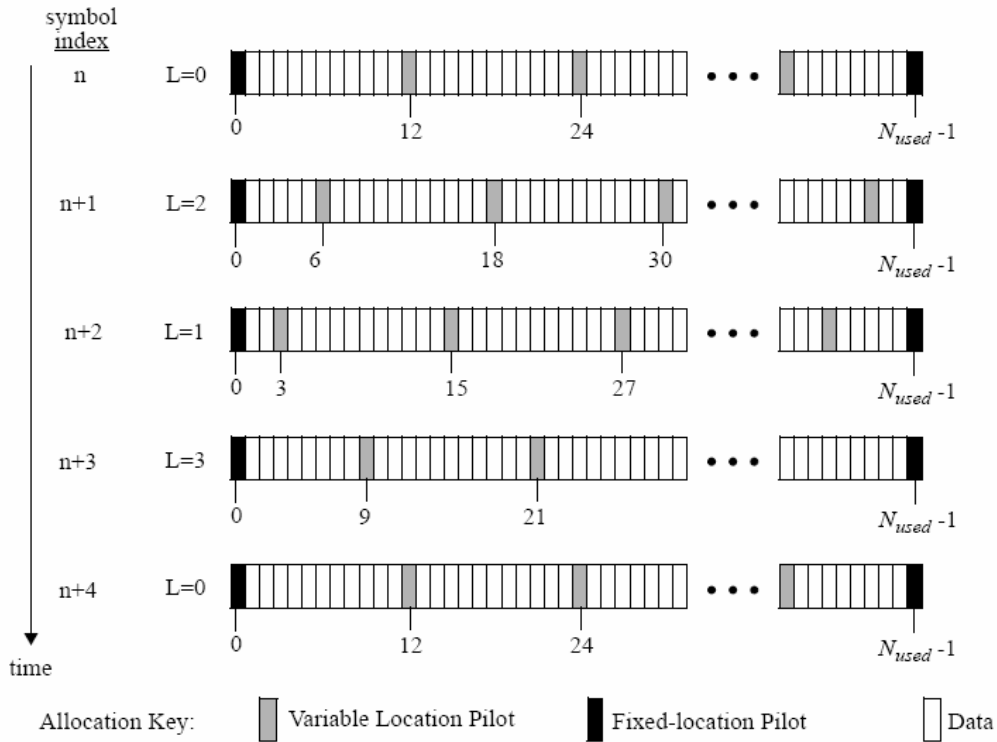
Figure 3.4 Carrier Allocation of DL 802.16a OFDMA [11]

Table 3.2 Detailed Carrier Allocation of DL 802.16a OFDMA [11]

Parameter	Value
Number of dc carriers	1
Number of guard carriers, left	173
Number of guard carriers, right	172
N_{used}, Number of used carriers	1702
Total number of carriers	2048
$N_{varLocPilots}$	142
Number of fixed-location pilots	32
Number of variable-location pilots which coincide with fixed-location pilots	8
Total number of pilots[a]	166
Number of data carriers	1536
$N_{subchannels}$	32
$N_{subcarriers}$	48
Number of data carriers per subchannel	48
BasicFixedLocationPilots	{0,39, 261, 330, 342, 351, 522, 636, 645, 651, 708, 726, 756, 792, 849, 855, 918, 1017, 1143, 1155, 1158, 1185, 1206, 1260, 1407, 1419,1428, 1461, 1530,1545, 1572, 1701}
$\{PermutationBase_0\}$	{3, 18, 2, 8, 16, 10, 11, 15, 26, 22, 6, 9, 27, 20, 25, 1, 29, 7, 21, 5, 28, 31, 23, 17, 4, 24, 0, 13, 12, 19, 14, 30}

3.1.3 802.16a OFDMA Space-Time Coding (STC)

In 802.16a standard, a simple scheme of transmitter diversity is defined as an optional mode. The special optional mode is mainly based on Alamouti's scheme [2]. In this optional mode, we assume that the number of antennas at BS is two and the number at SS is one. A simple illustration of BS and SS is shown in Figure 3.5. The process before TX diversity encoder is quite similar to the general mode configuration. However, after the diversity encoder, the new space-time code words are modulated by two independent IFFT processors. Once the transform is completed, the OFDM symbols are converted into analog signal, and then they will be transmitted on different antennas of BS. For this special transmission mode, BS will require extra hardware in its design. This modification is also shown in the upper part of Figure 3.5.

Table 3.3 Encoding pattern of 802.16a STC mode

	Antenna 0	Antenna 1
time t	S_0	S_1
time t+T	$-S_1^*$	S_0^*

Detailed encoding flow of Tx diversity encoder is described in Figure 3.6. The encoding procedures are applied to each subcarrier and both on space and time domains. Table 3.3 gives a clear description on this procedure.
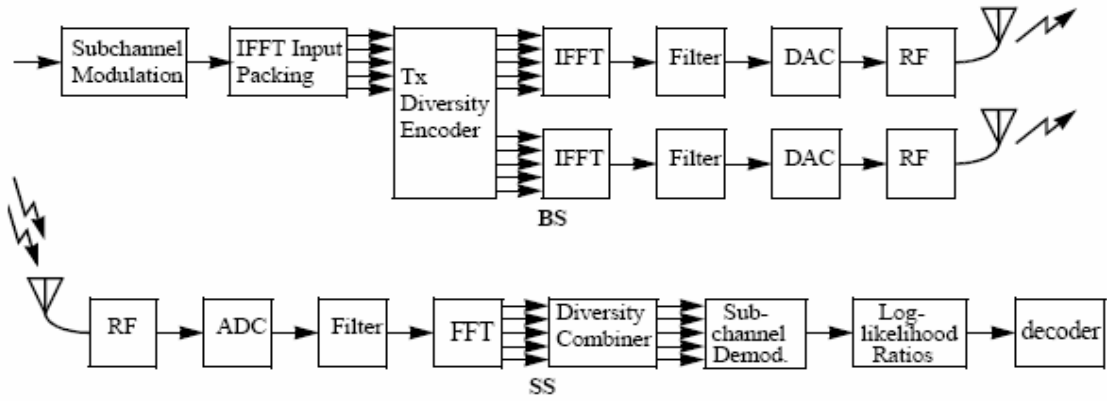
Figure 3.5 Tx/Rx architecture of 802.16a with STC [11]
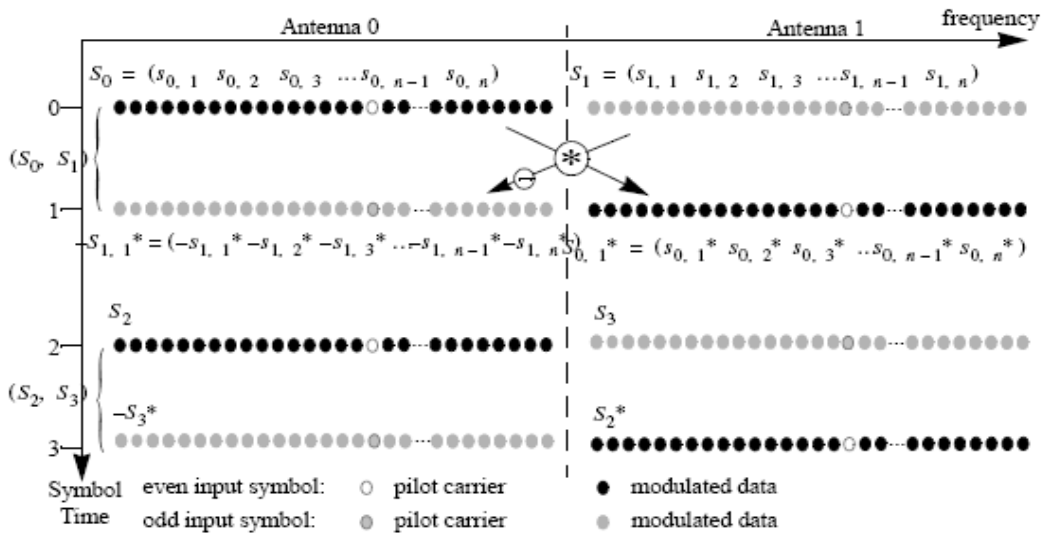
Figure 3.6 Transmitter symbol arrangement of 802.16a STC [11]

3.2 IEEE 802.11n WWiSE Proposal

According to WWiSE 802.11n proposal [12], the frame structure of this system is quite similiar to 802.11a system. The proposal keeps major features of 802.11a to sustain backward-compatibility to the legacy system. The frame structure of 802.11a will be explored, and then extended to WWiSE's proposed system.

3.2.1 Physical Layer Parameters of WWiSE

The system operates at 5 GHz license-free band, which has an advantage of large bandwidth for license-exempt usages. The system has a sampling rate of 20 MHz and FFT length of 64 points. A typical OFDM block duration consists of 80 samples. 64 samples of them are modulated data and 16 samples for guard interval, and their purposes have been introduced in 2.1.2 already. Among the total 64 subcarriers of an OFDM symbol, 12 tones on both sides of channel band are guard band to avoid interference to other nearby system. Besides 4 pilot tones, 48 subcarriers are used for data transmission. The main features of WWiSE physical layer are listed in Table 3.4.

Table 3.4 Main features of WWiSE baseband Mandatory Mode

Sampling rate	20MHz
Number of FFT points	64
Number of data subcarriers	48
Number of pilot subcarriers	4
Subcarrier spacing	0.3125 MHz (=20MHz/64)
OFDM symbol period	4μs (80 samples)
Cyclic prefix period	0.8μs (16 samples)
FFT symbol period	6.2μs (64 samples)
Modulation scheme	BPSK,QPSK,16QAM,64QAM
Short training sequence duration	8μs
Long training sequence duration	8μs
Long training symbol GI duration	1.6μs

3.2.2 Frame Structure of WWiSE Mandatory Mode

Figure 3.7 shows the basic structure of an 802.11a frame. A frame consists of three parts, which are Preamble, SIGNAL, and DATA, respectively. Preamble part is inserted into the frame to assist synchronization and channel estimation. SIGAL part contains the length, modulation type, ECC coding rate, and other information of following DATA part. The modulation of SIGNAL is fixed to BPSK, and the coding rate of convolution code is 1/2. DATA part is the main element of a whole frame and carries data from transmitter. This thesis will focus on channel estimation skills. Our studies will be concentrated on design of Preamble part.
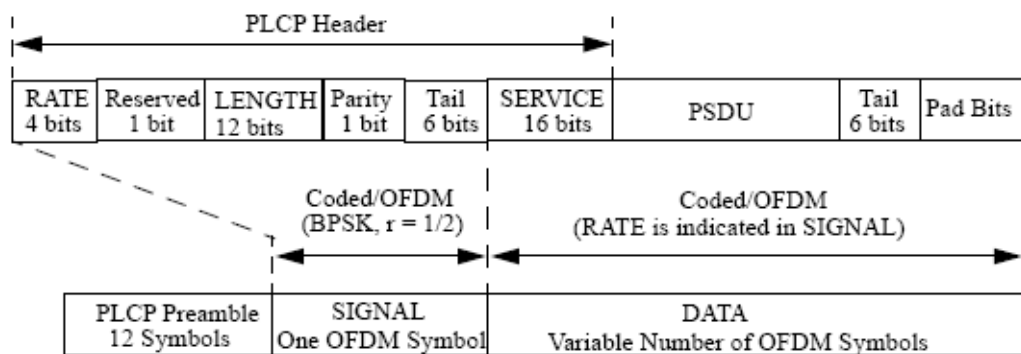
Figure 3.7 Frame structure of WWiSE 802.11n proposal [13]

In Figure 3.8, a clear illustration of 802.11a frame is shown. This figure shows two types of training field, the short training field (STF) and long training field (LTF). In the advice of IEEE standard [14], there are ten STFs for auto gain control (AGC), coarse frequency offset estimation, and timing synchronization. After these STFs, there are two LTFs for channel estimation. In Chapter 4, we will focus on the arrangement of LTFs to complete our channel estimation.
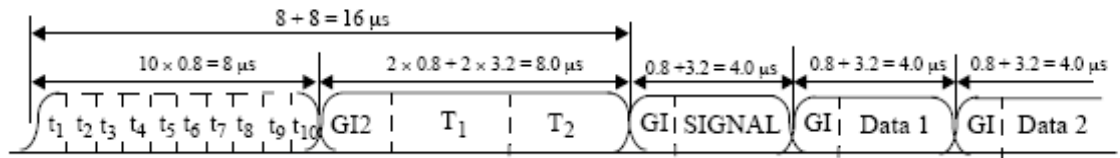
Figure 3.8 Detailed frame structure of 802.11n system [13]

In [12], WWiSE proposed a prototype system for 802.11n MIMO OFDM system based on 802.11a standard as we mentioned in this subsection. For example, if there are two transmitting antennas, training sequence of the first antenna is similar to 802.11a, and training sequence of the second antenna will be cyclic-shift version of the first antenna. This special structure is shown in Figure 3.9. Note that guard interval $GI2_1$ in this figure is cyclic-shift version (1600ns) of GI2. We can extend this case to four-antenna scenario as we show in Figure 3.10. The shift length is described in each field of this figure. In following discussion, the case of two antennas will be focused for simplicity consideration.
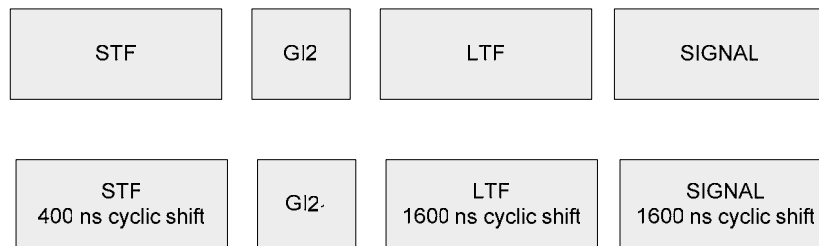
Figure 3.9 Frame structure of WWiSE system with two transmission antennas

[12]
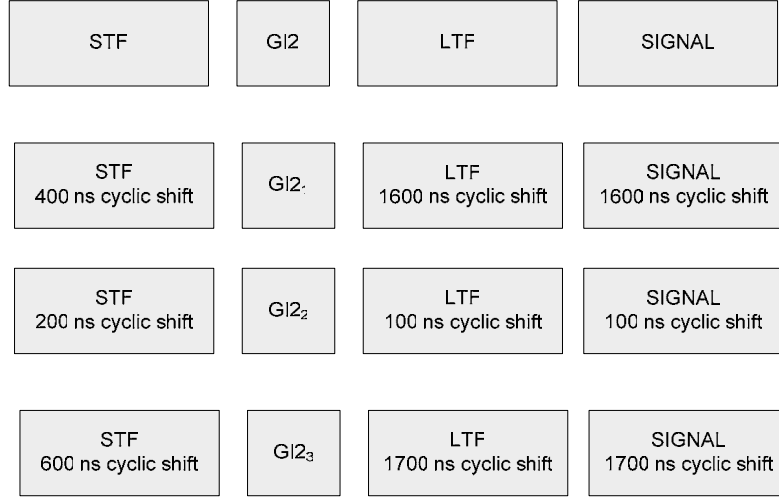
Figure 3.10 Frame structure of system WWiSE with four transmission antennas

[12]

3.2.3 The Code Structure of Space-time Block Code

From Table 3.3, the transmission model of space-time block code can be described in following equations. Assume the channel responses h_0 and h_1 are static in a STBC symbol (two consecutive OFDM symbols).

$$
\begin{aligned}
h_0(t) = h_0(t+T) = h_0 = \alpha_0 e^{j\theta_0} \\
h_1(t) = h_1(t+T) = h_1 = \alpha_1 e^{j\theta_1}
\end{aligned}
\tag{3.2}
$$

And the received signal r_0 and r_1 are

$$
\begin{aligned}
r_0 = r(t) = h_0 S_o + h_1 S_1 + v_0 \\
r_1 = r(t+T) = -h_0 S_1^* + h_1 S_0^* + v_1
\end{aligned}
\tag{3.3}
$$

Finally, we define the estimated signal $\hat{S}_0$ and $\hat{S}_1$ as

$$\hat{S}_0 = \frac{h_0^* r_0 + h_1 r_1^*}{|h_0|^2 + |h_1|^2}$$

$$\hat{S}_1 = \frac{h_1^* r_0 - h_0 r_1^*}{|h_0|^2 + |h_1|^2}$$

(3.4)

Substituting (3.2) to (3.4), we get

$$\hat{S}_0 = S_0 + \frac{h_0^* v_0 + h_1 v_1^*}{(\alpha_0^2 + \alpha_1^2)}$$

$$\hat{S}_1 = S_1 + \frac{-h_0 v_1^* + h_1^* v_0}{(\alpha_0^2 + \alpha_1^2)}$$

(3.5)

When the number of data streams is three and four, we use the following space-time block codes, H_3 and H_4, to encode the data. The decoders for H_3 and H_4 are derived in the Appendix of [14].

$$H_3 = \begin{pmatrix} S_1 & S_2 & \dfrac{S_3}{\sqrt{2}} \\ -S_2^* & S_1^* & \dfrac{S_3}{\sqrt{2}} \\ \dfrac{S_3^*}{\sqrt{2}} & \dfrac{S_3^*}{\sqrt{2}} & \dfrac{\left(-S_1 - S_1^* + S_2 - S_2^*\right)}{2} \\ \dfrac{S_3^*}{\sqrt{2}} & -\dfrac{S_3^*}{\sqrt{2}} & \dfrac{\left(S_2 + S_2^* + S_1 - S_1^*\right)}{2} \end{pmatrix}$$

(3.6)

$$H_4 = \begin{pmatrix} S_1 & S_2 & \dfrac{S_3}{\sqrt{2}} & \dfrac{S_3}{\sqrt{2}} \\ -S_2^* & S_1^* & \dfrac{S_3}{\sqrt{2}} & -\dfrac{S_3}{\sqrt{2}} \\ \dfrac{S_3^*}{\sqrt{2}} & \dfrac{S_3^*}{\sqrt{2}} & \dfrac{\left(-S_1 - S_1^* + S_2 - S_2^*\right)}{2} & \dfrac{\left(-S_2 - S_2^* + S_1 - S_1^*\right)}{2} \\ \dfrac{S_3^*}{\sqrt{2}} & -\dfrac{S_3^*}{\sqrt{2}} & \dfrac{\left(S_2 + S_2^* + S_1 - S_1^*\right)}{2} & -\dfrac{\left(S_1 + S_1^* + S_2 - S_2^*\right)}{2} \end{pmatrix}$$

(3.7)

Chapter 4
Channel Estimations for MIMO OFDM Systems

4.1 Preamble Design for MIMO OFDM Systems

In [15], several types of pilot arrangements are proposed for MIMO OFDM systems. In this thesis, three of them will be discussed. In this section, these pilot arrangement methods will be introduced briefly. The pilot arrangements concerned are all-pilot preamble, space-time coded preamble, and scattered preamble, respectively. The same spatial arrangement may combine different time-frequency preamble formats, such as block type (802.11n) and comb type (802.16a with STC). A simple category of pilot arrangement is shown in Figure 4.1. After a general study, channel estimation in both 802.11n and 802.16a systems will be discussed.
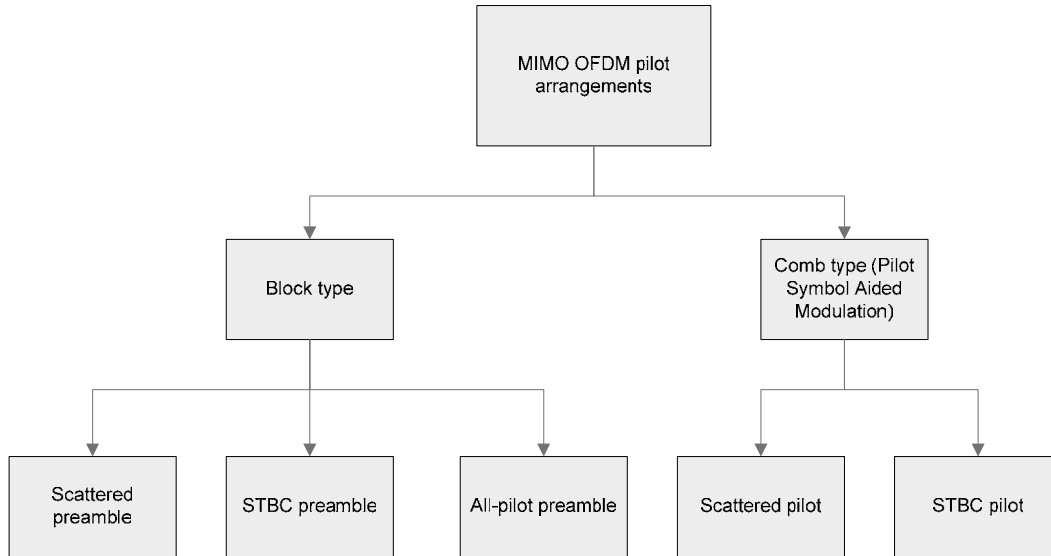
Figure 4.1 Classification of pilot arrangement in MIMO OFDM

4.1.1 Scattered Preamble

This preamble format is proposed in [15]. The scattered pilot preambles organize subcarriers in a single all-pilot-preamble symbol into several groups for different antennas. The transmission signal on each antenna can be expressed in the form of (4.1) and (4.2). The illustration of scattered preamble and data symbols is shown in Figure 4.2.

For pilot symbol assisted modulation (PSAM) OFDM symbol

$$
\begin{aligned}
X_1 &= (P \quad 0 \quad d \quad d \quad P \quad 0 \quad d \quad d \quad \cdots) \\
X_2 &= (0 \quad P \quad d \quad d \quad 0 \quad P \quad d \quad d \quad \cdots)
\end{aligned}
$$

(4.1)

where P is pilot tone and d is data tone

For block type OFDM preambles (802.11n-like)

$$
\begin{aligned}
X_1 &= (P \quad 0 \quad P \quad 0 \quad P \quad 0 \quad P \quad 0 \quad \cdots) \\
X_2 &= (0 \quad P \quad 0 \quad P \quad 0 \quad P \quad 0 \quad P \quad \cdots)
\end{aligned}
$$

(4.2)

34
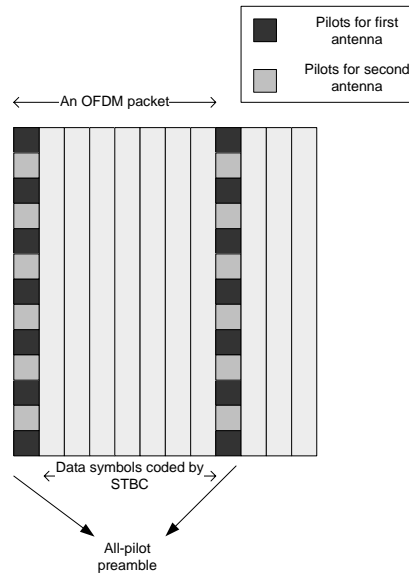
Figure 4.2 Frame structure of a 2x1 MIMO OFDM system with scattered pilot

4.1.2 Space-time Coded Preamble

According to [2], space-time block code (STBC) can be applied to MIMO system so that the diversity of multiple antenna systems can be utilized. If the transmitted symbols are known, one can obtain the channel response from space-time coded OFDM symbols. The transmission scheme of this space-time coded preamble is depicted in Figure 4.3, and it can be seen how channel estimator (for preambles) and combiner (for data symbols) work. Table 4.1 lists transmission sequence of the space-time symbols between two antennas, and Figure 4.4 shows total arrangement of a whole packet in this kind of pilot arrangement.
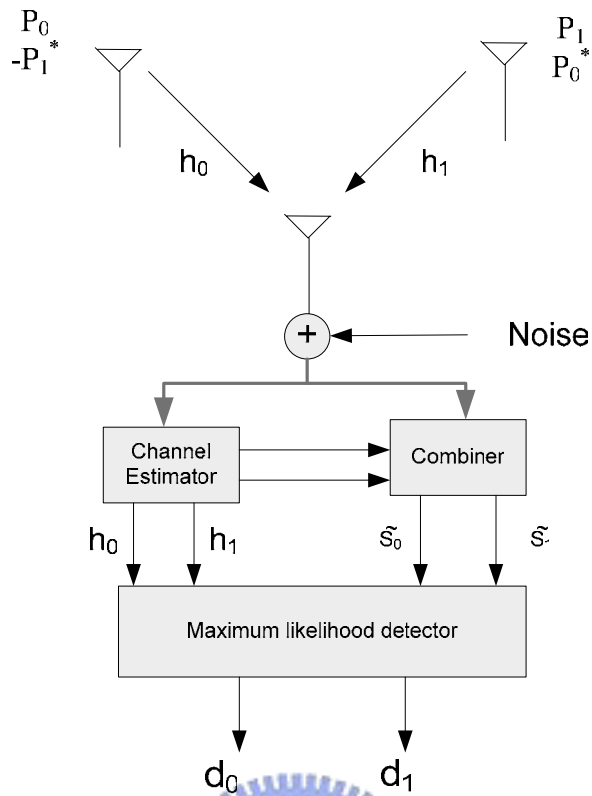
Figure 4.3 Receiving and decoding structure of a 2x1 space-time coded system
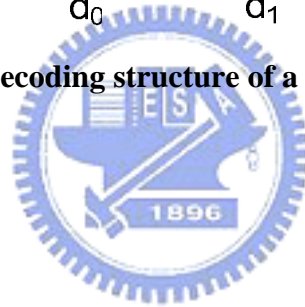
Table 4.1 Training symbol arrangement of space-time coded preamble

	Antenna 0	Antenna 1
time t	P_0	P_1
time t+T	$-P_1^*$	P_0^*

←——An OFDM packet——→

P_0 -P_1* P_0 -P_1*

P_1 P_0* P_1 P_0*

← Data symbols coded by → STBC

Space-time coded preable
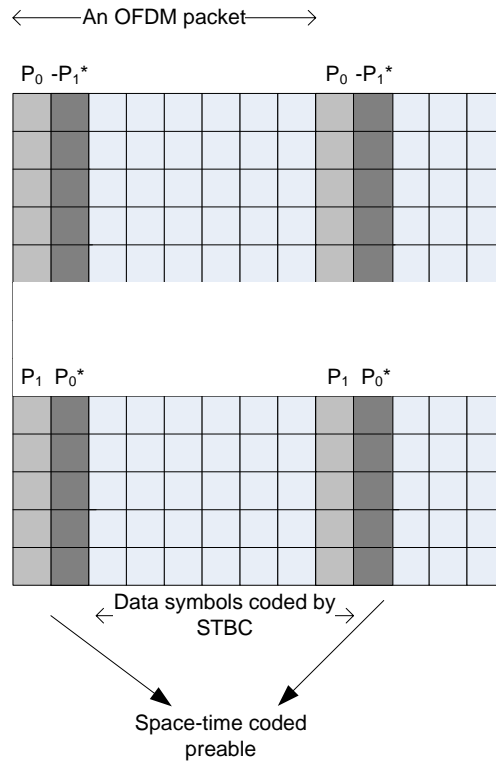
Figure 4.4 Frame structure a 2x1 MIMO OFDM system with space time coded pilot

4.1.3 All-pilot Preambles

In a SISO OFDM system with packet transmission, the all-pilot preambles are often used. As introduced in Section 3.2.2, 802.11a system adopts this frame structure to perform channel estimation with its LTF preambles. If 802.11n system is needed to backward-compatible to 802.11a, the 802.11n system must reserve the feature of all-pilot preambles. As explained in section 3.2.2, WWiSE uses cyclic-shift version of original LTF for antennas other than the first one. However, this structure may experience severely co-channel (CCI) effect because pilots from different antennas occupy the same tones at the same time. For scattered preambles and space-time coded preambles mentioned previously, this problem can be avoided by tone-interleaving skills and space time block coding. The issue of CCI cancellation will be discussed later in this chapter.

4.2 Channel Estimation Techniques for MIMO

OFDM System

In [16], the authors mainly introduce the methods to detect channel response on pilot tones based on LS and MMSE methods for SISO OFDM systems. For MIMO OFDM systems, the channel estimation problems may be more complicated. Due to the special structure of space-time coding and co-channel interference, some additional processing must be integrated into the MIMO OFDM system to solve these problems. In this section, we will study channel estimation methods for MIMO OFDM systems.
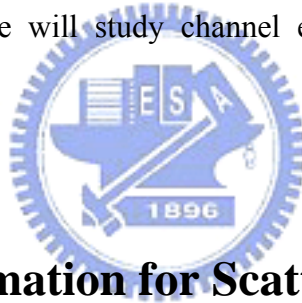
4.2.1 Channel Estimation for Scattered Preambles

Scattered preamble described in (4.2) is explored further here. To explain the estimation process, an example is given. The number of transmitter antennas is two, and the total amount of subcarriers in an OFDM symbol is 64. In this case, the frequency domain expression of two OFDM preambles P_1 and P_2 can be described by (4.3).

$$
\begin{aligned}
P_1 &= (P_0^1 \quad 0 \quad P_2^1 \quad 0 \quad P_4^1 \quad 0 \quad \cdots \quad P_{62}^1 \quad 0) \\
P_2 &= (0 \quad P_1^2 \quad 0 \quad P_3^2 \quad 0 \quad P_5^2 \quad \cdots \quad 0 \quad P_{63}^2)
\end{aligned}
\tag{4.3}
$$

P_k^m is the pilot symbol at tone k from the mth antenna

In preamble symbol which belongs to a transmission packet, the channel effect and additive white noise can be modeled as.
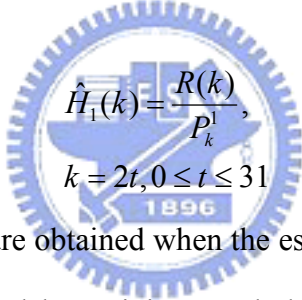
$$R(k) = \sum_{m=1}^{2} H_m(k) P_k^{m} + w(k)$$

$R(k)$ is the received symbol,

and $H_m(k)$ is the response at the kth tone from the mth antenna

(4.4)

Therefore, the received symbol vector R is

$$R = [H_1(0)P_0^1 \quad H_2(1)P_1^2 \quad H_1(2)P_2^1 \quad H_2(3)P_3^2 \quad \cdots \quad H_1(62)P_{62}^1 \quad H_2(63)P_{63}^2] \quad (4.5)$$

For H_1 estimation, the tones $R(0)$ $R(2)$ $\cdots$ $R(62)$ may be used for LS estimation. The general form of estimation is like (4.6). The result can be also applied to channel response for the second antenna, and the extension to more than two antennas is straightforward.

$$\hat{H}_1(k) = \frac{R(k)}{P_k^1},$$
$$k = 2t, 0 \le t \le 31$$

(4.6)

However, only half the tones are obtained when the estimation in (4.6) is applied. The response on the tones occupied by training symbol from another antenna must be derived with interpolation techniques. In following discussion, some popular interpolation techniques are considered.

4.2.1.1 Piecewise Linear Interpolation

Linear interpolation is quite simple and intuitive among all interpolation skills. The interpolation skills are based on linearity assumption of unknown subcarrier responses between known two known subcarrier intervals. If known subcarrier data is inserted for each M subcarrier, the segment length is M, and then subcarrier response interpolation in the mth segment can be obtained by

$$\hat{H}(mM+l) = \frac{M-l}{M}\hat{H}(mM) + \frac{l}{M}\hat{H}((m+1)M)\,, 0 < l < M \qquad (4.7)$$

4.2.1.2 SPLINE Interpolation
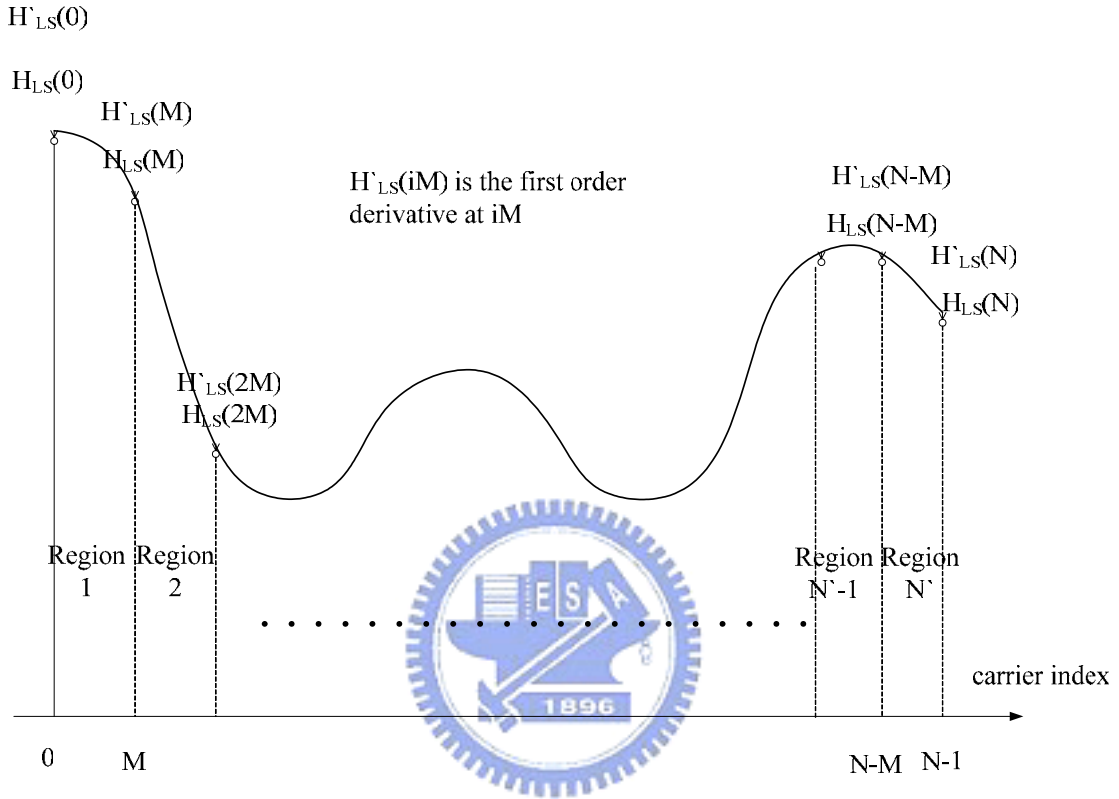
Figure 4.5 Illustration of channel segmentation and the required known

parameters for cubic spline interpolation

For generalization, specific-order spline functions can be derived such as the widely used cubic spline for channel interpolation. It is based on the third-order curve-fitting polynomial $Y_i = Ax_i^3 + Bx_i^2 + Cx_i + D$. Sufficient equations are required to solve this problem because there are total 4N' unknown variables. All the divisional polynomial coefficients are solved based on continuous assumption at the segment boundary, with the first and second derivative continuity of the pilot channel values on segment boundaries. Therefore, (2N')+(N'-1)+(N'-1) equations can be set

up from the constraints, with two more from the assumption of zero first order derivative value of the very first and last carrier channel value.

4.2.1.3 Transform-Domain Interpolation

DFT-based channel estimators have been proposed in [17,18]. These estimators are based on the techniques performed in transform domain to accomplish the estimation. Fast DFT algorithms can be utilized to reduce the transform complexity. In the following, we will describe this method in detail. The DFT-based channel estimator has a principal restriction on placement of pilot subcarriers. That is, pilot subcarriers must be equi-spaced along frequency direction. A typical pilot pattern is shown in Figure 4.6. As the figure describes, DFT estimator can be applied only when D_f is a constant. In such case, pilot tones can be viewed as a downsampled version of frequency response on all tones.
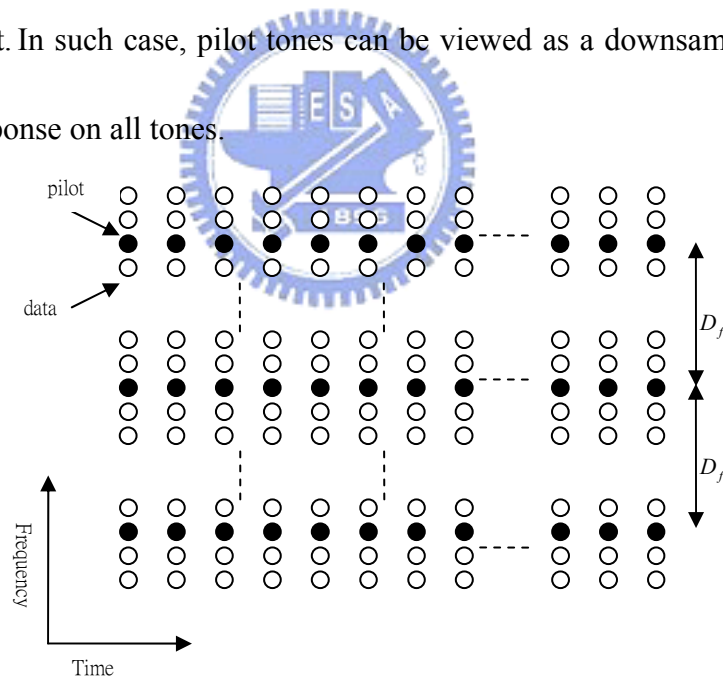
Figure 4.6 Regular pilot placement

When scattered pilots are used in MIMO OFDM, interpolations are needed to obtain channel response of interleaving tones for different antennas. In this case, transform domain methods are good choices because of the equi-spaced pilot tones in preambles.

We can find different channels between different antenna pairs with interpolation skills.

In this subsection, we will discuss non-sample spaced channel effect in general wireless channels. As mentioned in Chapter 2, radio channel impulse responses can be modeled as several delay paths with random distributed gain (usually Rayleigh distribution). However, delay intervals are always assumed to be sample spaced. In real transmission environment, this assumption is not true for most cases. In the following parts of this subsection, this effect will be explored while transform-domain interpolation methods are used in MIMO OFDM channel estimation.

According to [19], the continuous channel impulse response can be expressed in (4.8), where v is the total number of channel delay taps, and ε_l is delay time for each tap. In (4.9), the frequency domain response is obtained by DFT, where τ_l is the delay interval normalized to sampling period T_c. And T_c equals to T/N.

$$h(t) = \sum_{l=0}^{v-1} \alpha_l \delta(t - \varepsilon_l) \qquad (4.8)$$

$$H_{discrete}(k) = \sum_{l=0}^{v-1} \alpha_l e^{-j2\pi k \frac{\varepsilon_l}{NT_c}} = \sum_{l=0}^{v-1} \alpha_l e^{-j\frac{2\pi k \tau_l}{N}}$$
$$k = 0, 1, 2 \cdots, N-1 \qquad (4.9)$$
$$T_c \equiv sampling\ period$$

To obtain the equivalent discrete-time impulse response, IDFT is performed on $H_{discrete}(k)$.

$$h_{discrete}(n) = IDFT\{H_{discrete}(k)\}$$

$$= \frac{1}{N}\sum_{l=0}^{\nu-1}\alpha_l(iT_s)e^{-j\frac{\pi(n+(N-1)\tau_l)}{N}}\frac{\sin(\pi\tau_l)}{\sin(\pi(\tau_l-n)/N)}, \quad n=0,1,2,\cdots,N-1 \tag{4.10}$$

If the delay intervals are all sample-spaced, i.e. $\{\tau_l\}$ are all integers, $h_{discrete}(n)$ can be

simplified to

$$h_{discrete}(n) = \sum_{l=0}^{\nu-1}\alpha_l(iT_s)\delta(n-\tau_l), \quad n=0,1,2,\cdots,N-1 \tag{4.11}$$

Table 4.2 Channel parameters for indoor wireless channel (Model 1)

Tap No.	Delay (ns)	Delay (samples)	Power (dB)	Amplitude Distribution
1	0	0	0	Rayleigh
2	36	0.72	-5	Rayleigh
3	84	1.68	-13	Rayleigh
4	127	2.54	-19	Rayleigh

Table 4.3 Channel parameters for indoor wireless channel (Model 2)

Tap No.	Delay (ns)	Delay (samples)	Power (dB)	Amplitude Distribution
1	0	0	0	Rayleigh
2	176	3.52	-8	Rayleigh
3	274	5.48	-15	Rayleigh
4	560	11.2	-18	Rayleigh

According to (4.8)-(4.10), the continuous channel response and the discrete channel response can be both illustrated in Figure 4.7 and Figure 4.8. The channel model is cited from [20]. Model 1 is in the environment of typical office, and Model 2 is in an airport hall. In Figure 4.7 and Figure 4.8, one can see that the delay spread of Model 1 is smaller than Model 2, which means that the delay taps are more concentrated in Model 1 than in Model 2. By observing the impulse response plot in Figure 4.7, we can see the aliasing effect in 'high time' part due to non-sample spaced channel. However, this effect seems not very obviously in Model 2. To explain this effect, we may examine (4.8)-(4.10) to find the answer. If we check sinusoid ratio part in (4.10), it would become (4.12).

$$w(n) = \frac{1}{N} \times \frac{\sin(\pi \tau_l)}{\sin(\pi(\tau_l - n)/N)} \tag{4.12}$$

Equation (4.12) can be viewed as the gain of interference produced by other taps in continuous impulse response. It is plotted in Figure 4.9. Here, $\tau_l = 4.48$ and N=64 are chosen as an example. It can be seen that Model 2 has larger attenuations on the multipath taps other than the main path. Additionally, the multipath taps are located at loose positions, so that the introduced aliasing effect is smaller than in Model 1. Therefore the aliasing effect is not so significant in Model 2.
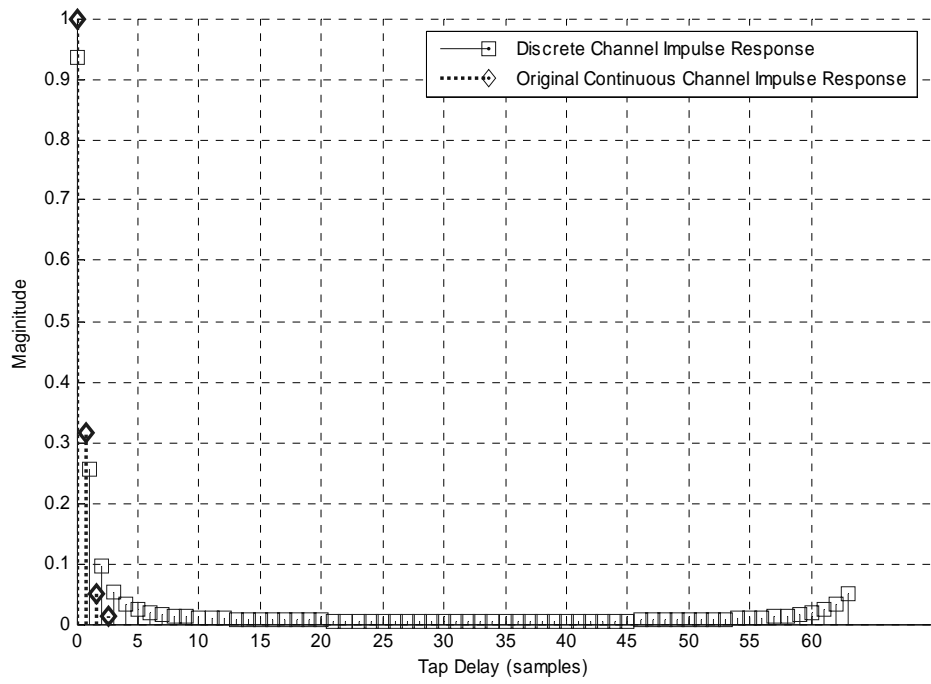
Figure 4.7 Continuous and discrete impulse responses of indoor model 1
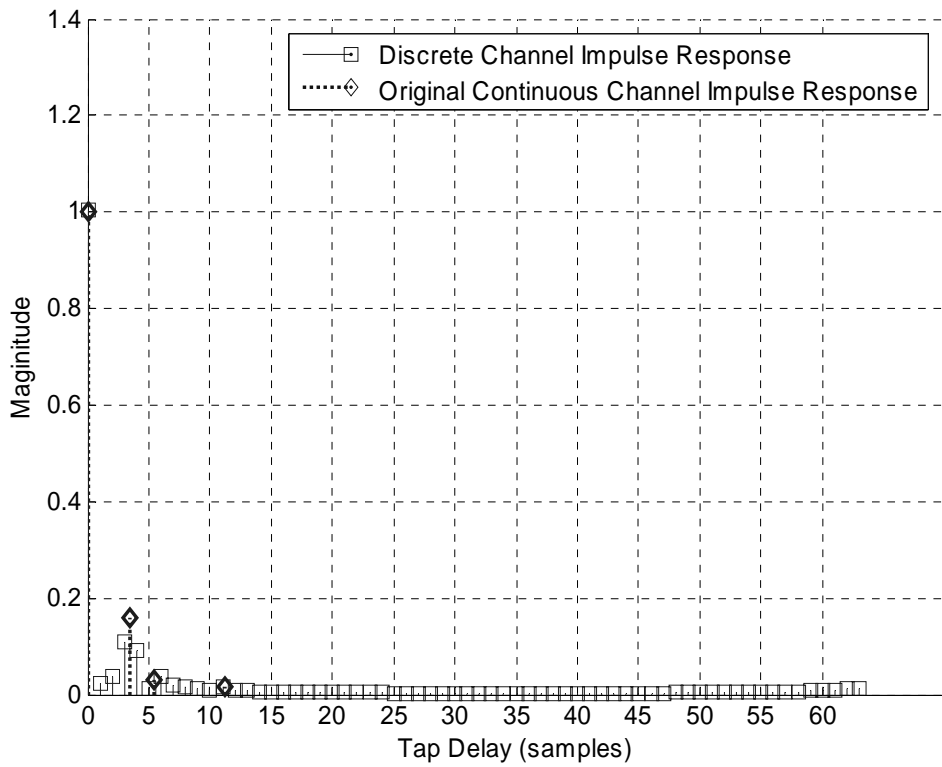
Figure 4.8 Continuous and discrete impulse responses of indoor model 2
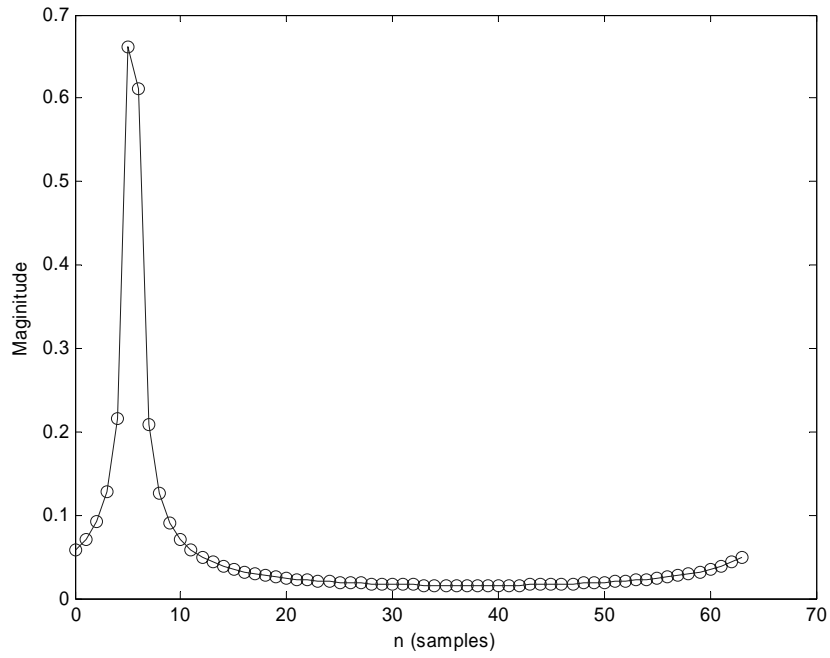
Figure4.9 Magnitude plot of tap weight of non-sample spaced channel
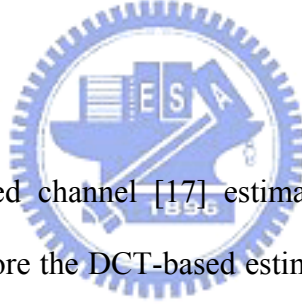
Unfortunately, DFT-based channel [17] estimator is sensitive to non-sample spaced channel effect. Therefore the DCT-based estimator [19] is applied to this kind of MIMO OFDM system to improve the performance of transform domain channel estimator. In remaining part of this subsection, we will explain how non-sample spaced effect impacts the performance of typical DFT-based estimator. After that, we will show how DCT-based channel estimator compensates this drawback.

The DFT-based estimator starts with Least Square estimation of channel frequency response at pilot subcarriers. The LS estimation is described by (4.13). We assume the maximum delay spread is $\tau_{max} T_c$ and Δ is the minimum integer that is larger than τ_{max}. Then we shift the channel impulse response by $-\Delta/2$ so that the

power of channel impulse response is centered around $n = 0$. The shift process can be carried out by phase rotation in the frequency domain, as shown by equation (4.14).

$$\hat{H}_p(k) = \frac{Y_p(k)}{P(k)} = H_p(k) + \frac{N_p(k)}{P(k)} = H_p(k) + \tilde{N}_p(k)$$

where $\hat{H}_p(k)$ isthe estimated response at k^{th} subcarrier,

$Y_p(k)$ is the received signal,   (4.13)

$P(k)$ is the pilot,

and $N_p(k)$ is noise

$$\hat{H}'_p(k) = \hat{H}_p(k) \times e^{j\pi\frac{\Delta k}{M}}$$

where M is the number of pilot tones $\qquad\qquad$ (4.14)

Next, M-point IDFT of $\hat{H}'_p(k)$ is performed

$$\hat{h}_p(n) = IDFT_k\{\hat{H}'_p(k)\} = \frac{1}{M}\sum_{k=0}^{M-1}\hat{H}'_p(k)e^{-j\frac{2\pi nk}{M}} \quad n = 0,1,2,\cdots,M-1 \quad (4.15)$$

By the concept of interpolation, the estimated channel impulse response is obtained by zero padding. To reduce the aliasing effect, zeros must be padded to the region with less power. Sine we have centered the power around $n = 0$, zeros are padded in the middle of $\{\hat{h}_p(n)\}_{n=0}^{M-1}$.

$$\hat{h}(n) = \begin{cases} \hat{h}_p(n) & 0 \le n \le M/2 - 1 \\ 0 & otherwise \\ \hat{h}_p(M + n - N) & N - M/2 \le n \le N - 1 \end{cases} \qquad (4.16)$$

After that we perform N-point DFT on $\hat{h}(n)$, which results in interpolation in frequency domain, as shown below.

$$H'(k) = \sum_{n=0}^{N-1}\hat{h}(n)e^{-j\frac{2\pi nk}{N}} \qquad k = 0,1,2,\cdots,N-1 \qquad (4.17)$$

Finally, the estimated channel frequency response $\hat{H}(k)$ is obtained by removing phase rotation effect from $H'(k)$. That is (4.18).

$$\hat{H}(k) = H'(k) \times e^{-j\pi\frac{\Delta k}{N}} \qquad k = 0,1,2,\cdots,N-1 \qquad (4.18)$$

The whole estimation process of DFT-based estimator is shown in Figure 4.10.
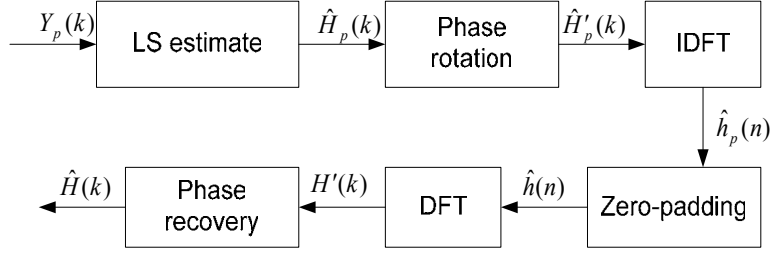
Figure 4.10 DFT-based channel estimator

Basic idea of the DCT-based channel estimator [19] is to make the input data symmetric so that the high frequency component is reduced, and then apply DFT-based interpolation algorithms. As a result, IDCT or DCT based channel estimation will be obtained. Although mirror-duplicating can be done in time domain, it can also be done by defining the extended pilot channel frequency response as [19]

$$\hat{H}_{2M}(k) = \begin{cases} \hat{H}_p(k) & 0 \le k \le M-1 \\ 0 & k = M \\ \hat{H}_p(2M-k)e^{-\frac{j\pi(2M-k)}{M}} & M+1 \le k \le 2M-1 \end{cases} \quad (4.19)$$

This design is compatible with the conventional inverse discrete cosine transform. For both two approaches, high frequency components are less significant than DFT-based approach, because the processed data are symmetric. Therefore, interpolation by using $\hat{H}_{2M}(k)$ would be better than the original DFT-based estimation.

With $\hat{H}_{2M}(k)$, we can perform its DFT-based interpolation to get the estimated channel frequency response. To achieve IDCT/DCT-based algorithm, each step of DFT-based estimator will be translated to DCT-related operation. First, we perform IDFT on the extended $\hat{H}_{2M}(k)$ to get the time-domain signal

$$\hat{h}_{2M}(n) = \frac{1}{2M} \sum_{k=0}^{2M-1} \hat{H}_{2M}(k) e^{\frac{j2\pi nk}{2M}}$$

$$= \frac{1}{2M} \hat{H}_{2M}(0) + \frac{1}{2M} \sum_{k=1}^{M-1} \left[\hat{H}_{2M}(k) e^{\frac{j2\pi nk}{2M}} + \hat{H}_{2M}(2M-k) e^{-\frac{j2\pi nk}{2M}} \right]$$

$$= \frac{1}{2M} \hat{H}_{p}(0) + \frac{1}{2M} \sum_{k=1}^{M-1} 2 e^{-\frac{j\pi k}{2M}} \hat{H}_{p}(k) \cos(\frac{(2n+1)\pi k}{2M})$$

$$= \frac{1}{\sqrt{2M}} \sum_{k=0}^{M-1} w(k) \hat{H}_{p}'(k) \cos(\frac{(2n+1)\pi k}{2M})$$

$$= \frac{1}{\sqrt{2M}} \hat{h}(n) \qquad n = 0,1,2,\cdots,2M-1$$

where $\hat{H}_{p}'(k) = \begin{cases} \dfrac{1}{\sqrt{2}} \hat{H}_{p}(k) & k = 0 \\[2mm] e^{-\frac{j\pi k}{2M}} \hat{H}_{p}(k) & 1 \le k \le M-1 \end{cases}$ and $\hat{h}_{2M}(n) = \hat{h}_{2M}(2M-n-1)$ (4.20)

and $w(k) = \begin{cases} \dfrac{1}{\sqrt{M}} & k=0 \\[2mm] \sqrt{\dfrac{2}{M}} & k \ne 0 \end{cases}$

This shows that the time-domain signal $\hat{h}_{2M}(n)$ can be obtained by performing IDCT

on $\hat{H}_{p}'(k)$ followed by a constant multiplication. Next, continuing the interpolation by

zero-padding $\hat{h}_{2M}(n)$, we can get the corresponding time-domain signal to the target

upsampled channel response, which is what we want to solve in the end.

$$\hat{h}_{2N}(n) = \begin{cases} \hat{h}_{2M}(n) & 0 \le n \le M-1 \\ 0 & otherwise \\ \hat{h}_{2M}(n-2N+2M) & 2N-M \le n \le 2N-1 \end{cases} \qquad (4.21)$$

Finally, the estimated channel frequency response is obtained by performing DFT on

$\hat{h}_{2N}(n)$.

$$
\begin{aligned}
\hat{H}_{2N}(k) &= \sum_{n=0}^{2N-1} \hat{h}_{2N}(n) e^{-\frac{j2\pi nk}{2N}} \\
&= \sum_{n=0}^{M-1} \hat{h}_{2M}(n) e^{-\frac{j2\pi nk}{2N}} + \sum_{n=2N-M}^{2N-1} \hat{h}_{2M}(n-2N+2M) e^{-\frac{j2\pi nk}{2N}} \\
&= \sum_{n=0}^{M-1}\left[\hat{h}_{2M}(n) e^{-\frac{j2\pi nk}{2N}} + \hat{h}_{2M}(2M-n-1) e^{-\frac{j2\pi(2N-1-n)k}{2N}} \right] \\
&= \frac{1}{\sqrt{2M}} \sum_{n=0}^{M-1}\left[\hat{h}(n) e^{-\frac{j2\pi nk}{2N}} + \hat{h}(n) e^{\frac{j2\pi(n+1)k}{2N}} \right] \\
&= \frac{1}{\sqrt{2M}} e^{\frac{j\pi k}{2N}} \sum_{n=0}^{M-1} 2\hat{h}(n) \cos(\frac{(2n+1)\pi k}{2N}) \\
&= w_k' w_k \sum_{n=0}^{M-1} \hat{h}(n) \cos(\frac{(2n+1)\pi k}{2N})
\end{aligned}
\qquad (4.22)
$$

$$
where \quad w_k' = \frac{1}{\sqrt{2}} \quad k=0 \ , \quad w_k' = e^{\frac{j\pi k}{2N}} \quad k=1,2,\cdots,N-1
$$

This equation is equivalent to a DCT operation combined with one constant multiplication. It is obvious that in the interpolation process, $\hat{h}(n)$ can be obtained by IDCT and $\hat{H}_{2N}(k)$ is the DCT transform of $\hat{h}(n)$ followed by one multiplication. Therefore, the whole IDFT-based interpolation can be replaced by DCT-based operations. This IDCT/DCT-based channel estimator [19] is shown in Figure 4.11. We also show the equivalent channel estimations by IDCT-based interpolator and IDFT-based interpolator in Figure 4.12, where

$$
\widetilde{H}_p(k) = \hat{H}_p(k) e^{-j\frac{\pi k}{M}} \qquad k=1,2,\cdots,M-1 \qquad (4.23)
$$
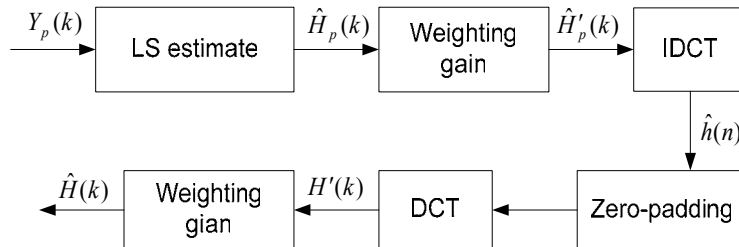
Figure 4.11 IDCT/DCT-based channel estimator
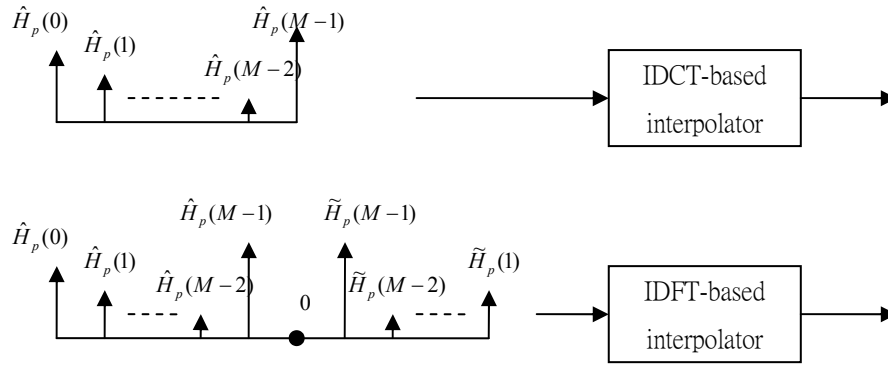
Figure 4.12 Equivalent channel estimators by IDCT/DCT-based interpolator and

IDFT-based interpolator

When we discuss 802.11n-like MIMO OFDM system, the scattered pilot makes the channel estimation easier compared to cyclic-shift preamble (no co-channel interference problem). Once the preamble signal is received, the channel response on pilot tones can be obtained by LS method. After that, we can further obtain responses on all subcarriers with interpolation skills. Transform domain interpolation is a good solution for such equi-spaced pilots. However, conventional DFT-based estimator suffers from non-sample spaced effect, as mentioned in previous part of this subsection. A comparison among different interpolation skills is presented in Chapter 5.

4.2.2 Channel Estimation for Space-time Coded Preamble

As introduced in 4.1.2, channel response can be detected if the pilots from transmitter are known. In Figure 4.3, it shows the special frame structure of space-time coding OFDM mentioned before. The assumption [2] in this system is that the channel responses between two consecutive OFDM symbols are the same. [2] also

assumes that the frequency response is flat in our concerned signal bandwidth, and this is true while OFDM system separates the large transmission band into N narrow subcarriers. Finally, the transmission signal on the kth subcarrier can be expressed as

$$P = \begin{bmatrix} P_1(k) & P_2(k) \\ -P_2^*(k) & P_1^*(k) \end{bmatrix}$$
(4.22)

According to [21], the received signals at consecutive time slots are y_1 and y_2, which are formulated as

$$y_1(k) = h_1 P_1(k) + h_2 P_2(k) + w_1(k)$$
$$y_2(k) = -h_1 P_2^*(k) + h_2 P_1^*(k) + w_2(k)$$
(4.23)

The channel response on this subcarrier can be estimated with the following two equations (4.24a) and (4.24b).

$$\hat{h}_1 = \frac{y_1 \cdot P_1^*(k) - y_2 \cdot P_2(k)}{|P_1(k)|^2 + |P_2(k)|^2}$$
(4.24a)

$$\hat{h}_2 = \frac{y_1 \cdot P_2^*(k) + y_2 \cdot P_1(k)}{|P_1(k)|^2 + |P_2(k)|^2}$$
(4.24b)

Where $\hat{h}_1$ and $\hat{h}_2$ denote estimations of channels h_1 and h_2, respectively, and (4.25a) and (4.25b) can be obtained from (4.23).

$$\hat{h}_1 = h_1 + \frac{P_1^*(k) \cdot w_1(k) - P_2(k) \cdot w_2(k)}{|P_1(k)|^2 + |P_2(k)|^2} = h_1 + w_1'(k)$$
(4.25a)

$$\hat{h}_2 = h_2 + \frac{P_2^*(k) \cdot w_1(k) - P_1(k) \cdot w_2(k)}{|P_1(k)|^2 + |P_2(k)|^2} = h_2 + w_2'(k)$$
(4.25b)

If the two previous equations (4.25a) and (4.25b) are observed, it can be obtained the new estimation error from white noise is turned to

$$w_1'(k) = \frac{P_1^*(k) \cdot w_1(k) - P_2(k) \cdot w_2(k)}{|P_1(k)|^2 + |P_2(k)|^2}$$
(4.26a)

$$w_2^{'}(k) = \frac{P_2^{*}(k) \cdot w_1(k) - P_1(k) \cdot w_2(k)}{\left|P_1(k)\right|^2 + \left|P_2(k)\right|^2} \qquad (4.26b)$$

4.2.2.1 Decision-direct Channel Tracking for Space-time Coded Preamble

While the preamble is sent to receiver, the channel is estimated with known preamble. Once the channel is estimated, the residual data symbols are extracted with the estimated channel. A common decision-direct tracking skill can be applied to the space-time coded MIMO OFDM system. The idea is to use the demodulated data subcarriers after demodulation as new pilots, and then estimate the current channel response again with demodulated data. Then channel response is updated with the new estimation.
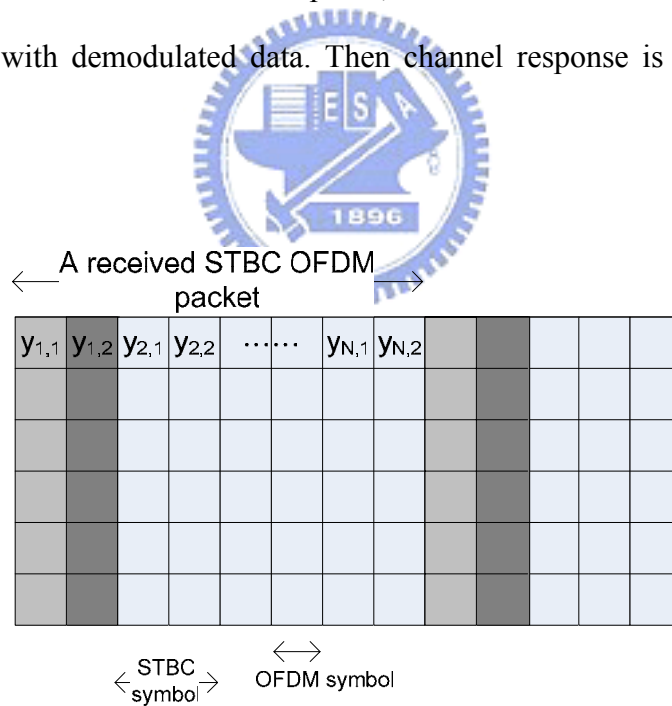
Figure 4.13 Illustration of received STBC symbol

In Figure 4.13, a received STBC OFDM symbol is shown to illustrate the decision-direct tracking skill. For preamble $y_{1,1}$ and $y_{1,2}$, the channel is estimated by (4.24a) and (4.24b). That is

$$\hat{h}_1 = \frac{y_{1,1} \cdot P_1^*(k) - y_{1,2} \cdot P_2(k)}{|P_1(k)|^2 + |P_2(k)|^2} \qquad (4.27a)$$

$$\hat{h}_2 = \frac{y_{1,1} \cdot P_2^*(k) + y_{1,2} \cdot P_1(k)}{|P_1(k)|^2 + |P_2(k)|^2} \qquad (4.27b)$$

where $y_{i,j}$ is the jth OFDM symbol of the ith STBC symbol.

The data of STBC symbols are extracted from the channel estimates as

$$\hat{x}_{n,1} = \frac{\hat{h}_{n,1}^* \cdot y_{1,1} + \hat{h}_{n,2} \cdot y_{1,2}}{|\hat{h}_1|^2 + |\hat{h}_2|^2} \qquad (4.28a)$$

$$\hat{x}_{n,2} = \frac{\hat{h}_2^* \cdot y_{n,1} - \hat{h}_1 \cdot y_{n,2}}{|\hat{h}_1|^2 + |\hat{h}_2|^2} \qquad (4.28b)$$

Then $\hat{x}_1$ and $\hat{x}_2$ are demodulated by constellation demapping, so that $\tilde{x}_1$ and $\tilde{x}_2$ are the decoded data. With these known data, the current channel response can be again estimated and updated by (4.29a) and (4.29b).

$$\hat{h}_{n,1} = \frac{y_{n,1} \cdot \tilde{x}_{n,1}^* - y_{n,2} \cdot \tilde{x}_{n,2}}{|\tilde{x}_{n,1}|^2 + |\tilde{x}_{n,1}|^2} \qquad (4.29a)$$

$$\hat{h}_{n,2} = \frac{y_{n,1} \cdot \tilde{x}_{n,2}^* + y_{n,2} \cdot \tilde{x}_{n,1}}{|\tilde{x}_{n,1}|^2 + |\tilde{x}_{n,1}|^2} \qquad (4.29b)$$

After that, it can be used to update the previous estimation by the following smoothing process. That is,

$$\hat{h}_{n,i} = (1-\alpha)\hat{h}_{n-1,i} + \alpha\hat{h}_{n-2,i} \qquad (4.30)$$

where α is the forgetting factor

Performance improvement of the improved skills will be shown in Chapter 5.

4.2.3 Channel Estimation with All-pilot Preamble

While using all-pilot preamble in MIMO OFDM system, the main difficulty is the co-channel interference. The received preamble in frequency domain expression is the summation of signals from multiple antennas. For this reason, the interference must be cancelled before channel is estimated. In this subsection, the solution proposed by [22] will be studied first. After that, the complexity issue will be explored. Finally, a modification is proposed for this algorithm.

For convenience of the ensuing discussion, let's define a MIMO channel response as

$$H_i[n,k] = \sum_{l=0}^{K_0-1} h_i[n,l] W_N^{kl} \qquad (4.31)$$

where W_N^{kl} is defined as $e^{-j(2\pi kl/N)}$,
l is time-domain tap index,
k is the subcarrier number,
n is the OFDM symbol index,
i is the transmission antenna index,
N is the number of subcarriers,
K_0 is the number of the most significant taps in impulse response,
$H_i(n,k)$ is the frequency response of the ith MIMO channel,
$h_i(n,l)$ is the impulse response of the ith MIMO channel

The received signal at the n_R^{th} antenna can be expressed as (4.32).

$$r_{n_R}[n,k] = \sum_{i=1}^{N_T} H_i[n,k] t_i[n,k] + w[n,k] \qquad (4.32)$$

where r_{n_R} is the received signal of n_R^{th} received antenna,
t_i is the known preamble signal,
w is the additive noise,
N_T is the number of transmission antennas

For a general case (N_T transmit antennas), to estimate channel response, one can define the following square error cost function (4.33)

$$C\left(\left\{ \tilde{h}_i[n,l]; i=1,\cdots,N_T \right\} \right) = \sum_{k=0}^{N-1} \left| r_{n_R}[n,k] - \sum_{i=1}^{N_T} \sum_{l=0}^{K_0-1} \tilde{h}_i[n,l] W_N^{kl} t_i[n,k] \right|^2 \quad (4.33)$$

where $\tilde{h}_i[n,l]$ is the estimation of the ith channel response

It can be easily shown that the optimum least-square-error (LSE) solution can be solved from the following normal equation.

$$\sum_{k=0}^{N-1} \left(r_{n_R}[n,k] - \sum_{i=1}^{N_T} \sum_{l=0}^{K_0-1} \tilde{h}_i[n,l] W_N^{kl} t_i[n,k] \right) W_N^{-kl_0} t_j^*[n,k] = 0,$$

$$\text{where } j = 1 \cdots N_T,$$

$$\text{and } l_0 = 0,1,\cdots K_0 - 1 \quad (4.34)$$

One can define these parameters q_{ij} and p_j to simplify (4.34).

$$q_{ij}[n,l] \equiv \sum_{k=0}^{N-1} t_i[n,k] t_j^*[n,k] W_N^{-kl} \quad (4.35)$$

$$p_j[n,l] \equiv \sum_{k=0}^{N-1} r_{n_R}[n,k] t_j^*[n,k] W_N^{-kl} \quad (4.36)$$

Hence (4.34) can be transformed into

$$\sum_{i=1}^{N_T} \sum_{l=0}^{K_0-1} \tilde{h}_i[n,l] q_{ij}[n,l_0 - l] = p_j[n,l_0], \, j = 1 \cdots N_T \quad (4.37)$$

Furthermore, one can define the vectors and matrix,

$$
\tilde{h}[n] \equiv \begin{pmatrix} \tilde{h}_1[n] \\ \vdots \\ \tilde{h}_{N_T}[n] \end{pmatrix}, \quad p[n] \equiv \begin{pmatrix} p_1[n] \\ \vdots \\ p_{N_T}[n] \end{pmatrix}, \quad Q[n] \equiv \begin{pmatrix} Q_{11}[n] & \cdots & Q_{N_T 1}[n] \\ \vdots & \ddots & \vdots \\ Q_{1N_T}[n] & \cdots & Q_{N_T N_T}[n] \end{pmatrix}, \quad (4.38)
$$

where

$$
\tilde{h}_i[n] \equiv (\tilde{h}_i[n,0], \tilde{h}_i[n,1], \cdots, \tilde{h}_i[n,K_0-1])^T \tag{4.39}
$$

$$
p_i[n] \equiv (p_i[n,0], p_i[n,1], \cdots, p_i[n,K_0-1])^T \tag{4.40}
$$

$$
Q_{ij}[n] \equiv \begin{pmatrix} q_{ij}[n,0] & q_{ij}[n,-1] & \cdots & q_{ij}[n,-K_0+1] \\ q_{ij}[n,1] & q_{ij}[n,0] & \cdots & q_{ij}[n,-K_0+2] \\ \vdots & \vdots & \ddots & \vdots \\ q_{ij}[n,K_0-1] & q_{ij}[n,K_0-2] & \cdots & q_{ij}[n,0] \end{pmatrix} \tag{4.41}
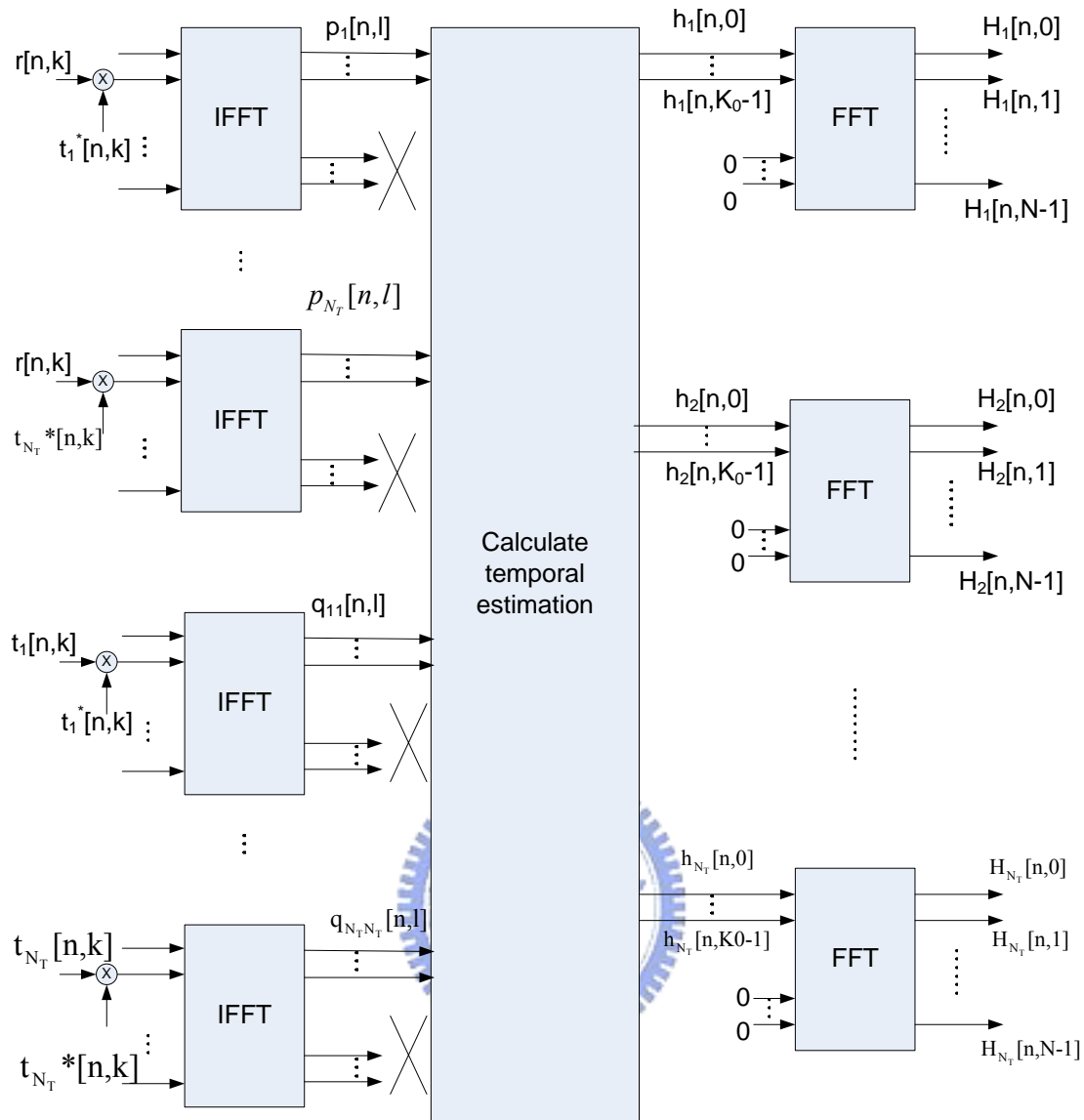$$

As a result, (4.37) can be rewritten as (4.42).

$$
Q[n]\tilde{h}[n] = p[n] \tag{4.42}
$$

One can solve the equation (4.42) by

$$
\tilde{h}[n] = Q^{-1}[n]p[n] \tag{4.43}
$$

The overall process of this LSE MIMO channel estimation technique can be illustrated by Figure 4.14.

Figure 4.14 Function structure of LS channel estimation for MIMO OFDM systems using all-pilot preambles

4.2.3.1 Complexity Analysis of LS Channel Estimator for MIMO OFDM System Using All-pilot Preambles

From 4.2.3, it can be found that the complexity of LS estimator is high due to plenty of matrix operations, such as matrix multiplications and inversions. According to [23], the complexity of matrix inversion is proportional to $O(N_0^3)$ for general

cases, where N_0 is the dimension of the matrix. The detailed numbers of operations

with Gaussian elimination are listed in Table 4.4.

Table 4.4 Computational Complexity of matrix inversion with Gaussian

elimination ($N_0 \equiv N_T \times K_0$)

Operation	Division	Multiplication	Addition
Number	$\frac{1}{2}N_0(N_0+1)$	$\frac{1}{2}(N_0-1)N_0(N_0+1)$	$\frac{1}{2}(N_0-1)N_0(N_0+1)$

Unfortunately, Q[n] is a $N_T \times K_0$ by $N_T \times K_0$ matrix, as shown in Table 4.4,

its inversion is always hard to obtain due to high complexity. A simplified scheme is

proposed in [22,24], the main idea is to estimate only K_0' delay taps in time domain,

and hence the matrix dimension is reduced to $N_T \times K_0'$ by $N_T \times K_0'$. As a result,

(4.40) to (4.43) becomes (4.44) to (4.49).

$$\bar{h}_i[n] \equiv (h_i[n,l_1],h_i[n,l_2],\cdots,h_i[n,l_{K_{0'}}])^T \tag{4.44}$$

$$\bar{p}_i[n] \equiv (p_i[n,l_1],p_i[n,l_2],\cdots,p_i[n,l_{K_{0'}}])^T \tag{4.45}$$

$$\bar{Q}_{ij}[n] \equiv \begin{pmatrix} \bar{q}_{ij}[n,0] & \bar{q}_{ij}[n,l_1-l_2] & \cdots & \bar{q}_{ij}[n,l_1-l_{K_{0'}}] \\ \bar{q}_{ij}[n,l_2-l_1] & \bar{q}_{ij}[n,0] & \cdots & \bar{q}_{ij}[n,l_2-l_{K_{0'}}] \\ \vdots & \vdots & \ddots & \vdots \\ \bar{q}_{ij}[n,l_{K_{0'}}-l_1] & \bar{q}_{ij}[n,l_{K_{0'}}-l_2] & \cdots & \bar{q}_{ij}[n,0] \end{pmatrix} \tag{4.46}$$

$$\bar{h}[n] \equiv \begin{pmatrix} \bar{h}_1[n] \\ \vdots \\ \bar{h}_{N_T}[n] \end{pmatrix}, \quad \bar{p}[n] \equiv \begin{pmatrix} \bar{p}_1[n] \\ \vdots \\ \bar{p}_{N_T}[n] \end{pmatrix}, \quad \bar{Q}[n] \equiv \begin{pmatrix} \bar{Q}_{11}[n] & \cdots & \bar{Q}_{N_T 1}[n] \\ \vdots & \ddots & \vdots \\ \bar{Q}_{1N_T}[n] & \cdots & \bar{Q}_{N_T N_T}[n] \end{pmatrix} \tag{4.47}$$

$$\overline{Q}[n]\overline{h}[n] = \overline{p}[n] \qquad\qquad (4.48)$$

$$\overline{h}[n] = \overline{Q}^{-1}[n]\overline{p}[n] \qquad\qquad (4.49)$$

## 4.2.3.2 Proposed Method for the Decision of Significant Number of Channel Taps

In 4.2.3.1, it is shown that the complexity of LS estimator can be reduced if small K_0 is chosen. In Chapter 5, the simulation results show that a proper K_0 brings good MSE performance, and the simulations exploit the fact that a proper value of K_0 is the number of those most significant taps in time-domain. In [22], the detection of K_0 is not studied for this LS estimator. For this reason, we propose a simple method to improve this drawback of the methods.

According to the simulations in Chapter 5, the mean square error is large when K_0 is also large. While K_0 decreases and is closed to significant length of the channel, MSE is also reduced. An intuitive idea to decide K_0 is to use a large initial value for coarse estimation. Then a fine estimation of K_0 is conducted based on the result of coarse estimation.

The significant length of the channel is defined as the first tap-number at which the multi-path power is below the threshold. With threshold of 10^{-3}, the result falls at a reasonable performance. This criterion is illustrated in Figure 4.15. The overall flow of proposed modification is illustrated in Figure 4.16. The simulations for performance verification will be shown in Chapter 5
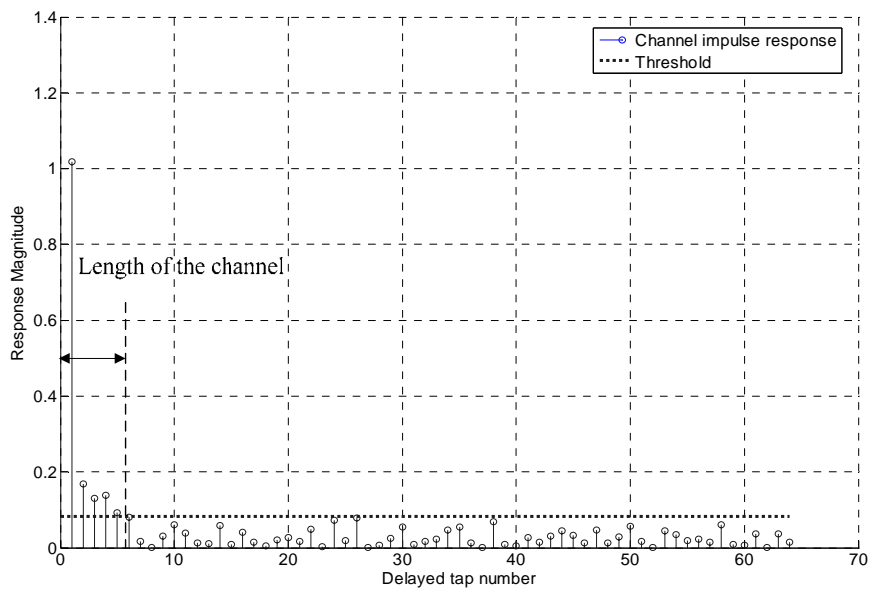
Figure 4.15 Criteria for length of the estimated channel
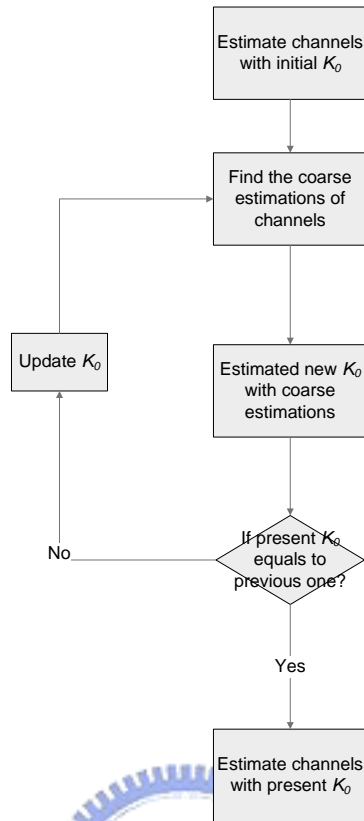
Figure 4.16 Flow chart for proposed channel length detection algorithm

Chapter 5
Simulations and Comparisons

In this chapter, we will present the simulation results on MIMO OFDM system channel estimation techniques. As we mentioned in Chapter 4, several kinds of pilot arrangements and corresponding estimation techniques are involved in our studies. After general evaluation on channel estimation techniques, we will discuss channel estimation issues of two popular standard, 802.16a with STC and 802.11n (WWiSE).

5.1 Simulation Environment and Parameters

The studies begin with simulations on a general MIMO OFDM system. Main system features are listed in Table 5.1 for simplicity. The overall system flow is shown in Figure 5.1. In our studies, we assume no synchronization errors in the system (i.e. perfect synchronization). Only inner transceiver is considered, and channel coder will not be considered. Both 802.11n-lke (packet type transmission) and 802.16a with STC (PSAM with STC) systems are also considered in our simulations.

Table 5.1 Simulated 802.11n-like MIMO system parameters

Sample Period	50 ns
Total number of carriers	64
Total number of carriers	52
The number of data carriers	48
Symbol period	$4\,\mu s$
Guard Interval	$0.8\,\mu s$
Modulation	QPSK
Sampling frequency	20MHz
Carrier spacing	312.5 kHz
Normalized Doppler shift frequency	0.01
ST-coding for data	STBC
Number of Tx/Rx	2-4/1-4

5.1.1 Channel Models

For both 802.11n-like and 802.16a with STC systems, two channel models are considered. The specific static impulse response of each channel model is listed below. Table 5.2 and Table 5.3 are for 802.11n-like systems. They are indoor wireless model at 5.3 GHz. Table 5.4 is channel model A for 802.16a proposed by ETSI (European Telecommunications Standards Institute). Table 5.4 is a model provided by ATTC (Advanced Television Technology Center). The channels are modeled as Rayleigh fading channels, and we assume uncorrelated between antennas (i.e. the correlation matrices are set to be identity matrices).

Table 5.2 Static parameters for indoor wireless channel (Model 1)

Tap No.	Delay (samples)	Power (dB)
1	0	0
2	1	-5
3	2	-13
4	3	-19

Table 5.3 Static parameters for indoor wireless channel (Model 2)

Tap No.	Delay (samples)	Power (dB)
1	0	0
2	4	-8
3	5	-15
4	11	-18

Table 5.4 Static parameters for ETSI model A (Model 3)

Tap No.	Delay (samples)	Power (dB)
1	0	0
2	4	-5
3	8	-7
4	12	-8.87
5	20	-10
6	30	-10

Table 5.5 Static parameters for ATTC model E (Model 4)

Tap No.	Delay (samples)	Power (dB)
1	0	0
2	2	-1
3	17	-9
4	36	-10
5	75	-15
6	137	-20

5.2 Channel Estimation for 802.11n-like Systems

In this subsection, different 802.11n-like (block type) MIMO OFDM systems such as all-pilot preamble, scattered preamble, and space-time coded preamble, will be explored. Space-time coded preamble, all-pilot preamble (the same as WWiSE), and scattered preamble are involved in our discussion. Except the pilot arrangement in preamble, all the other system parameters are the same as Table 5.1.

5.2.1 Channel Estimation for Space-Time Coded

Preamble MIMO OFDM

(a)
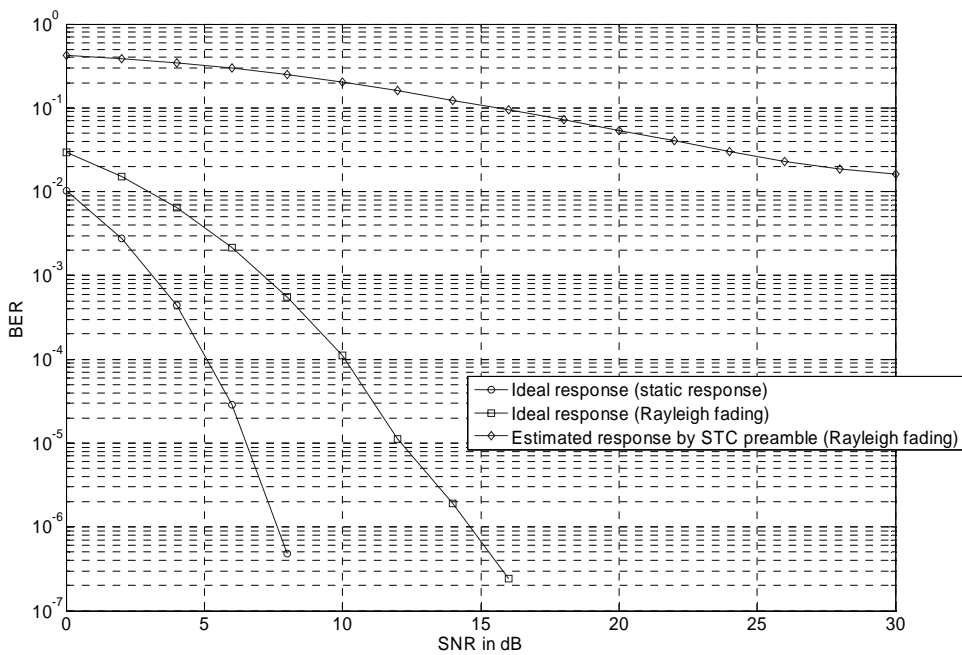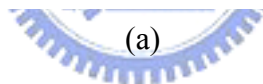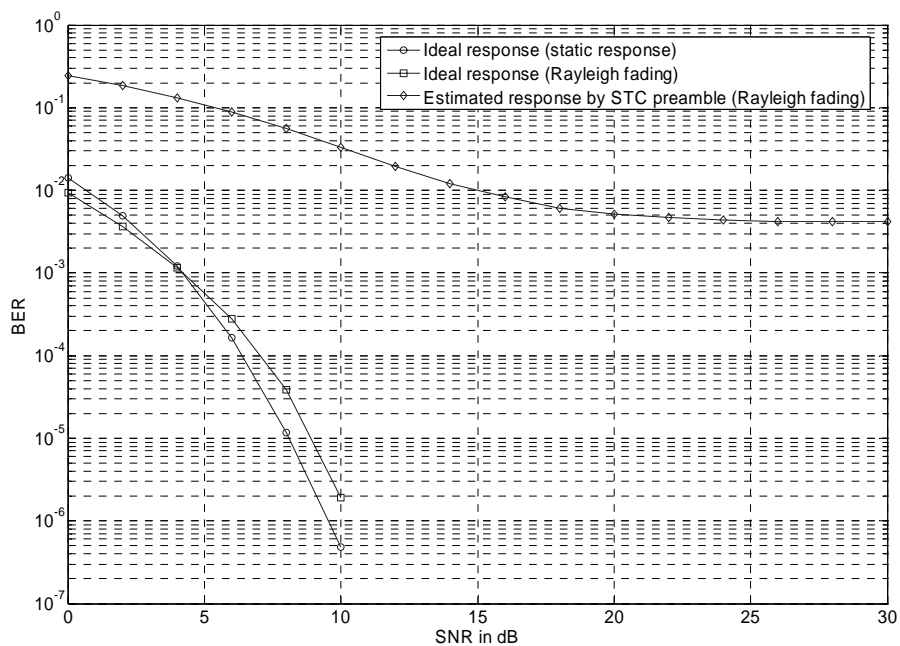
Figure 5.1 BER comparison of space-time coded preamble system (2 x 1) for two different channel conditions (a) Model 1 (b) Model 2

In this kind of MIMO OFDM system, both data and preambles are coded by space-time block code. When receiver starts to extract incoming OFDM symbols, the channel response is obtained by known space-time coded preamble. The channel is estimated of channel is from equations (4.25a) and (4.25b). The assumption of static channels between consecutive symbols is not valid in time-varying channels. Although noise is suppressed as shown in (4.26a) and (4.26b), the failure of static assumption degrades the performance. In Figure 5.1 (a) and (b), performance degeneration can be observed from the result of the static channel and time-varying channel.

After the decision-direct tracking skill is applied to this system, one can see that the BER curves in both Figure 5.2(a) and 5.2(b) are below the curves without decision-direct channel tracking. It shows that this skill is useful to combat time-varying channels. In Figure 5.3, the estimated responses at both head and tail of the packet are drawn. One can find that they are close to the actual responses. In this simulation, the number of OFDM symbols in a packet is 20, and the forgetting factor α described in equation (4.30) is set to 0.1. The normalized Doppler frequency f_dT is 0.1.
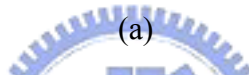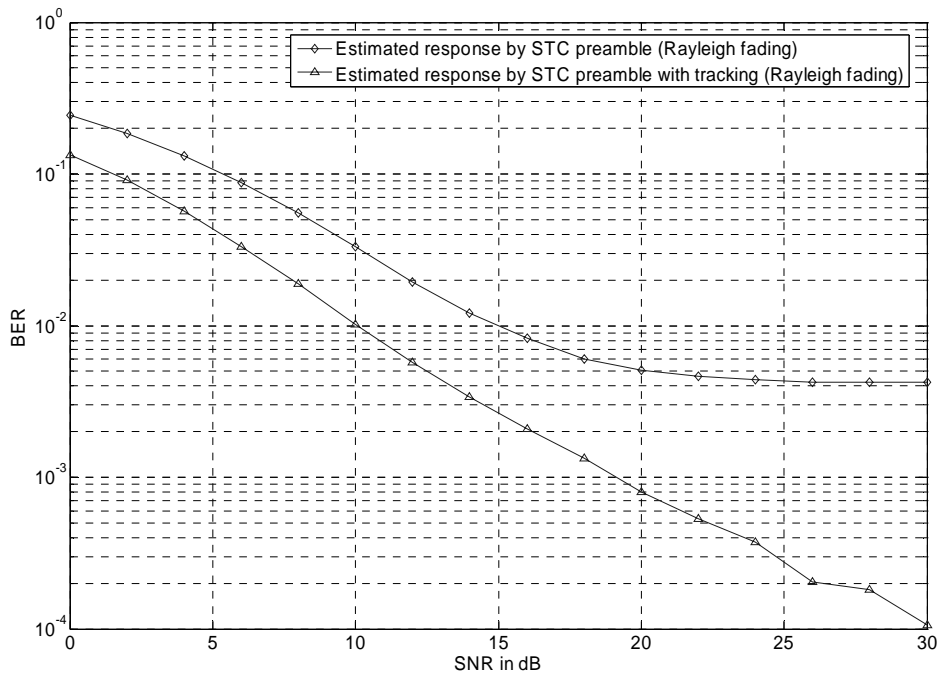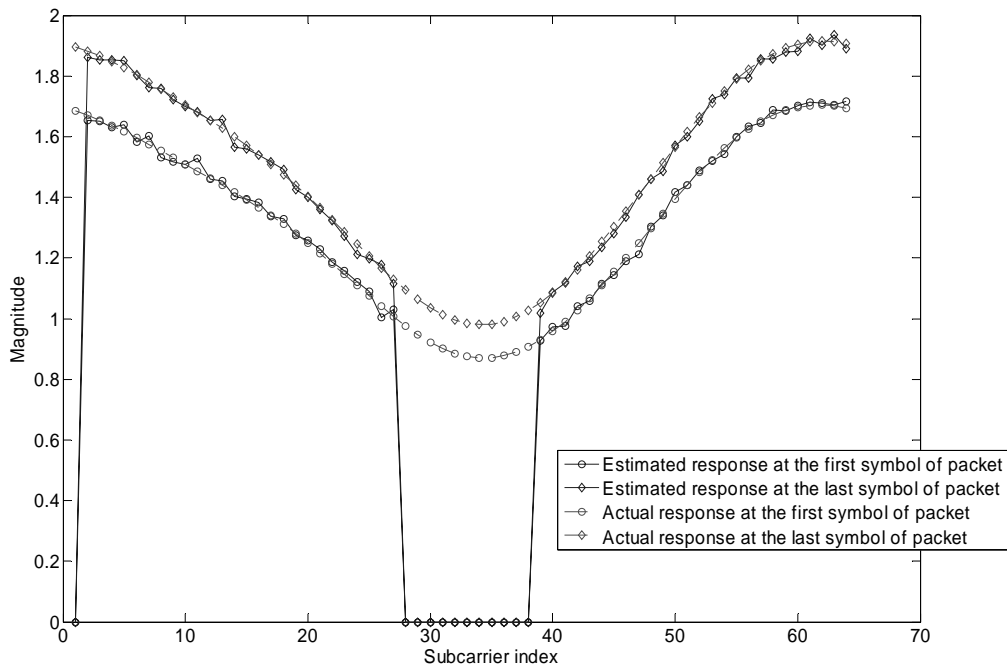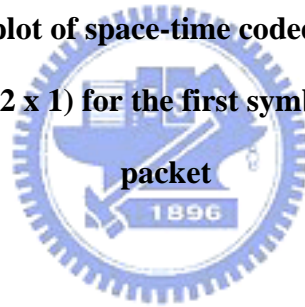
(a)
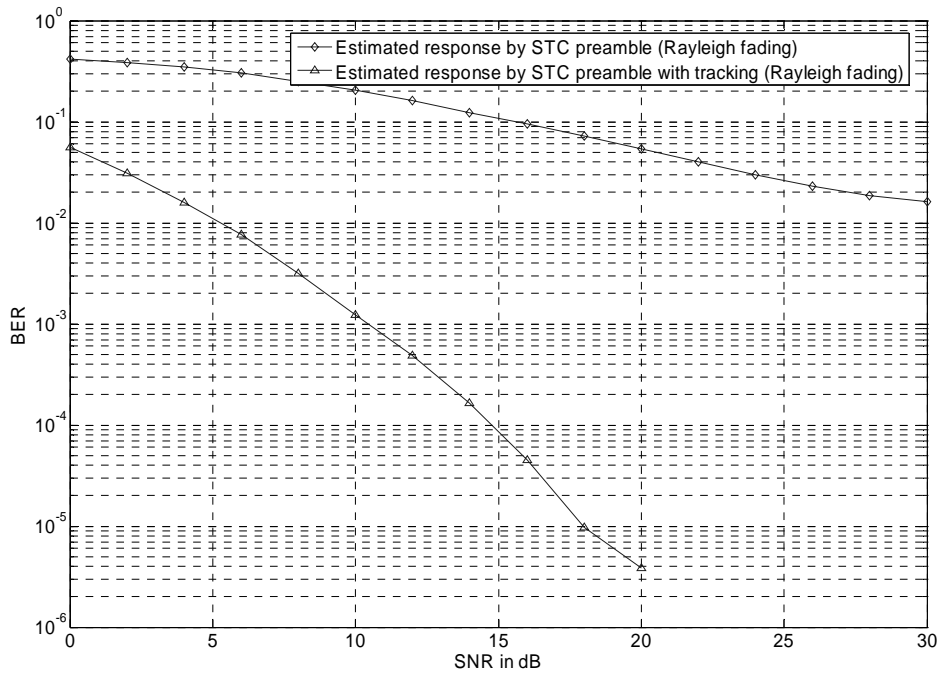
(b)

Figure 5.2 BER comparison of space-time coded preamble system with

decision-direct tracking (2 x 1) for two different channel conditions (a) Model 1

(b) Model 2

Figure 5.3 Response plot of space-time coded preamble system with

decision-direct tracking (2 x 1) for the first symbol and the last symbol in a

**packet**

5.2.2 Channel Estimation for All-pilot Preamble

MIMO OFDM

When we further investigate channel estimation in all-pilot preamble MIMO

OFDM system, the parameter K_0 must be chosen carefully. As mentioned in

Chapter 4, K_0 equals to the number of most significant taps in time domain. To

illustrate this property, we consider another channel model other than Model 1 and 2.

This channel has a larger delay spread that can demonstrate the influence of K_0. The
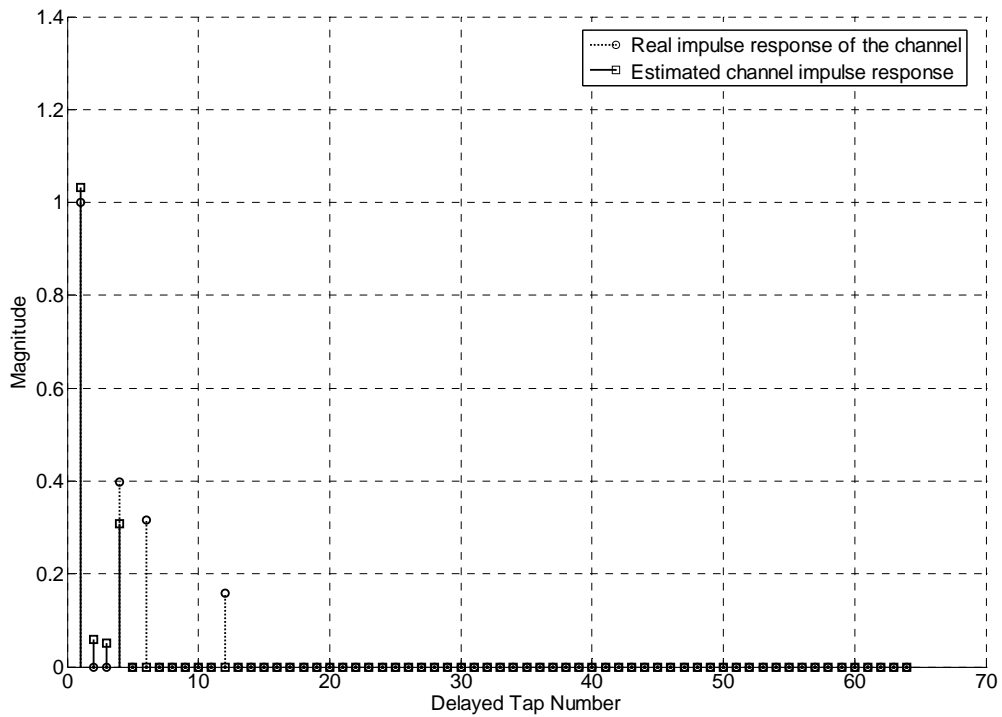
delay taps of this channel is at 0, 4, 5, and 11 samples. The power attenuation in dB is 0, 4, 5, and 8, respectively.
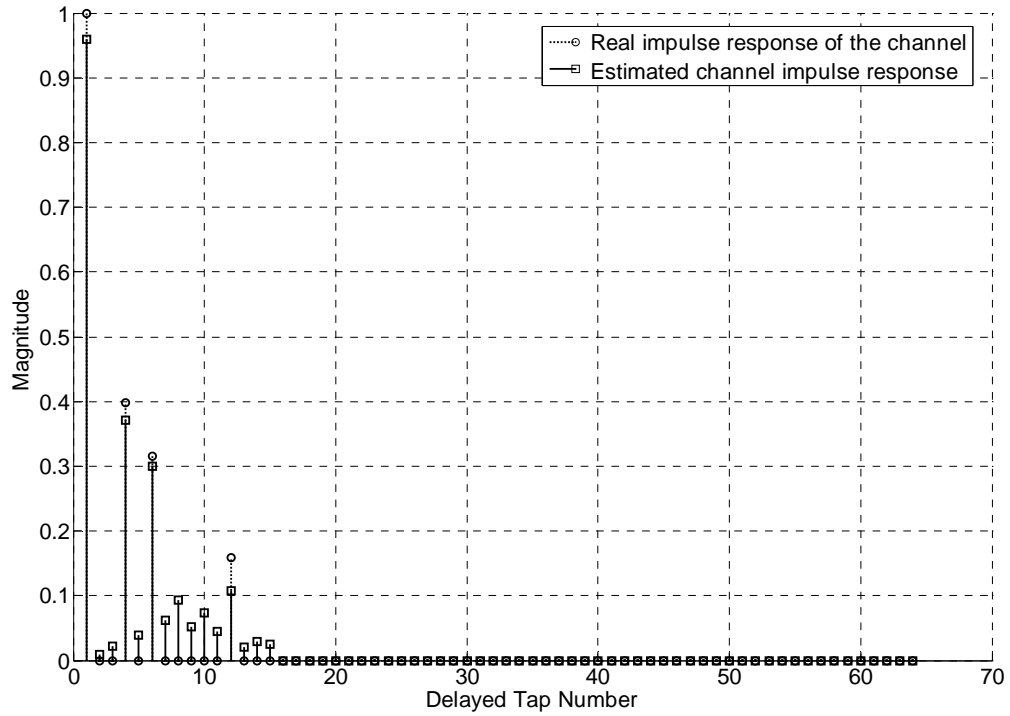

(a)
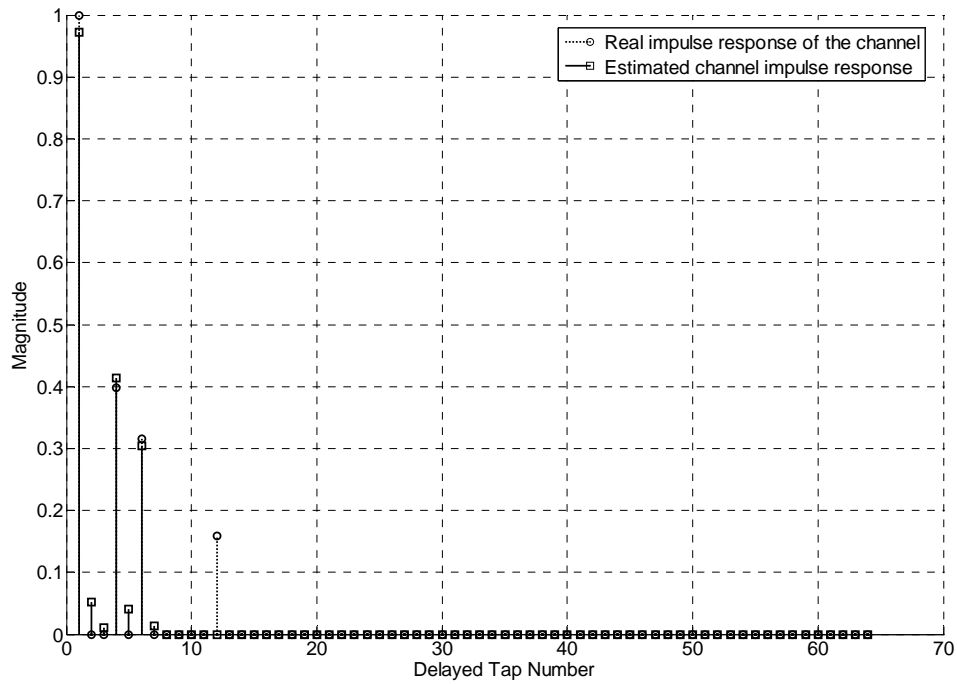
(b)

(c)

Figure 5.4 Estimated channel responses for three different K_0 **(a)** K_0=15 **(b)**

K_0=7 **(c)** K_0=4

From the observation of previous simulations, K_0 is a critical factor of performance. To verify the influence of K_0, a static two-ray channel is used for simulations. In order to evaluate performances of various K_0, the multipath power of each tap is set to a large value to emphasize their difference. The delay taps of this channel is at 0 and 14 samples. The power attenuation in dB is 0 and 3. In Figure 5.5, MSE versus K_0 plot is illustrated under noiseless condition with the static two-ray channel. One can see that MSE has the lowest value when K_0 equals to 15. The

MSE is large when K_0 is smaller than 15 because a significant tap is lost. The MSE

increases with K_0 when K_0 is greater than 15.
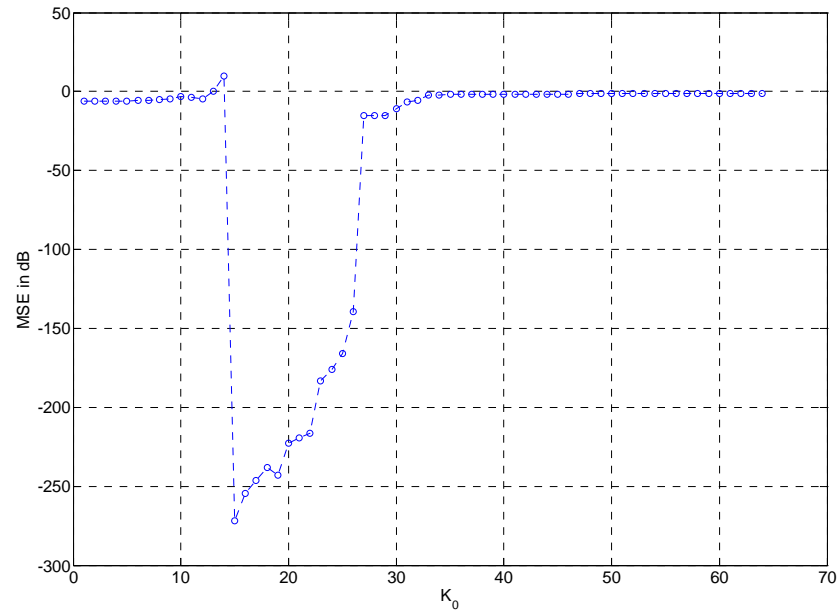
Figure 5.5 Averaged MSE versus K_0 of an all-pilot preamble system, N_T=2,

assumed a static two-ray model
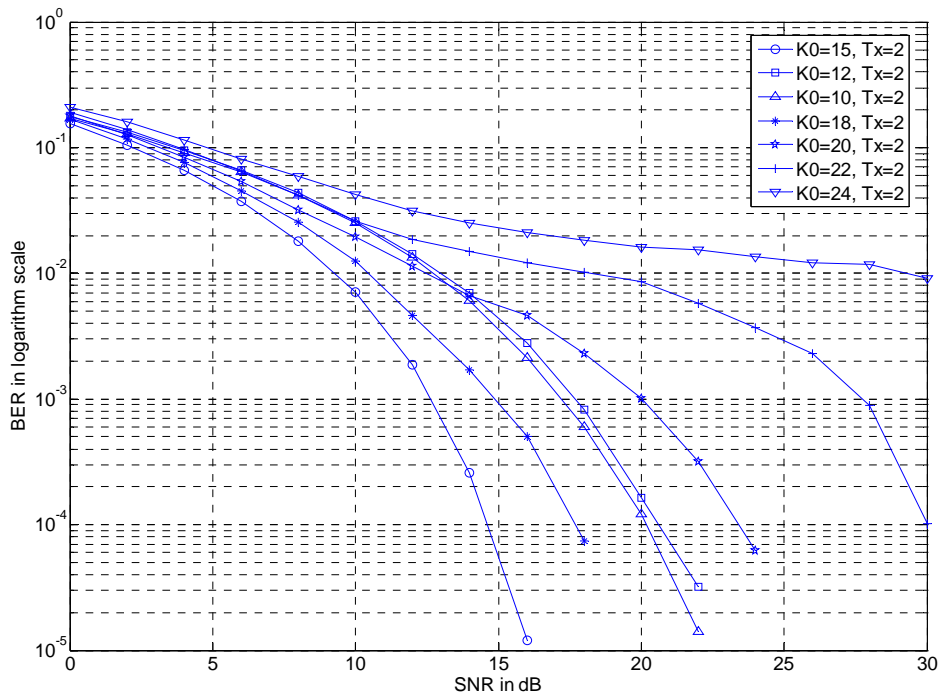
Figure 5.6 BER comparison due to various K_0 values, all-pilot-preamble, with

N_T=2, N_R =1, assumed a static two-ray model

The BER comparison is shown in Figure 5.6. The BER versus SNR curves show the

same trend as the MSE curve. The curve K_0=15 outperforms all other curves. From

this result, one can conclude that the best choice of K_0 is length of the channel.


In the following simulations, Rayleigh fading channels are assumed. The power

delay profiles are set to Model 1 and Model 2. In a single packet, there are 10 OFDM

symbols. From Figure 5.4 to 5.6, we can obtain two conclusions. First, K_0 should be

large enough to include all the delay taps in time domain. In 5.4 (b) and 5.4 (c), K_0

is smaller than the maximum delay spread (8 in this case). Therefore, there are more

noticeable mismatches between estimated taps and the actual taps, than in the case of

enough K_0. Another conclusion is that K_0 should not be too large. A more than

enough K_0 will include noise and CCI on those null taps. For example, all four

major taps are well caught by the extra channel estimator as shown in Figure 5.4 (a),

but additional interference can also be observed on those 15 taps (K_0=15). The

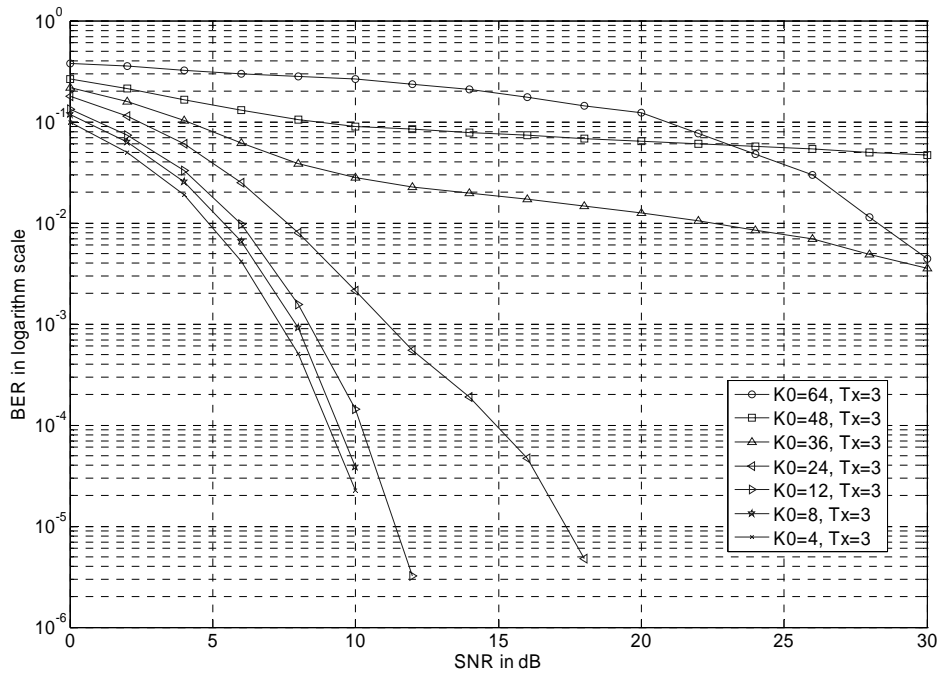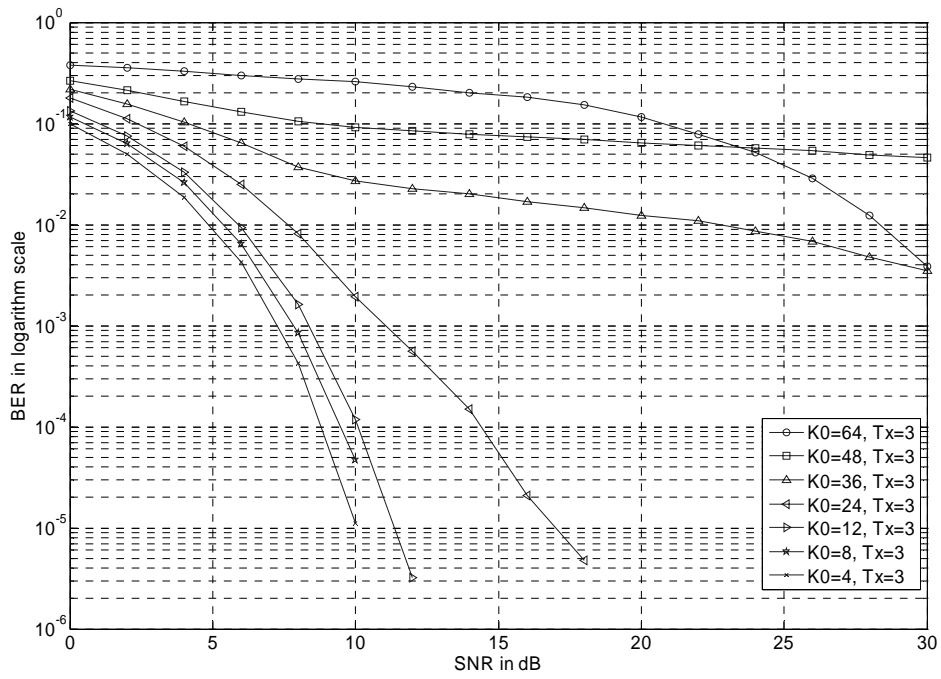mentioned two conditions cause the performance degradation in the channel

estimation.
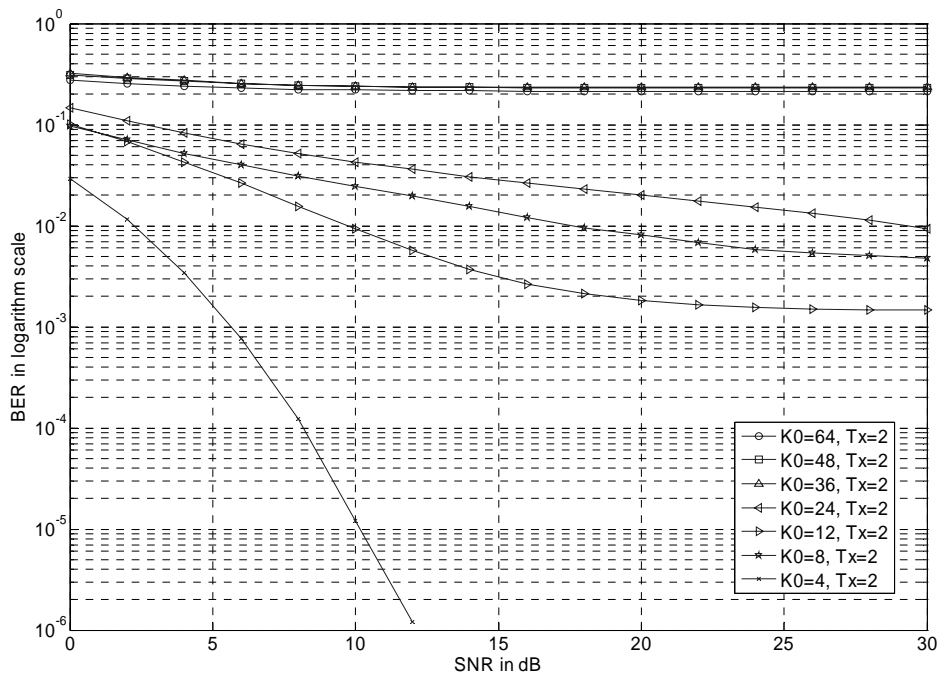
(a)
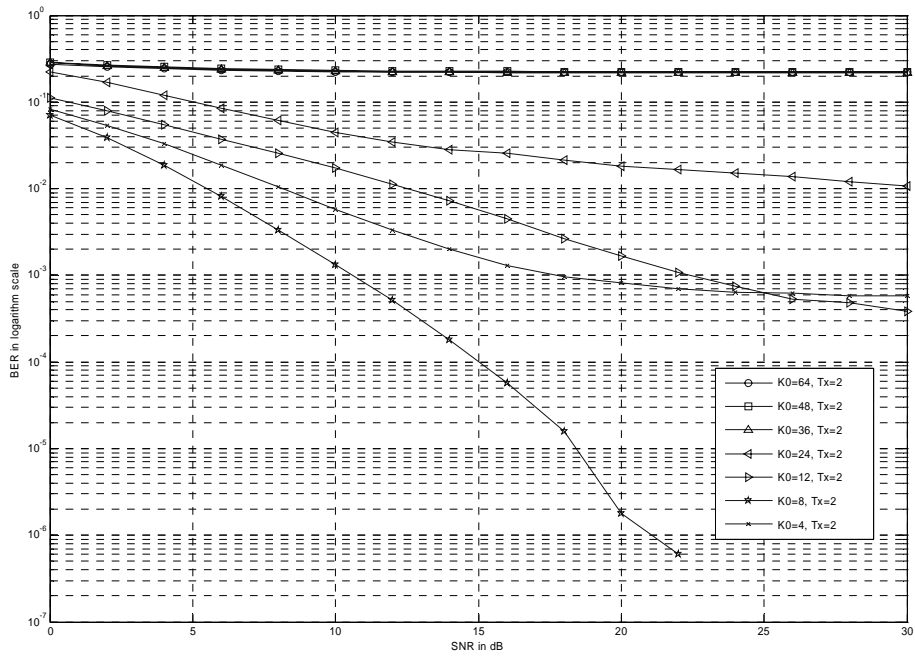
(b)

Figure 5.7 BER comparison due to various K_0 values, all-pilot-preamble, with
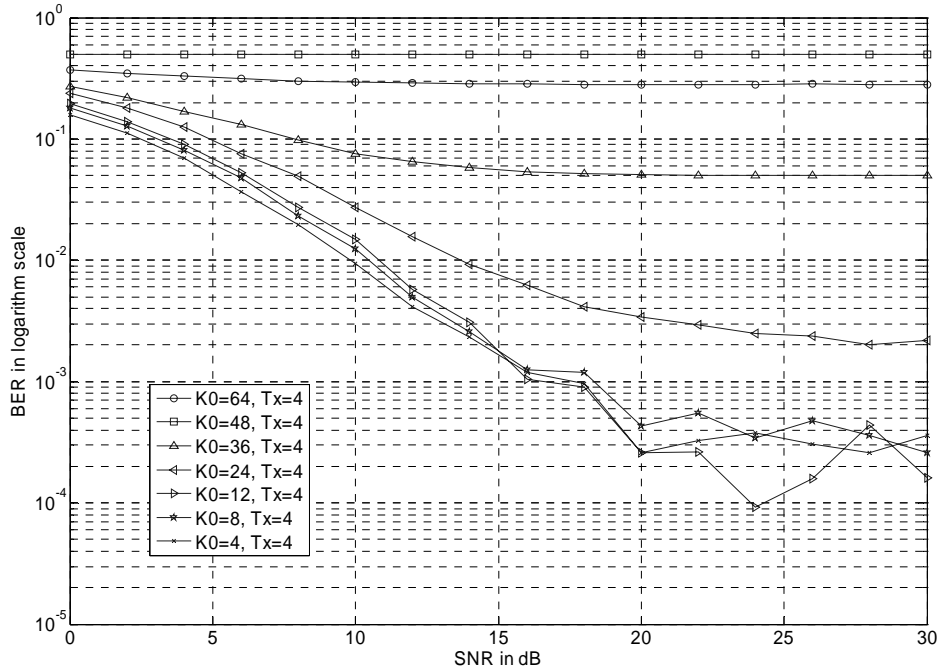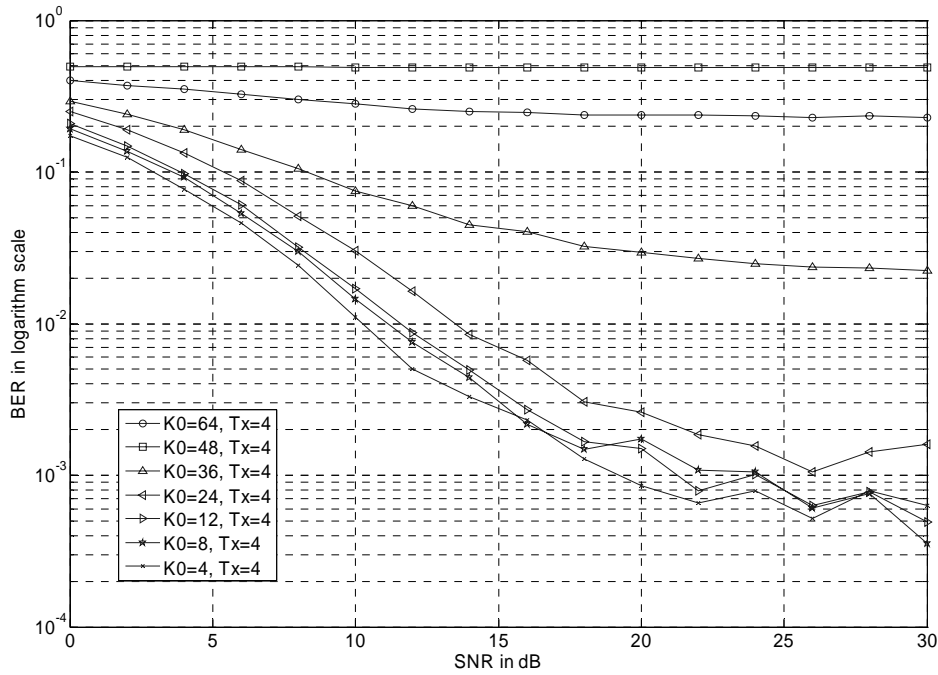
$N_T=2, N_R =1$ **(a) Model 1 (b) Model 2**

(a)

(b)

Figure 5.8 BER comparison due to various K_0 values, all-pilot-preamble, with

$N_T=3$, $N_R=1$ (a) Model 1 (b) Model 2

(a)

BER in logarithm scale

SNR in dB

Legend:
- K0=64, Tx=4
- K0=48, Tx=4
- K0=36, Tx=4
- K0=24, Tx=4
- K0=12, Tx=4
- K0=8, Tx=4
- K0=4, Tx=4

(b)

Figure 5.9 BER comparison due to various K_0 values, all-pilot-preamble, with N_T=4, N_R =1 (a) Model 1 (b) Model 2

In Figure 5.7 (a) and (b), BER versus SNR curves with different K_0 are shown for N_T=2. According to previous statements, inadequate K_0's have worse performances than that of exact K_0. However, the lengths of Model 1 and Model 2 indoor wireless channels are not very long, and the multipath powers of last few paths are quite small (smaller than -13 dB). The small taps are not very significant compared with additive noise. For this reason, the performance degradation with small K_0 is not obviously in our simulations. When we discuss the simulation results, it is noted that the maximum delay spread of is 3 in Model 1, and 11 in Model 2. In Figure 5.7 (a), K_0=4 provides best performance among several different K_0. In

(b), $K_0=8$ outperforms other K_0's. As a result, decision of K_0 is crucial to the

performance of the channel estimation. Set K_0 to the maximum delay spread is a

good choice. In Figure 5.8 and 5.9, one can see that the influence of CCI increases

when the number of transmission antennas is larger. There are significant error floors

in high SNR condition while the number is 4. In Figure 5.10 to 5.12, the cases of

multiple receiver antennas are simulated. One can see that the receiver diversity

provides better performance while multiple receiver antennas are used. For example,

the error floor in Figure 5.9(a) is improved in Figure 5.12.
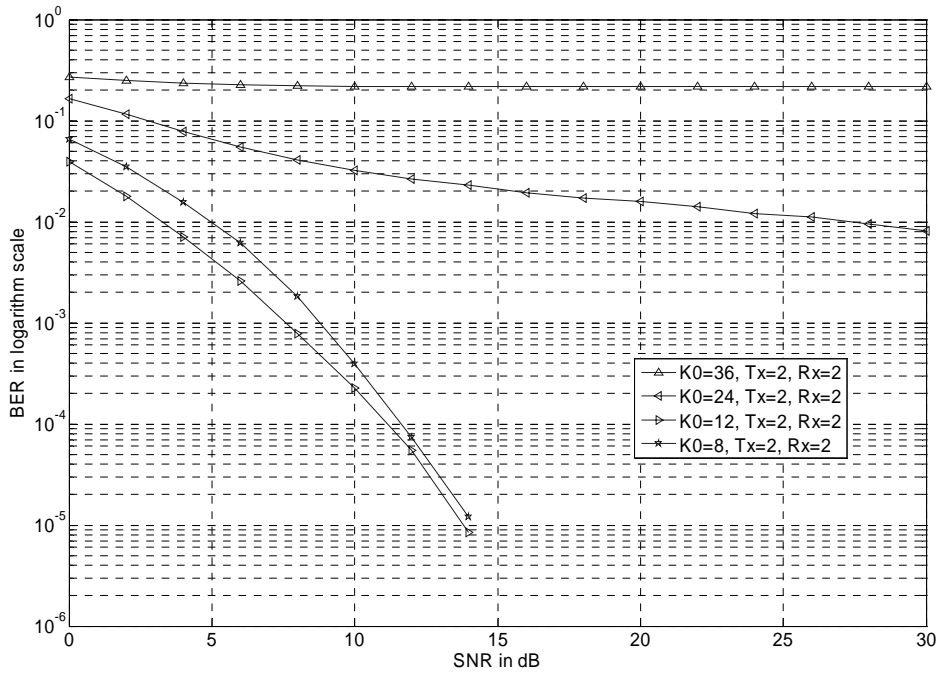
Figure 5.10 BER comparison due to various K_0 values, all-pilot-preamble,
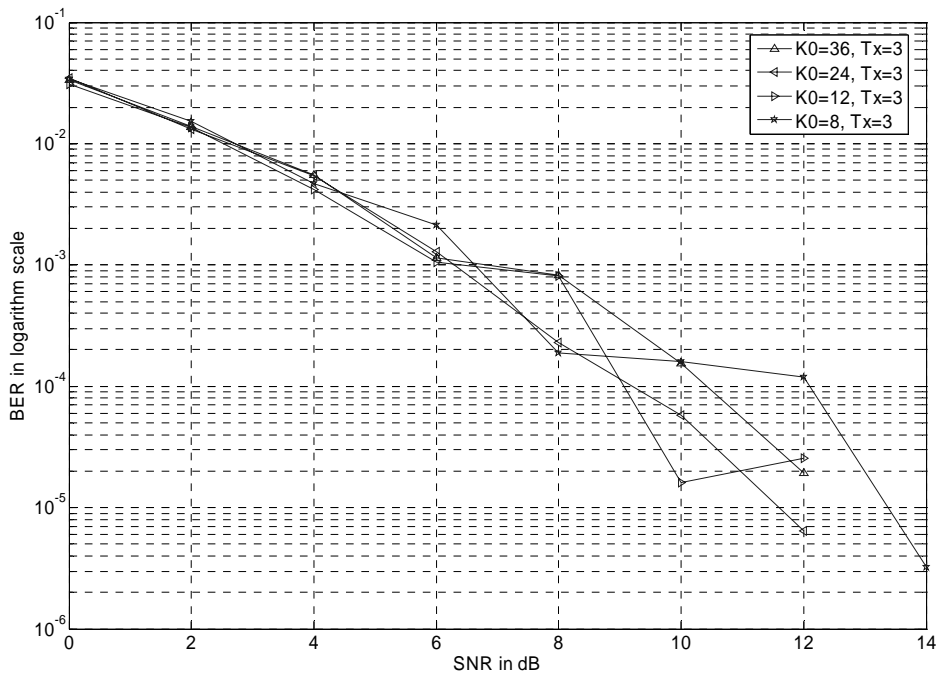
$N_T=2$, $N_R=2$ (Model 1)

Figure 5.11 BER comparison due to various K_0 values, all-pilot-preamble,

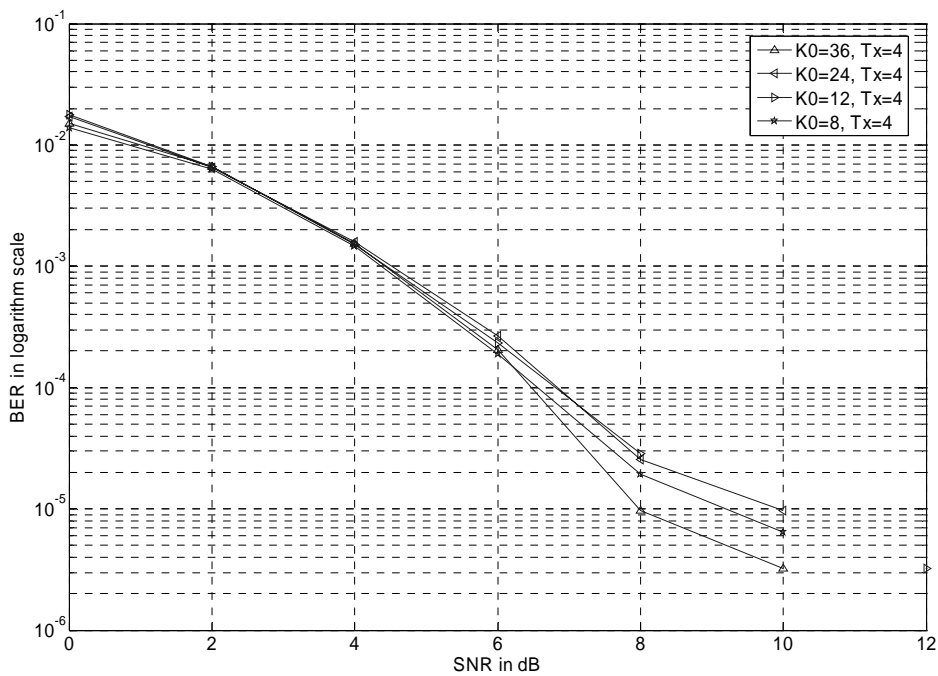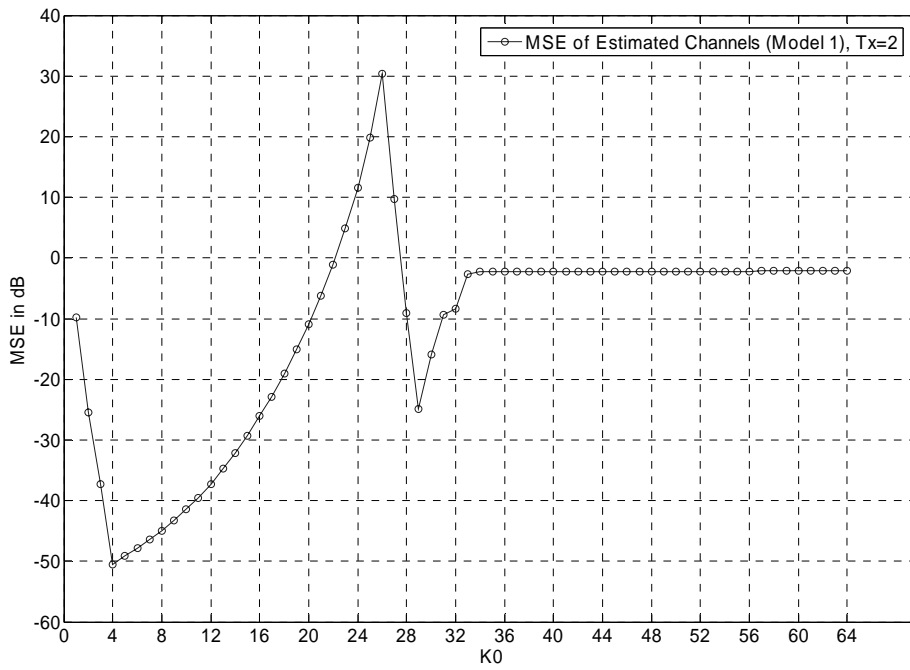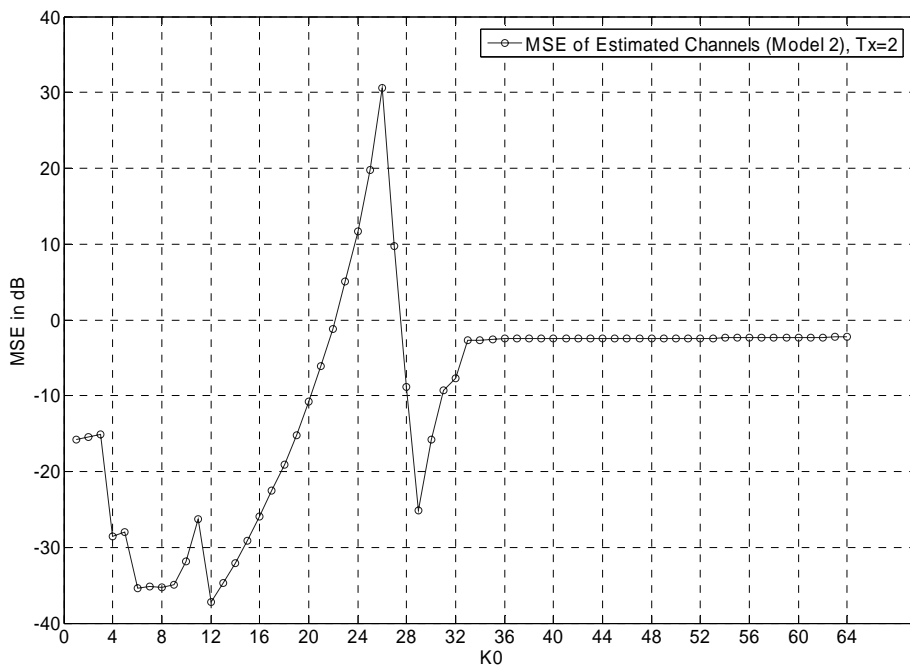**$N_T=3$, $N_R=3$ (Model 1)**

Figure 5.12 BER comparison due to various K_0 values, all-pilot-preamble,

$N_T=4$, $N_R=4$ (Model 1)

(a)

(b)

Figure 5.13 Averaged MSE versus K_0 **of all-pilot preamble system,** $N_T=2$ **(a)**

Model 1 (b) Model 2

81

(a)

(b)

Figure 5.14 Averaged MSE versus K_0 **of all-pilot preamble system,** $N_T=3$ **(a)**
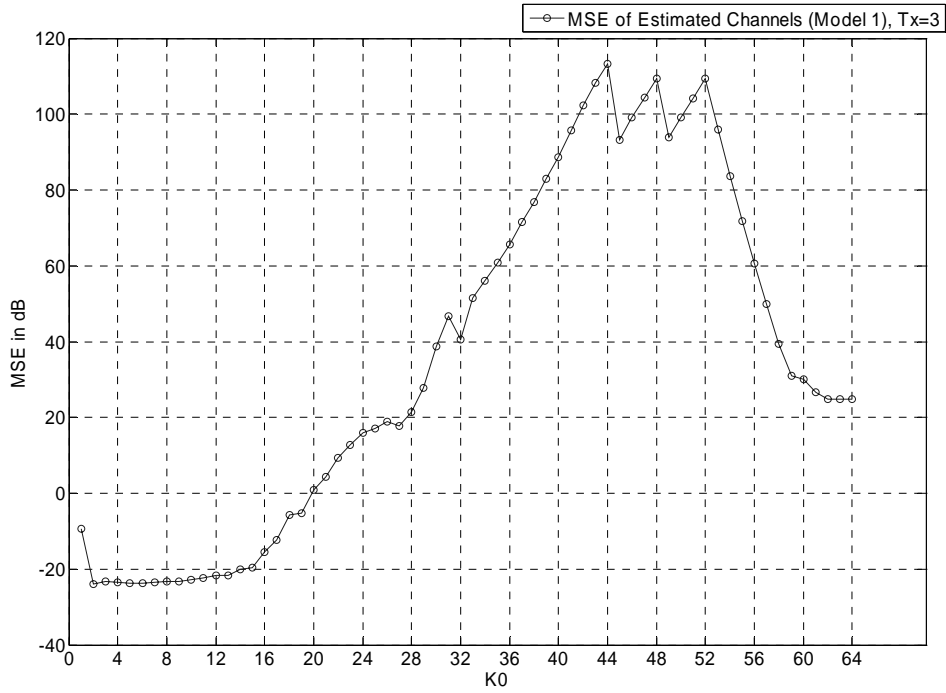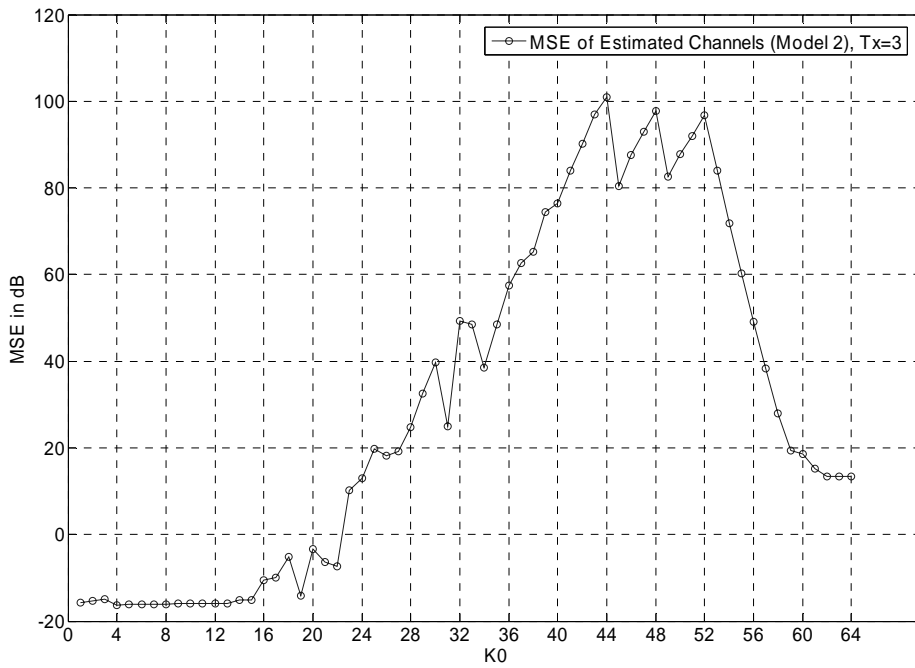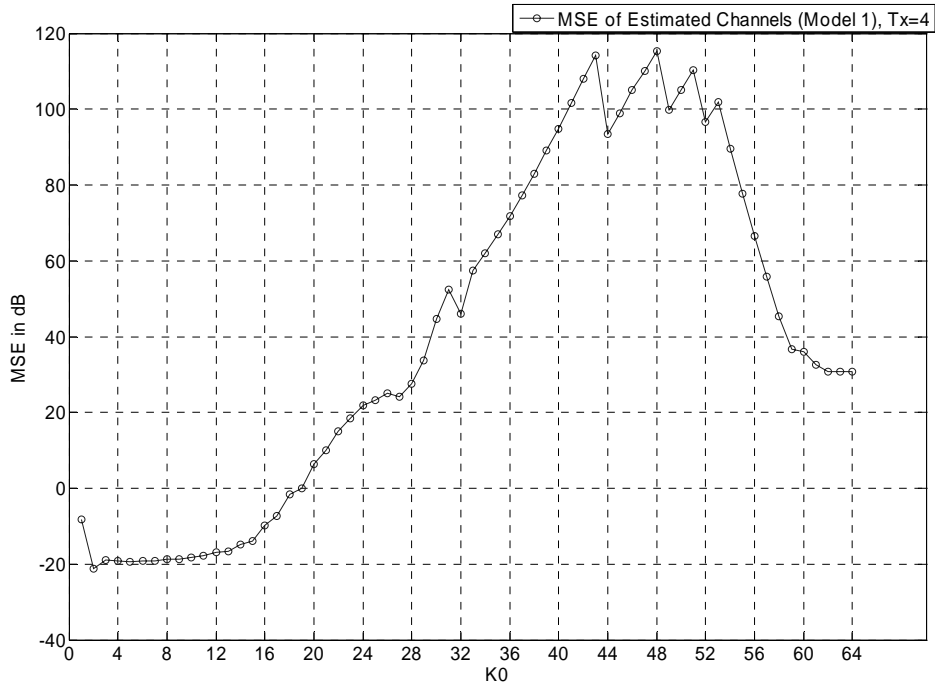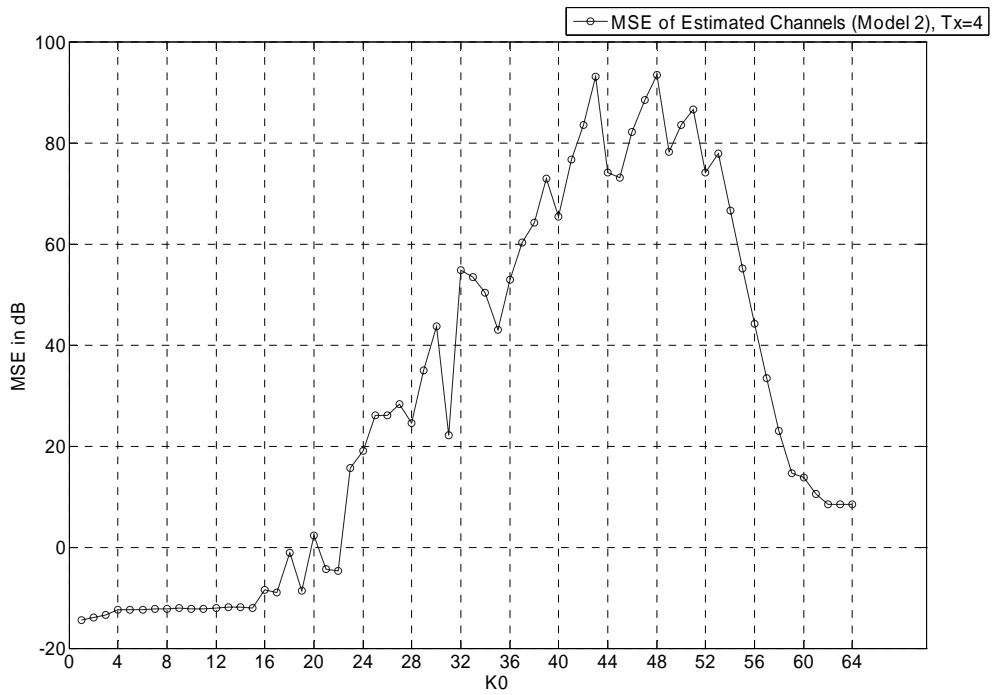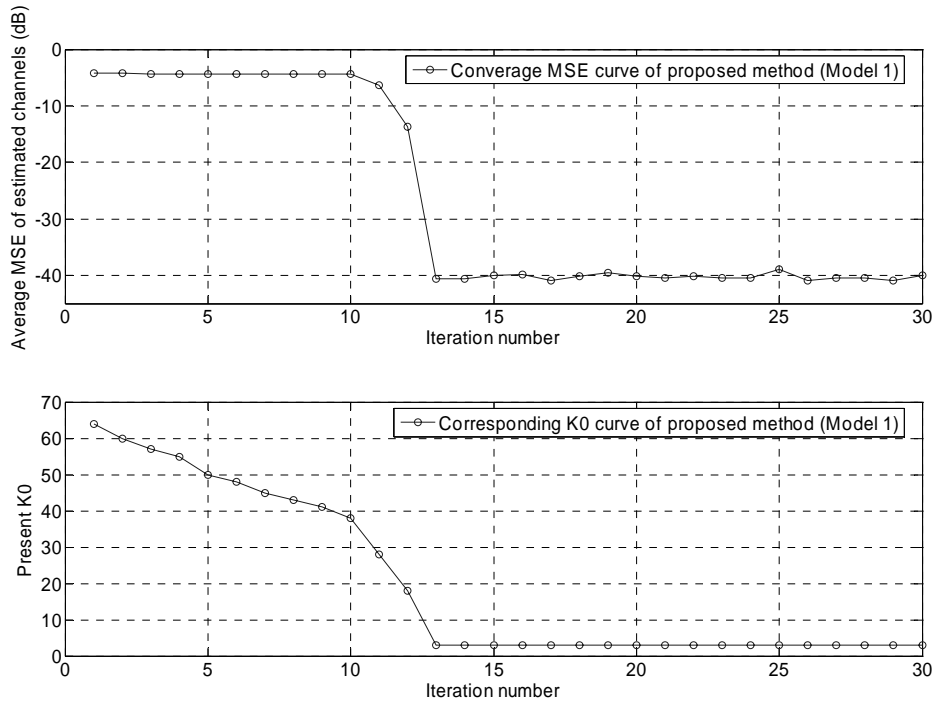
Model 1 (b) Model 2

(a)

(b)

Figure 5.15 Averaged MSE versus K_0 **of all-pilot preamble system, with** $N_T=4$

(a) Model 1 (b) Model 2

The MSE versus K_0 plot is also shown in Figure 5.13 to Figure 5.15. In the figures, the channels are estimated with SNR set to 40dB. MSE in this plot is the mean of both estimated channels from two antennas. In this case, co-channel interference dominates the MSE performance. One can obtain that if K_0 is smaller than the max delay spread (4 in Model 1 and 12 in Model 2), the MSE is relative large due to insufficient K_0. If K_0 is chosen to be close to the max delay spread, the performance is relative good. As K_0 grows, the estimated channels include more taps with interference. For this reason, MSE gets larger in this region.

In Figure 5.16 to Figure 5.19, converge curves of the proposed modification for the LS estimator in 4.2.3.2 are presented. In every OFDM packet, the channel length is estimated again. The curves illustrate the converge of corresponding MSE and values of K_0. In Figure 5.16 to 5.19, one can see that the MSE converge to low value after a few iterations. For the case of four receiver antennas, the curve can't converge in present simulations. The improvement will be one of the future works.

Figure 5.16 MSE and K_0 **curves versus iteration no. of proposed** K_0 **decision**

algorithm, $N_T = 2$ **(Model 1)**
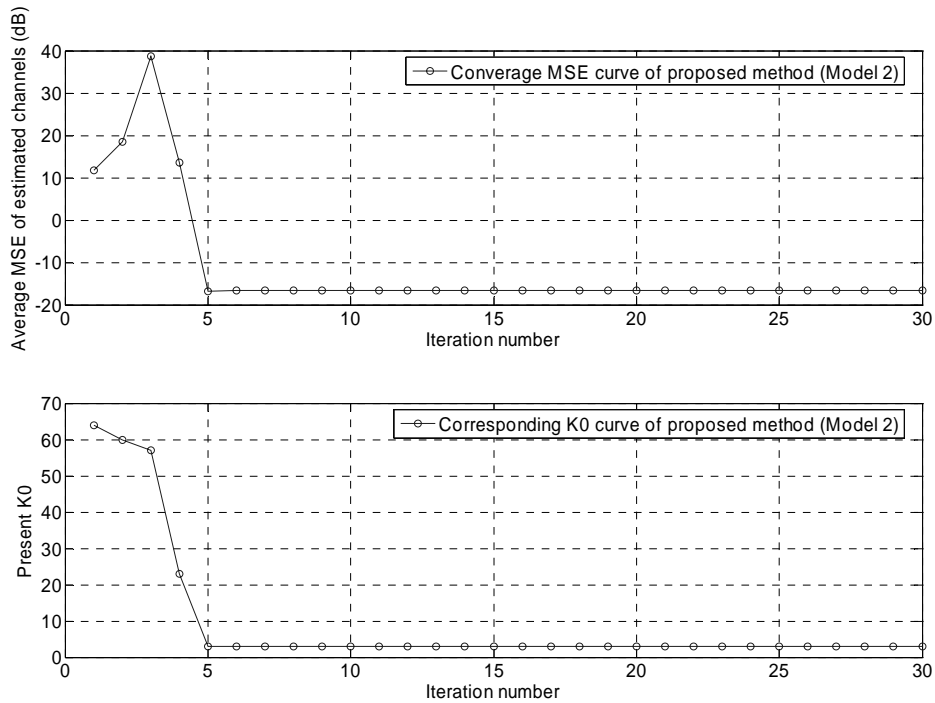
Figure 5.17 MSE and K_0 **curves versus iteration no. of proposed** K_0 **decision**

algorithm, $N_T = 2$ **(Model 2)**
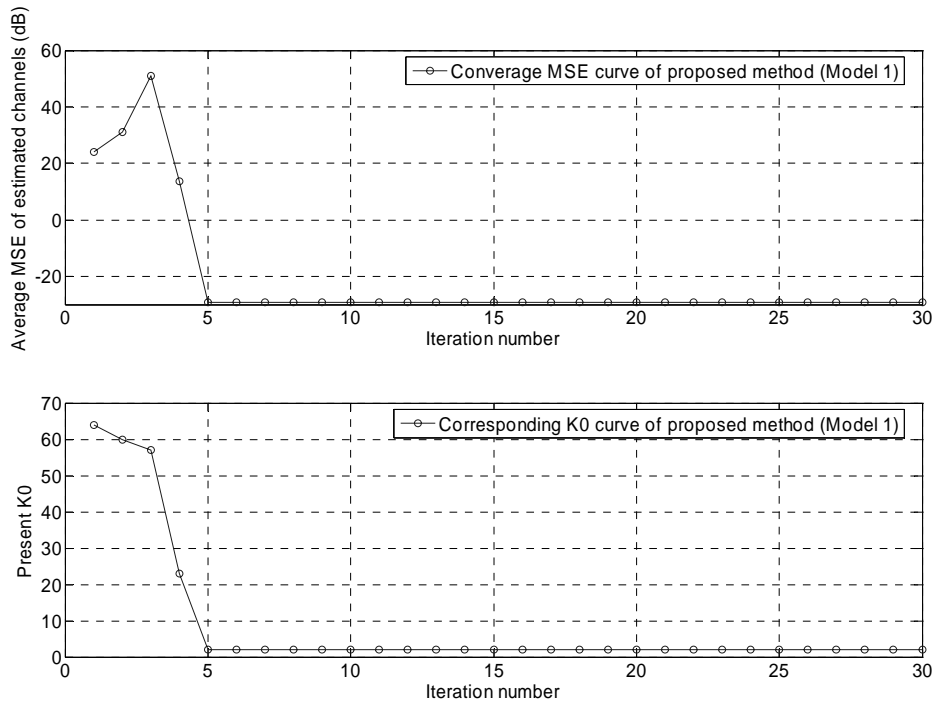
Figure 5.18 MSE and K_0 **curves versus iteration no. of proposed** K_0 **decision**

algorithm, $N_T = 3$ **(Model 1)**

Figure 5.19 MSE and K_0 curves versus iteration no. of proposed K_0 decision algorithm, $N_T = 3$ (Model 2)

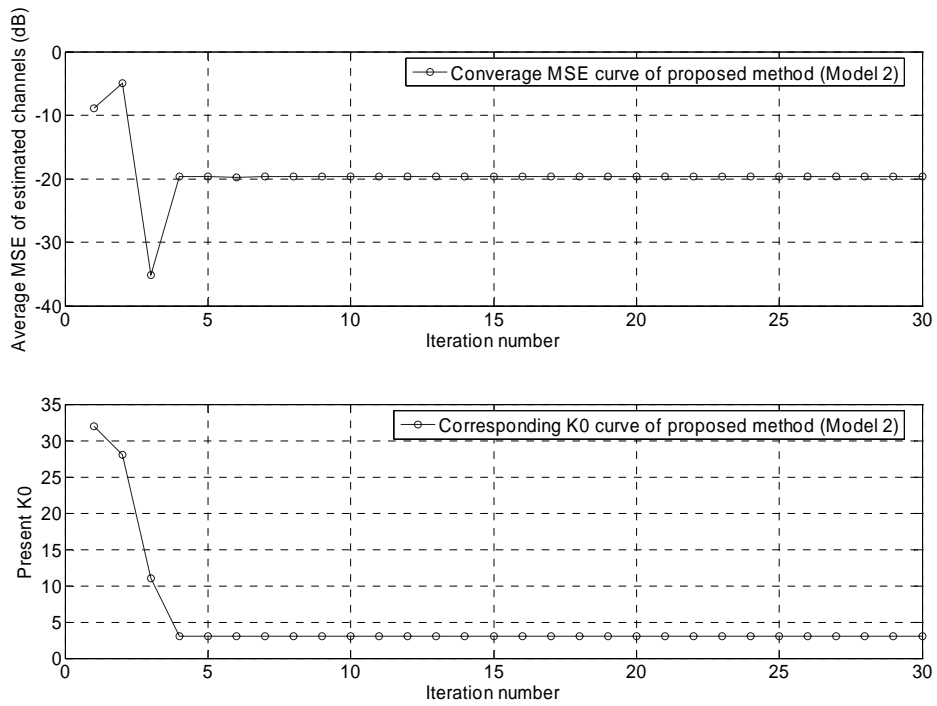# 5.2.3 Channel Estimation for MIMO OFDM Systems with Scattered Preamble

The scattered preamble MIMO OFDM system uses partial tones for each antenna to estimate channel parameters. After the responses on pilot tones are estimated by LS-based technique, there are still unknown responses on the non-pilot tones. These unknown values can be obtained by interpolation techniques. In our studies, transform-domain interpolation techniques are considered applied to those equi-spaced pilots. The equi-spaced pilots can be viewed as downsampled version of real channel response, and we can apply transform-domain interpolation techniques in this case.

(a)

(b)
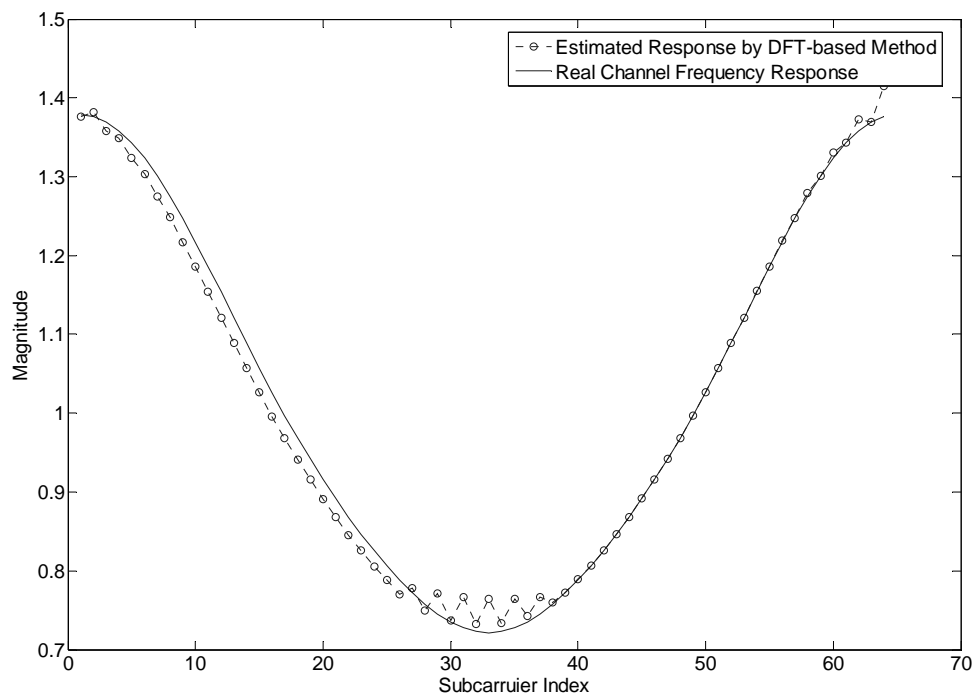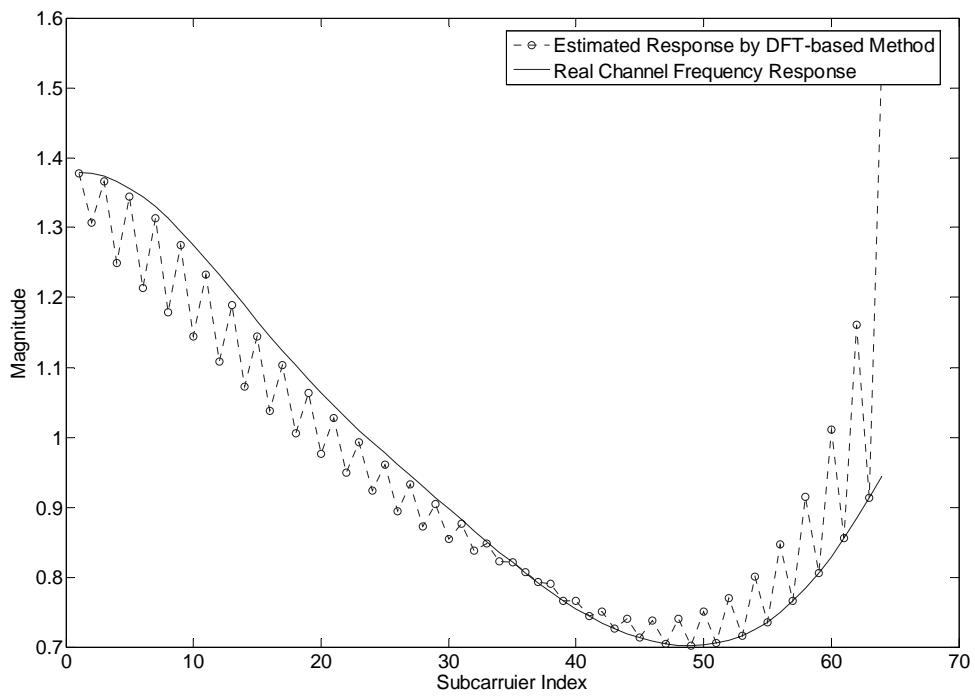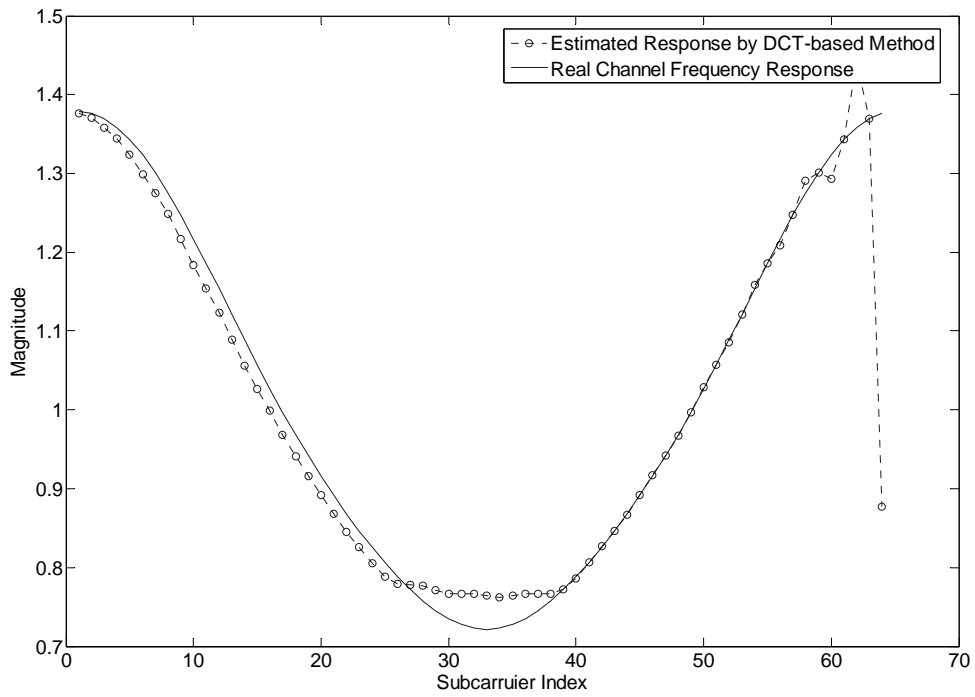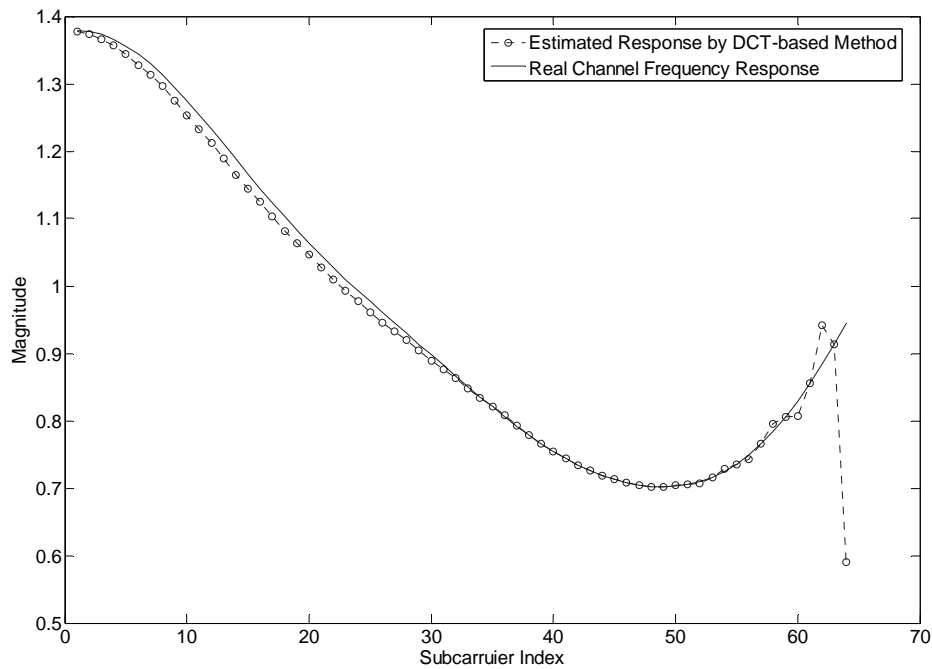
Figure 5.20 Estimated Responses by DFT and DCT-based estimators (a) DFT with sample spaced channel (b) DCT with sample spaced channel (c) DFT with non-sample spaced channel (d) DCT with non-sample spaced channel

In the following simulations, Rayleigh fading channels are assumed. The power delay profiles are set to Model 1 and Model 2. In a single packet, there are 10 OFDM symbols. The pilots from different antennas are located alternately in all subcarriers of preamble symbol. The estimated responses are shown in Figure 5.20 (a)-(d). In Figure 5.20 (a) and (b), the two estimators are applied to the sample spaced channel described in Table 5.2. As shown in the figure, the estimated responses are not much different. But in Figure 5.20 (c) and (d), we can find that the DFT-based estimator is not good for the non-sample spaced channel while DCT-based estimator works well.
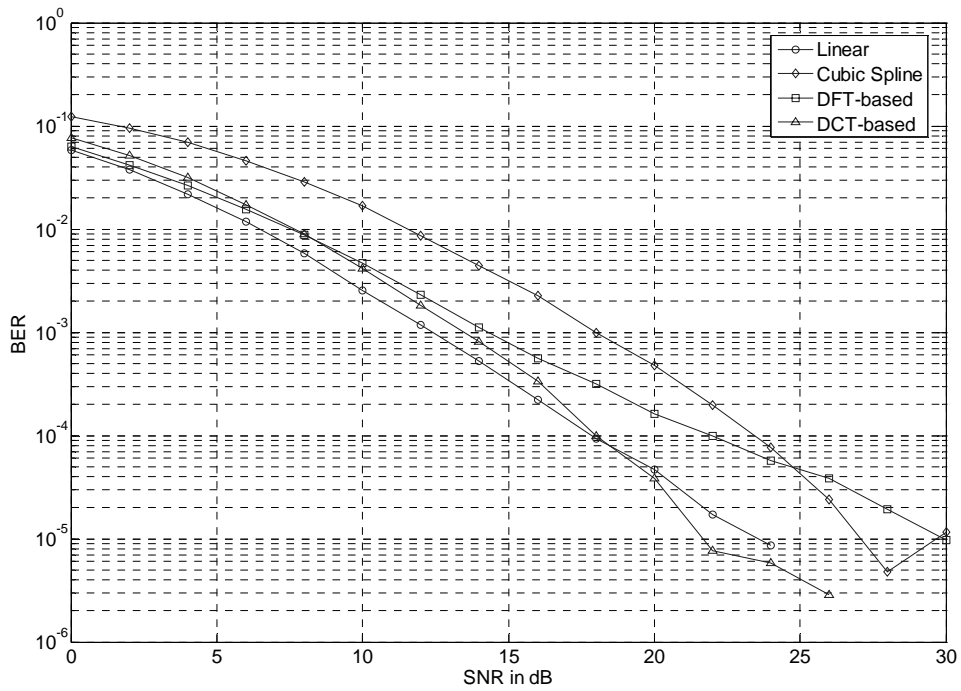
(a)
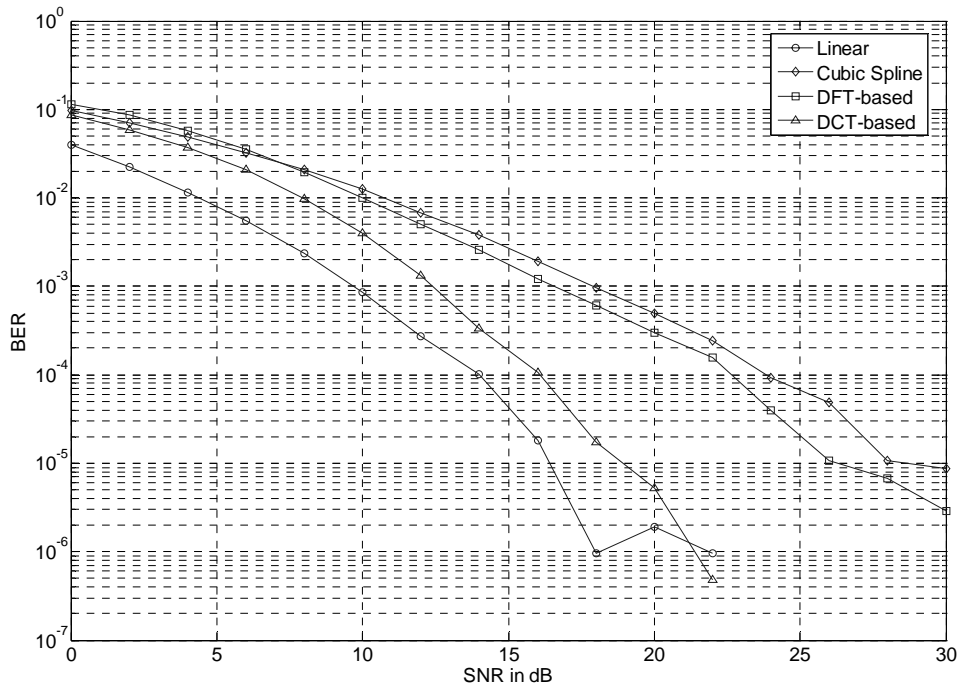
(b)

Figure 5.21 BER comparisons of various interpolation methods under

non-sample spaced channels (a) Model 1 (b) Model 2

90

The curves shown in Figure 5.21 are BER versus SNR for some major interpolations in non-sample-spaced channel Model 1 and 2. Since Model 2 has stronger frequency selectivity than model 1, it enhances the performance difference between those interpolation techniques. Unexpectedly, the performance of cubic spline interpolation is the worst of all those techniques. This would be against our intuition that cubic spline interpolation has the best function continuity of all those interpolation functions. However, this may be reasonable considering the additive noise effect on the accuracy of the assumed boundary function values and the derivative values of the interpolated segments. Comparing DFT and DCT -based channel estimators, we can find that the DCT-based estimator has better performance than conventional DFT-based estimator. It shows that the aliasing effect due to non-sample spaced channel effect mentioned in Chapter 4 can be mitigated by applying the DCT-based interpolation technique. However, the difference in the 802.11n-like systems is not so obviously compared with 802.16a system. The non-sample spaced effect may be considered to be stronger in typical 802.16a channel (e.g. ETSI A) than Model 1 and Model 2 channels. This is because the power and delay spread are relative large in typical 802.16a channels.

5.3 Channel Estimation for 802.16a OFDMA with STC

In this section, the channel estimation of 802.16a will be explored. 802.16a is an OFDM system with pilot symbol aided modulation . Therefore there are data tones and pilot tones in a single OFDM symbol. The channel estimation and data detection flows are shown in Figure 5.22. It is noted that interpolation techniques are required

after estimation on pilot tones. Compared to scattered block type MIMO OFDM systems, the estimation is more complicated due to special arrangement in 802.16a. When it comes to scattered block type systems, the pilot tones for each antenna are regularly distributed in preamble OFDM symbols. However, this is different in 802.16a system. As mentioned in Chapter 3, the pilots are classified into fixed and variable position types in 802.16a OFDMA, and it makes channel estimation more complicated. It will be further explored in this subsection.

Table 5.6 Simulation parameters of 802.16a STC system (2 x 1)

Bandwidth	10Mhz
Sample Frequency	11.42Mhz
Carrier Spacing	5.576KHz
GI Length	22.4μs(256 pts)
OFDM Symbol Length	201.75μs (2048 pts+256 pts)
N_{FFT}	2048 pts
Modulation	QPSK
Number of Fixed Pilots	32
Number of Variable Pilots	142
Number of Data Tones	1702
Space Time Coding	STBC
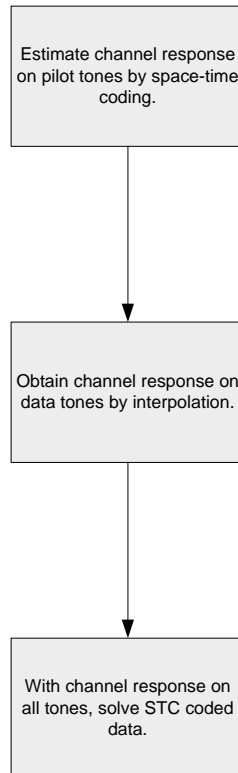
Figure 5.22 Channel estimation and data detection flow of 802.16a with STC

5.3.1 Pilot Sample Grouping for 2-D Channel

Estimations

For downlink of 802.16a system, each subcarrier appears as an pilot subcarrier once for every four consecutive OFDM symbols. In addition, the pilot tones repeat for every three subcarriers in frequency domain. This arrangement is shown in Figure 5.23 (a)-(c). If we want to compose more pilot subcarriers than in one symbol, we need to combine variable-position pilots from a few consecutive OFDM symbols. We will discuss several possible group schemes in the remaining subsection, and consider both BER and SER performance. Besides, buffer size (number of OFDM symbols reserved to do interpolation) will be considered in the studies.

Scheme 1, merging of multiple symbols: The pilot positions vary cyclically with different offset in consecutive OFDM symbols. One may assume the channel response varies slowly from symbol to symbol in a low mobility environment, and the response won't change very significantly. A most intuitive solution is to reserve four OFDM symbols in the buffer, and take the response estimated on the only pilot subcarrier as all other three data subcarriers in each column in Figure 5.23 (a). The solution is intuitive and simple, but this assumption may not be valid in a fast changing channel.

Scheme 2, bilinear interpolation on frequency and time axis: Linear interpolation can be applied to time and frequency axis. For the regularity of pilots in time domain, eight symbols may be reserved for our linear interpolation (at least two pilot subcarriers in the buffer). The detailed operation is illustrated in Figure 5.24 and equation 5.1, the data tone responses between pilot tones are obtained by interpolation and those on both sides of buffer are estimated by extrapolation from the nearest interval.
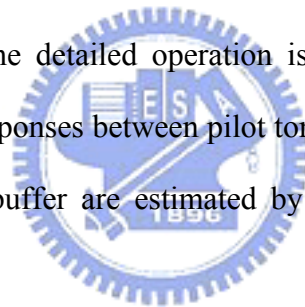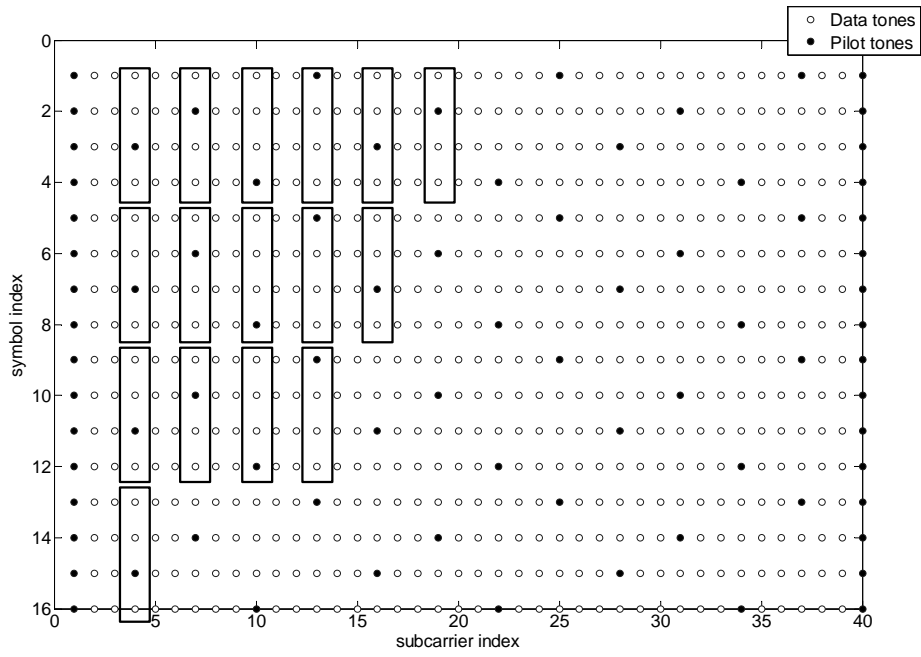
(a)
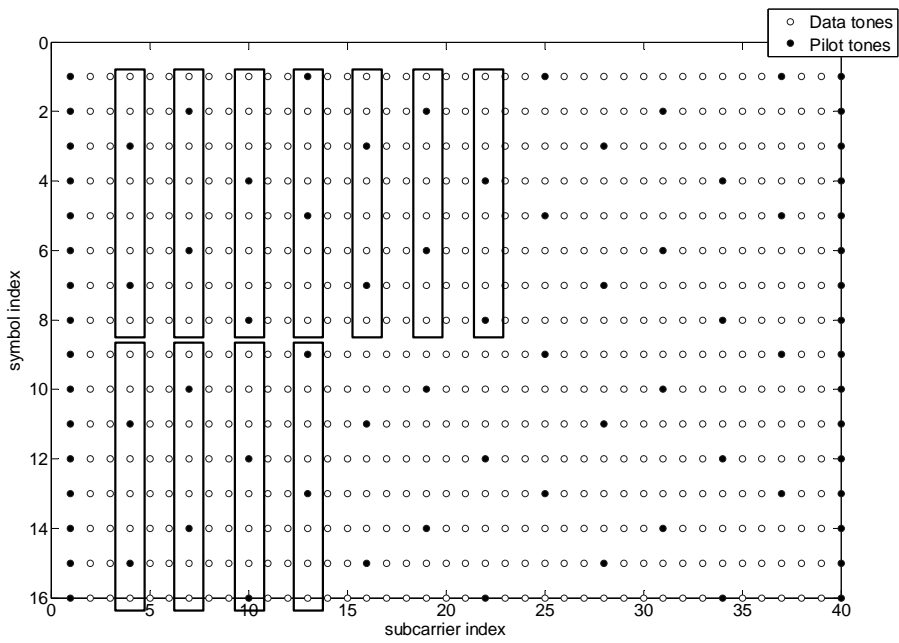
(b)

(c)

Figure 5.23 Pilot grouping schemes for 2-D channel interpolation (a) pilot merging of multiple symbols (b) pilot grouping for on time-axis (c) sliding windows for time-axis subcarrier response extrapolation
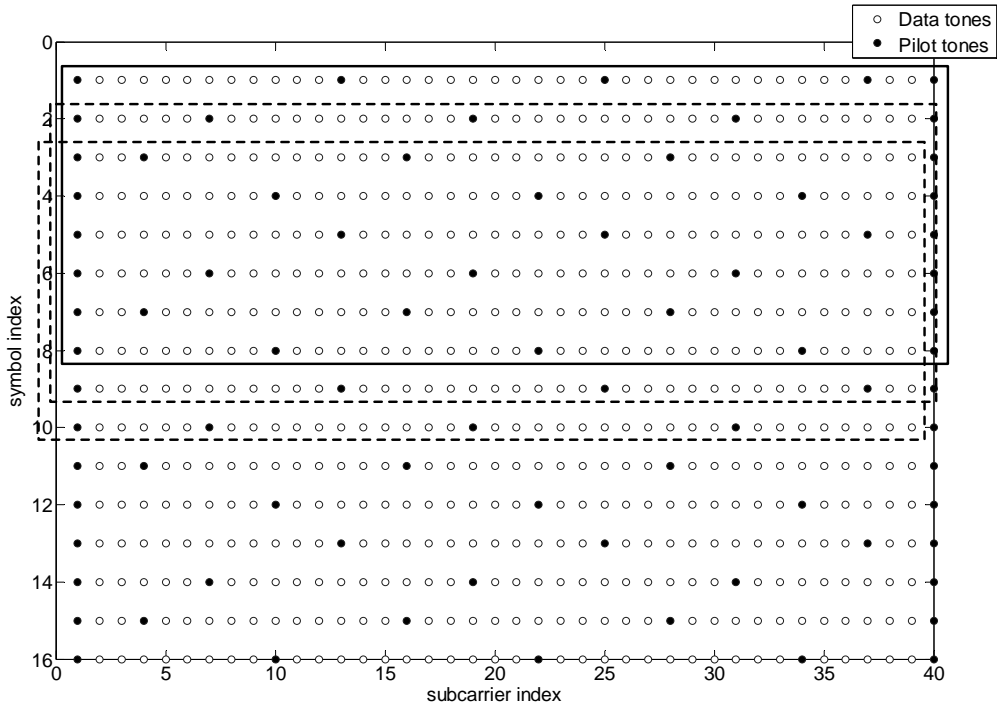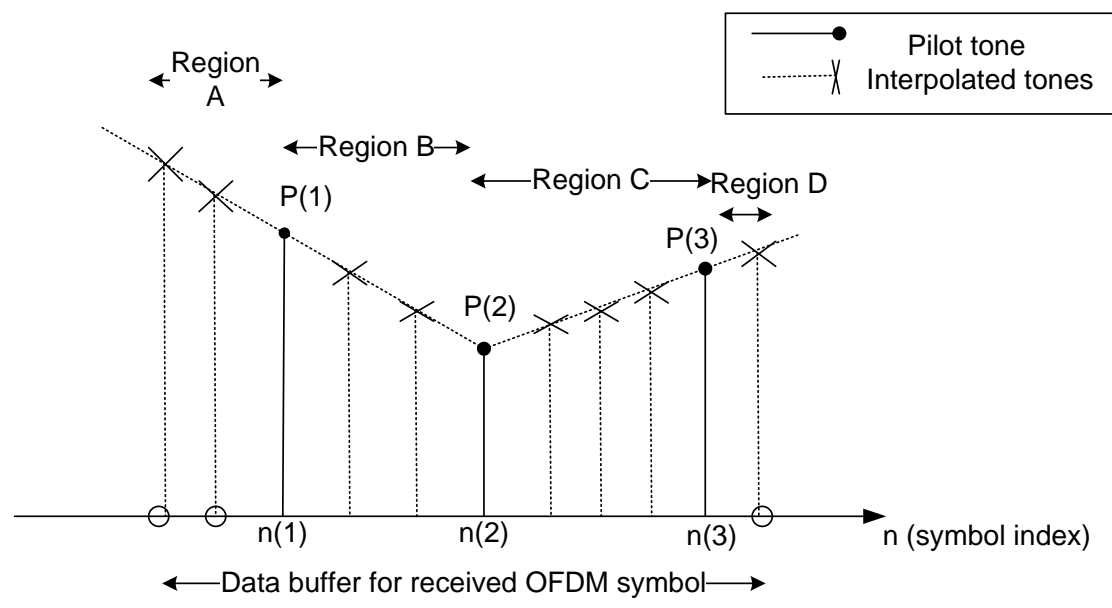

Figure 5.24 Interpolation and extrapolation region of data tone channel responses

Scheme 3, sliding window for channel extrapolation: When scheme 2 is used to find the channel on data subcarriers, results will not be obtained until the buffer is filled with eight (or other multiples of four) new symbols again. Hence we propose a scheme to reduce the latency. Once a new OFDM symbol is fed into the receiver, we will find the channel response on the data tones by extrapolation using two previous pilot tones. The flow is illustrated in Figure 5.25. The performance of these three schemes is shown in Figure 5.26 to Figure 5.27.

$$\begin{cases} \text{In region A, } X(n') = P(1) - (n' - n(1))\dfrac{P(2) - P(1)}{n(2) - n(1)} \\[2mm] \text{In region B, } X(n') = P(1) + (n' - n(1))\dfrac{P(2) - P(1)}{n(2) - n(1)} \\[2mm] \text{In region C, } X(n') = P(2) + (n' - n(2))\dfrac{P(3) - P(2)}{n(3) - n(3)} \\[2mm] \text{In region D, } X(n') = P(3) + (n' - n(3))\dfrac{P(3) - P(2)}{n(3) - n(2)} \end{cases} \qquad (5.1)$$
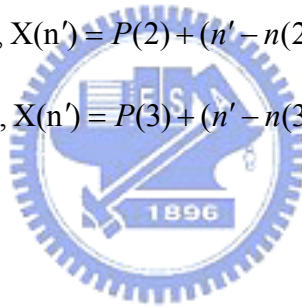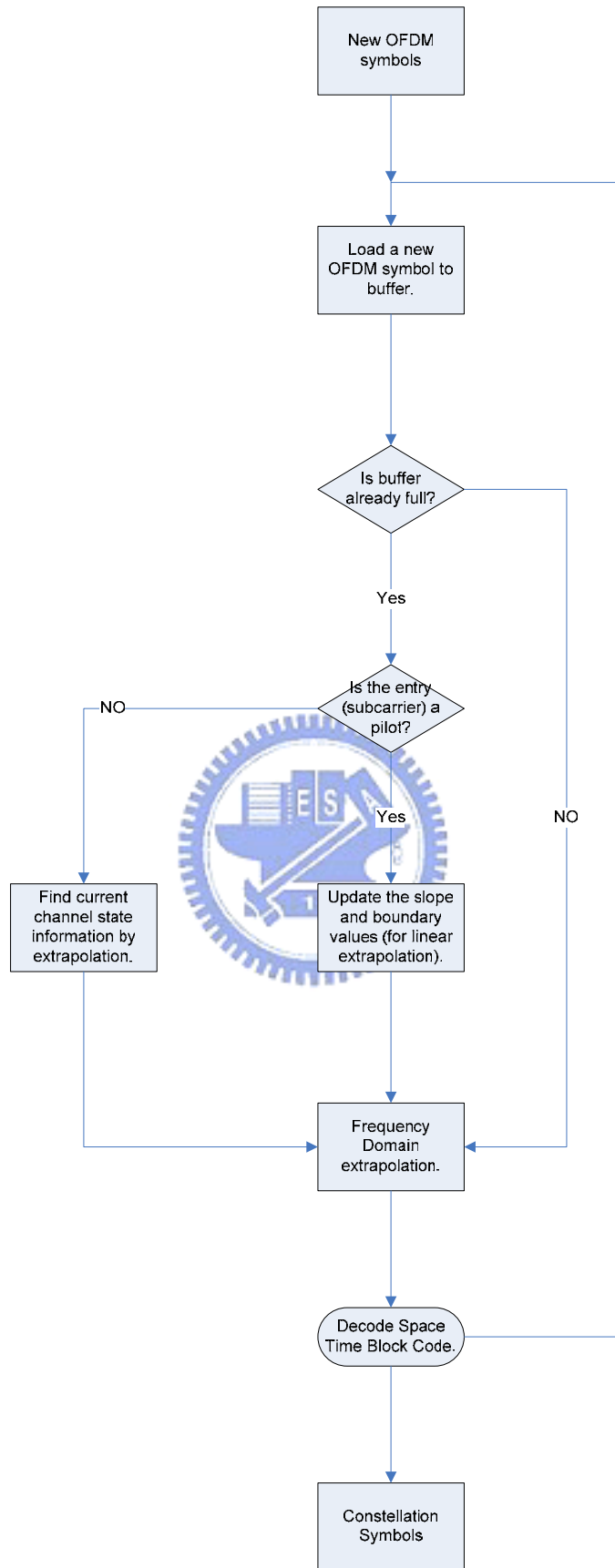
Figure 5.25 Extrapolation flow of scheme 3 for channel estimation

Figure 5.26 BER versus SNR plots based on various channel interpolations,

scheme 1 and scheme 2
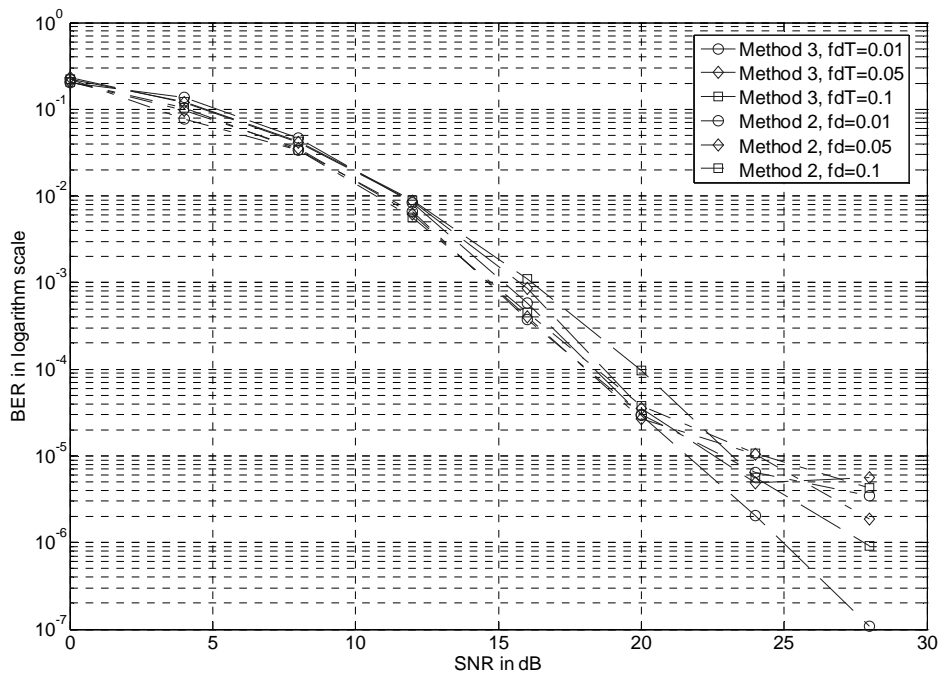
Figure 5.27 BER versus SNR plots based on various channel interpolations,

scheme 2 and scheme 3

In this simulation, channel Model 4 is used to emphasize the frequency-selectivity of channel response. In Figure 5.26 and Figure 5.27, the three mentioned schemes are applied to 802.16a system with STC system. One can see that scheme 1 -- directly combination of multiple symbols experience error floor in higher SNR und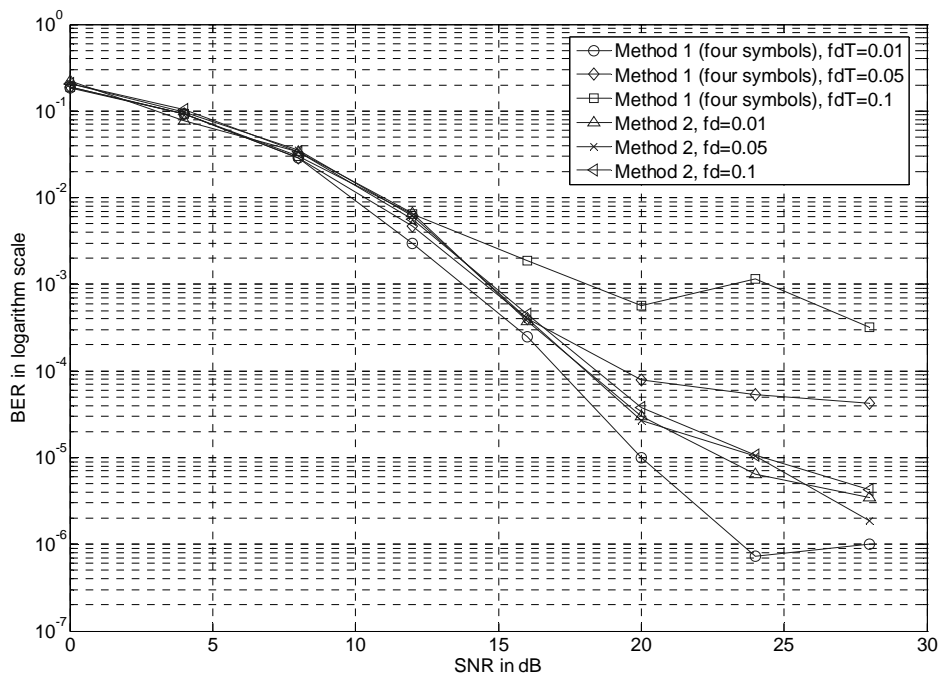er fast changing channel condition. Scheme 2 –interpolation on time-axis is better in BER than scheme 1, but main drawback of scheme 2 is that we will complete the operation only after every eight new symbols are received. Therefore scheme 3 continuously computes the estimated responses by extrapolation with pilot tones in sliding window. In Figure 5.26 and Figure 5.27, we can observe that the scheme 3 has a slightly poorer but comparable performance than scheme 2, but better than scheme 1. However, the main drawback of scheme 2 is reduced in scheme 3.
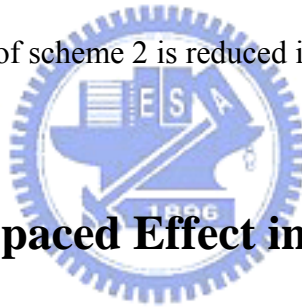
5.3.2 Non-sample Spaced Effect in 802.16a STC System

The non-sample spaced effect also exists in 802.16a STC system while transform domain interpolation techniques are considered. We test linear, cubic-spline, DFT-based, and DCT-based estimators in the simulations. The grouping scheme is scheme 2 in 5.3.1. In this simulation, Model 3 described in Chapter 4 is used here. In order to evaluate the performance under non-sample spaced channel, the taps of continuously channel model are located at 0, 3.5402, 8.1082, 12.448, 19.757, 28.664 samples.
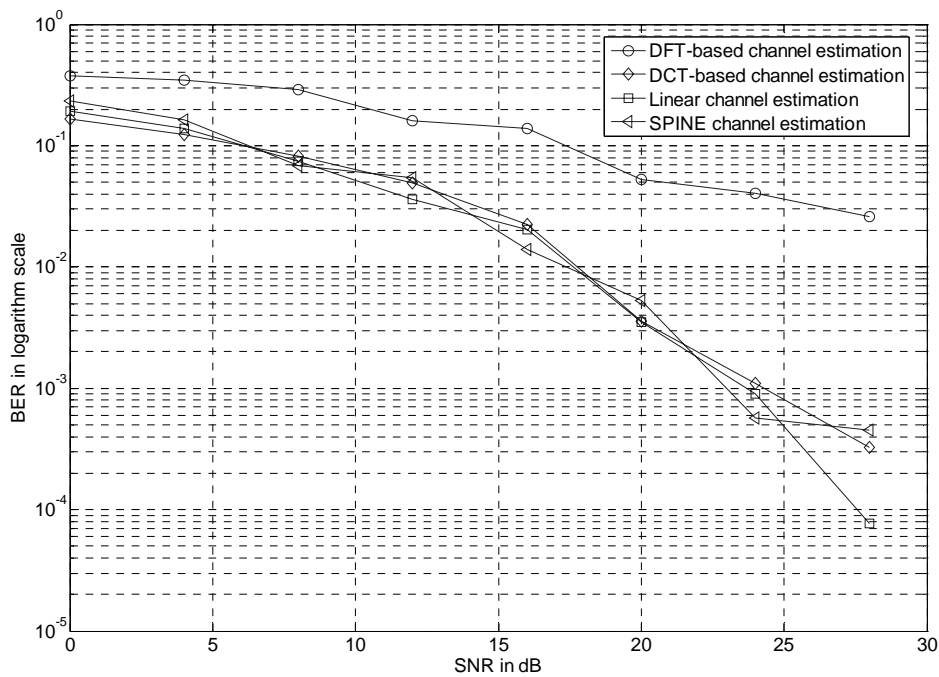
Figure 5.28 BER versus SNR plot of different estimators under non-sample

spaced channel

In Figure 5.28, DCT-based estimator is better than DFT-based estimator. Compared to Figure 5.6 (a) and (b), the improvement is more significant in 802.16a STC system. This is because the number of multipaths and the total power in Model 3 is larger than Model 1 and Model 2. As shown, DCT, linear, and cubic-spline estimators have almost equal performance.

Chapter 6
Conclusion

In this thesis, several kinds of channel estimation schemes for MIMO OFDM are considered. Before we start to discuss these approaches, the conventional Jakes' fading model is reviewed and the feature of spatial correlation is added to the conventional simulator. The simulation shows that the simulator can achieve the properties of MIMO channels. After that, a comparative investigation on these schemes is presented and analyzed in terms of bit error rate curves. Both 802.16a with STC and 802.11n-like systems are considered in our studies. In 802.11n-like systems with scattered preamble, the results show that the equi-spaced pilots are suitable for transform-domain interpolation skills. Under non-sample spaced channel, the results show that the DCT-based estimator improves the performance degeneration of DFT-based estimator. Among all interpolation skills, piecewise linear interpolation outperforms other interpolation skills in this scenario.

In the studies of STBC coded preamble MIMO OFDM system, a decision-direct channel tracking skill with smoothing process is applied to this system. The simulation results in 5.2.1 show that the tracking skill improves the performance of channel estimator in this system under time-varying channels. While we focus on all-pilot preamble MIMO OFDM systems, a LS-based estimator is applied to detect all-pilot MIMO preambles from interference of other antennas. For large matrix

inversion in this approach, a modification is also applied. In our simulations, different parameters (K_0) are tried to evaluate their corresponding performances. Both BER curves and MSE are presented. According to our simulations, the system has best performance while K_0 is set approximately to the maximum delay spread of the channel. The proposed decision algorithm for channel length is good for cases of two and three antennas, but not suitable for case of four antennas.

As for 802.16a system with STC, we consider different schemes to combine multiple OFDM symbols to improve estimation accuracy. Consider the accuracy and the latency. We discuss combination flow based on piecewise linear extrapolation with a sliding window. The simulations show that it performs well in this system.

This thesis focuses on existing MIMO OFDM channel estimation skills, and some advanced issues should be explored in the future. All the channel conditions in this thesis are assumed to be static in a single OFDM symbol. However, the ICI introduced by fast-fading channel should be studied and compensated. The method to detect channel length in Chapter 4 is not very robust for present studies. The improvement is another future work. The implementation of integrated IEEE 802.11n systems with data detection and synchronization is the next goal of our research. For this integrated work, more MIMO channel characteristics need to be added to present channel simulator.

Bibliography

[1]   V. Tarokh, A. Naguib, N. Seshadri, and A. R. Calderbank, "Space-time codes for high data rate wireless communication: performance criteria in the presence of channel estimation errors, mobility, and multiple paths," *IEEE Transactions on Communications*, vol. 47, pp. 199-207, 1999.

[2]   S. M. Alamouti, "A simple transmit diversity technique for wireless communications," *IEEE Journal on Selected Areas in Communications*, vol. 16, pp. 1451-1458, 1998.

[3]   S. Rappaport, *Wireless Communications Principles and Practice*, Prentice Hall, 1996.

[4]   S. Weinstein and P. Ebert, "Data Transmission by Frequency-Division Multiplexing Using the Discrete Fourier Transform," *IEEE Transactions on Communications*, vol. 19, pp. 628-634, 1971.

[5]   A. Peled and A. Ruiz, "Frequency domain data transmission using reduced computational complexity algorithms," *Proceedings of IEEE International Conference on Acoustics, Speech, and Signal Processing*, ICASSP '80, vol. 5, pp. 964-967, 1980.

[6]   W. C. Jakes, *Microwave Mobile Communications*, Wiley, 1974.

[7]   M. F. Pop and N. C. Beaulieu, "Limitations of sum-of-sinusoids fading channel simulators," *IEEE Transactions on Communications*, vol. 49, pp. 699-708, 2001.

[8]   A. Botonji, "MIMO channel models," M.S. thesis, Linkopings Universitet, Norrkoping, Sweden, 2004.

[9]   K. I. Pedersen, J. B. Andersen, J. P. Kermoal, and P. Mogensen, "A stochastic multiple-input-multiple-output radio channel model for evaluation of space-time coding algorithms," *Proceedings of Vehicular Technology Conference, 2000. IEEE VTS-Fall VTC 2000. 52nd*, vol. 2, pp. 893-897, 2000.

[10]   T. Klingenbrunn and P. Mogensen, "Modelling frequency correlation of fast fading in frequency hopping GSM link simulations," *Proceedings of Vehicular Technology Conference, 1999. VTC 1999 - Fall. IEEE VTS 50th*, vol. 4, pp. 2398-2402, 1999.

[11]   "IEEE Standard for Local and metropolitan area networks --- Part 16: Air Interface for Fixed Broadband Wireless Access Systems--- Amendment 2: Medium Access Control Modifications and Additional Physical Layer Specifications for 2-11 GHz," in IEEE Std 802.16a-2003 (Amendment to IEEE Std 802.16-2001), 2003, pp. 292.

[12] WWiSE, "WWiSE proposal," vol. 2004: Airgo Networks, Bermai, Broadcom, Conexant, Realtek, STMicroelectronics, Texas Instruments, 2004.

[13] "Information technology- telecommunications and information exchange between systems- local and metropolitan area networks- specific requirements part 11: wireless lan medium access control (MAC) and physical layer (PHY) specifications amendment 1: high-speed physical layer in the 5 GHz band," in ISO/IEC 8802-11:1999/Amd 1:2000(E); IEEE Std 802.11a-1999, 2000, pp. 83.

[14] V. Tarokh, H. Jafarkhani, and A. R. Calderbank, "Space-time block coding for wireless communications: performance results," *IEEE Journal on Selected Areas in Communications*, vol. 17, pp. 451-460, 1999.

[15] A. Dowler and A. Nix, "Performance evaluation of channel estimation techniques in a multiple antenna OFDM system," *Proceedings of Vehicular Technology Conference, 2003. VTC 2003-Fall. 2003 IEEE 58th*, vol. 2, pp. 1214-1218, 2003.

[16] J.-J. van de Beek, O. Edfors, M. Sandell, S. K. Wilson, and P. O. Borjesson, "On channel estimation in OFDM systems," *Proceedings of Vehicular Technology Conference, 1995 IEEE 45th*, vol. 2, pp. 815-819, 1995.

[17] Y. Zhao and A. Huang, "A novel channel estimation method for OFDM mobile communication systems based on pilot signals and transform-domain processing," *Proceedings of Vehicular Technology Conference, 1997 IEEE 47th*, vol.3, pp. 2089-2093, 1997.

[18] B. Yang, K. B. Letaief, R. S. Cheng, and Z. Cao, "Windowed DFT based pilot-symbol-aided channel estimation for OFDM systems in multipath fading channels," *Proceedings of Vehicular Technology Conference, 2000. VTC 2000-Spring Tokyo. 2000 IEEE 51st*, vol. 2, pp. 1480-1484, 2000.

[19] Y.-H. Yeh and S.-G. Chen, "DCT-based channel estimation for OFDM systems," *Proceedings of IEEE International Conference on Communications*, vol.4, pp. 2442-2446, 2004.

[20] X. Zhao, J. Kivinen, and P. Vainnikainen, "Tapped delay line channel models at 5.3 GHz in indoor environments," *Proceedings of Vehicular Technology Conference, 2000. IEEE VTS-Fall VTC 2000. 52nd*, vol. 1, pp. 1-5, 2000.

[21] V. Tarokh, S. M. Alamouti, and P. Poon, "New detection schemes for transmit diversity with no channel estimation," *Proceedings of IEEE International Conference on Universal Personal Communications*, vol. 2, pp. 917-920, 1998.

[22] Y. Li, N. Seshadri, and S. Ariyavisitakul, "Channel estimation for OFDM systems with transmitter diversity in mobile wireless channels," *IEEE Journal on Selected Areas in Communications*, vol. 17, pp. 461-471, 1999.

[23] Douglas (The Math Forum@Drexel), "Complexity of Matrix Inversion," April 25, 2001, http://mathforum.org/library/drmath/view/51908.html.

[24] Y. Li, "Simplified channel estimation for OFDM systems with multiple transmit antennas," *IEEE Transactions on Wireless Communications*, vol. 1, pp. 67-75, 2002.

[25] T.-Y. Tsai, "Channel Estimation Technique for Space-Time Block Coded Orthogoal Frequency Division Multiplexing System," M.S. thesis, Institute of Electronics, National Chiao Tung University, Hsin-Chu, Taiwan, 2003.

[26] Y.-H. Yeh, "Design of Pilot-Symbol-Aided Channel Estimation and Equalization for OFDM Systems," M.S. thesis, Institute of Electronics, National Chiao Tung University, Hsin-Chu, Taiwan, 2003.

[27] C.-C. Wu, "Pilot-Added Channel Estimation for OFDM systems," M.S. thesis, Institute of Electronics, National Chiao Tung University, Hsin-Chu, Taiwan, 2004.

Autobiography

詹偉廷，1981 年 1 月 5 日出生於台南市。2003 年自國立交通大學電機工程系畢業，隨即進入國立交通大學電子工程研究所攻讀碩士學位，致力於訊號處理與通訊系統研究。論文題目是多輸入多輸出之正交分頻多工通信系統通道估測設計